Thesis for The Degree of Doctor of Philosophy

Robust Design Framework for Cutting Tool Interface Design

Soner Camuz

Department of Industrial and Materials Science
Chalmers University of Technology
Gothenburg, Sweden, 2025

Robust Design Framework for Cutting Tool Interface Design

Soner Camuz

© Soner Camuz, 2025
except where otherwise stated.
All rights reserved.

ISBN 978-91-8103-168-3
Doktorsavhandlingar vid Chalmers tekniska högskola, Ny serie nr 5626.
ISSN 0346-718X

Department of Industrial and Materials Science
Chalmers University of Technology
SE-412 96 Göteborg,
Sweden
Phone: +46(0)31 772 1000

Cover:
Illustration of a CM390 indexable cutting tool assembly with magenta regions marking the insert and tool body interface.

Printed by Chalmers Digitaltryck,
Gothenburg, Sweden 2025.

"it can always get worse"
- Finnish saying

Robust Design Framework for Cutting Tool Interface Design
SONER CAMUZ
Department of Industrial and Materials Science
Chalmers University of Technology

Abstract

Failure to maintain an even pressure distribution and robustness in the positioning of inserts in indexable cutting tools can often result in critical failures during machining, such as increased wear and clamp screw fatigue, leading to costly design reiterations. Current locating schemes do not consider aspects such as external loads and non-linear material models, which are crucial to consider in indexable cutting tools as the loads acting on the insert and tool body often exceed the yield limit of materials. Therefore, this thesis proposes a framework with methodologies to assist engineers in the early design phases of indexable cutting tools to develop a robust positioning of the insert with the tool body interface. The framework focuses on optimizing the positioning of the insert, ensuring that the tool performs effectively under operational loads. By incorporating techniques such as Finite Element Analysis (FEA), genetic algorithms, stability analysis, and contact index optimization, the framework enables engineers to address key challenges like pressure distribution, insert movement, and fatigue, ultimately enhancing cutting tools' durability, reliability, and performance.

Applying the proposed framework to the existing insert design, R390-11T308M-MM2030 created a first-iteration prototype of the tool body interface. The prototype exhibited enhanced durability and reliability, ensuring more robust insert positioning under operational loads. The prototype maintained comparable efficiency to its predecessor and did not compromise the tool's overall productivity. This advancement suggests that further refinements could enhance the prototype's overall effectiveness, potentially leading to even more significant improvements in future iterations.

Keywords

Variation Simulation, Geometry Assurance, Cutting Tool Interface Design, Computer Aided Design, Computer Aided Engineering, Data-Driven Engineering, Robust Design

List of Publications

Appended publications

This thesis is based on the following publications:

[**Paper I**] **S. Camuz**, R. Söderberg, K. Wärmefjord, M. Lundblad, *Tolerance Analysis of Surface-to-Surface Contacts Using Finite Element Analysis 15th CIRP Conference on Computer Aided Tolerancing (Apr 2018), Vol. 75, p.250-255.*

Author's contribution: Conceptualization (Soner, Mikael), Methodology (Soner), Formal analysis (Soner), Investigation (Soner), Writing - Original Draft Preparation (Soner), Writing - Review & Editing (All)

[**Paper II**] **S. Camuz**, M. Bengtsson, R. Söderberg, K. Wärmefjord, *Reliability-Based Design Optimization of Surface-to-Surface Contact for Cutting Tool Interface Designs*
Journal of Manufacturing Science and Engineering (Feb 2019), Vol. 141, Issue 4, p.141(4).

Author's contribution: Conceptualization (Soner & Magnus), Methodology (Soner), Formal analysis (Soner), Investigation (Soner), Writing - Original Draft Preparation (Soner), Writing - Review & Editing (All).

[**Paper III**] **S. Camuz**, S. Lorin, K. Wärmefjord, R. Söderberg, *Nonlinear Material Model in Part Variation Simulations of Sheet Metals*
Journal of Computing and Information Science in Engineering (Jun 2019), Vol. 19, Issue 2, p.19(2).

Author's contribution: Conceptualization (Soner & Samuel), Methodology (Soner & Samuel), Formal analysis (Soner), Investigation (Soner), Writing - Original Draft Preparation (Soner & Samuel), Writing - Review & Editing (All).

[**Paper IV**] **S. Camuz**, A. Liljerehn, K. Wärmefjord, R. Söderberg, *Algorithm for Detecting Load-Carrying Regions within the Tip Seat of an Indexable Cutting Tool*
Journal of Computing and Information Science in Engineering (April 2024), Vol. 24, Issue 4.

Author's contribution: Conceptualization (Soner), Methodology (Soner), Formal analysis (Soner), Investigation (Soner), Writing - Original Draft Preparation (Soner), Writing - Review & Editing (All).

[**Paper V**] **S. Camuz**, A. Liljerehn, L. Lindkvist, R. Söderberg, K. Wärmefjord, *Robustness Optimization of the Tip Seat of an Indexable Cutting Tool*
Journal of Computing and Information Science in Engineering (April 2025), Vol. 25, Issue 4.

Author's contribution: Conceptualization (Soner), Methodology (Soner & Lars), Formal analysis (Soner), Investigation (Soner), Validation (Soner), Writing - Original Draft Preparation (Soner), Writing - Review & Editing (Soner, Anders, Rikard and Kristina).

Other publications

The following publications were published during my PhD studies, or are currently in submission/under revision. However, they are not appended to this thesis, due to contents overlapping that of appended publications or contents not related to the thesis.

[**i**] **S. Camuz**, M. Bengtsson, R. Söderberg, K. Wärmefjord, *Contact Variation Optimization for Surface-to-Surface Contacts*
ASME 2017 International Mechanical Engineering Congress and Exposition. Volume 2: Advanced Manufacturing (Nov 2017), Vol. 2.

Author's contribution: Conceptualization (Soner & Magnus), Methodology (Soner), Formal analysis (Soner), Investigation (Soner), Writing - Original Draft Preparation (Soner), Writing - Review & Editing (All).

[**ii**] **S. Camuz**, 2024. *A cutting tool.* EP24185199.7, *filed 28-07-2024*
Patent pending.

Acknowledgment

This study was carried out at the Department of Industrial and Materials Science at Chalmers University of Technology in Gothenburg and at AB Sandvik Coromant in Sandviken.

My first acknowledgment goes to my academic supervisors Rikard Söderberg and Kristina Wärmefjord for their support and motivational support throughout the years.

The deepest gratitude goes to the Department of Cutting Tool Research at AB Sandvik Coromant for their invaluable critiques, which pushed my ideas further and challenged me intellectually. I am especially grateful to my industrial supervisors, Mikael Lundblad and Anders Liljerehn, for their guidance and support.

I also thank the Swedish Agency for Innovation Systems (VINNOVA) and AB Sandvik Coromant for their financial support.

Finally, i would like to thank my parents and parents-in-law for their unconditional support through hardships and to my family, my wife Elin, and my daughters Elna and Ester for their love and patience.

Contents

Part I

Summary

Chapter 1

Introduction

This chapter provides an introduction to the conducted research, containing motivation and incentives, aim and scope, research questions and a brief outline[1]*.*

1.1 Background

Cutting tool manufacturers strive to enhance their products' reliability and longevity to meet the increasing demand for tools that offer predictable and lasting performance. Key factors influencing the reliability and durability of cutting tools include insert grade and geometry, machining parameters, and the tool's configuration relative to the workpiece.

Recent efforts to enhance reliability have prompted cutting tool manufacturers to investigate chamfered and serrated interfaces within the tool body. However, these attempts have occasionally resulted in excessive contact within the interface positioning, leading to multiple contact points that shift[2] based on the loads exerted on the indexable insert and, in turn, reduce the cutting tool's life expectancy. Alternatively, the forces and temperatures generated during the cutting process can plastically deform the insert-tool body interface, altering its positioning and creating multiple contact points. Altering the positioning of the insert is particularly devastating in cutting operations with transiently changing loads, such as milling and drilling, and has been shown to decrease life expectancy drastically in indexable cutting tools. Current robust design methodologies encounter significant challenges in achieving the desired robustness for indexable cutting tool positioning. These challenges arise from the inherent complexity of the tool-insert interface and the external loads exerted on the carbide insert. Ensuring consistent performance under varying

[1] Parts of this thesis have been reused from the author's previous licentiate thesis. S. Camuz, "Tolerance Analysis Framework for Cutting Tool Interface Design," Chalmers University of Technology, 2019. Accessed: Sep. 09, 2024. [Online]. Available: https://research.chalmers.se/en/publication/509701

[2] For instance, consider a four-legged chair with legs of varying heights. As the person sitting on it shifts their center of gravity, a different set of three legs will come into contact with the ground, creating a wobbling effect as the load's direction and magnitude change.

operational conditions is difficult due to the intricate interactions between the surfaces and the influence of transient forces during cutting operations. In new tool designs, issues with uneven pressure distribution often emerge during machining tests or after product release, leading to costly design revisions and a loss of anticipated quality. Therefore, methodologies to mitigate the impact of such variations are essential to ensure quality aspects like durability, reliability, and performance in cutting tool designs and reduce costs in product development of indexable cutting tools.

The conducted research combines three fields: positioning, variation simulation and metal cutting mechanics, (Fig. 1.1). Through literature reviews, it was identified that current methodologies require the incorporation of non-linear material behaviour, surface-to-surface contact formulations and the implementation of mechanical and thermal loads for geometry assurance of cutting tool design.

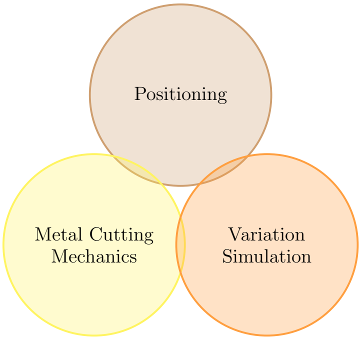

Figure 1.1: Venn diagram illustrating the addressed research fields and the knowledge gap between the three fields

Variation simulation refers to a collection of tools and methods designed to model how variations propagate through an assembly. These approaches help engineers understand and predict the impact of geometric and process deviations on the overall performance and functionality of a product. Each variation simulation method has specific advantages and disadvantages, depending on factors such as complexity, required accuracy, and computational resources, as shown in the comparative study by Shen et al. [1].

Early methods for variation simulation relied on 1D and 2D tolerance chain loops to model how deviations in individual components accumulate within an assembly. These approaches were used to predict stack-up effects, ensuring that components meet functional requirements, such as minimizing gaps or keeping assemblies flush.

As assembly complexity increases, the application of stack-up analysis using 1D/2D tolerance chain loops becomes challenging for 3D cases and when incorporating physical effects such as elasticity, thermal expansion, or deformation. These traditional methods lack the capability to account for nonlinear interactions and multidimensional variations in complex assemblies. To address these limitations, advanced approaches like Finite Element Analysis (FEA) and direct Monte Carlo simulations were introduced. These methods allow for more accurate predictions of assembly behavior by incorporating physics-based models, with the downside of increasing computational time.

Within sheet metal assemblies, Liu and Hu [2] introduced the use of influence coefficients (MIC) to establish a linear relationship between part deviations and assembly spring-back deviations to predict how final assembly tolerances. The linear relationship is retrieved through FEA and is valid as long as part deviations from nominal are small and stress-strain relationships are within the linear range.

To model how variations propagate through an assembly, different approaches can be taken, each with its advantages and disadvantages. A common practice are point-based approaches, such as the 3-2-1 locating scheme for rigid assemblies, where Söderberg and Lindkvist [3] incorporate robustness and geometrical stability evaluations to identify geometrically sensitive sheet metal assemblies. For compliant assemblies, the N-2-1 locating principle formulated by Cai et al. [4], and further expanded by Söderberg et al. [5], are the most common approaches in sheet metal applications and fixturing of workpieces. Point-based locating schemes require that the positioning between two or more parts are known and unchanged during operation. Dahlström and Lindkvist [6] present an approach for implementing a contact search algorithm in the MIC methodology to avoid penetration of contacting surfaces. The implementation shows significance in reducing computational time with a limited loss of accuracy.

Moos and Vezzetti [7] discuss the importance of non-linear material behaviour in resistance spot welding (RSW), where they, identified that the clamping force by the electrodes deviates and causes plastic deformations which in turn affect the assembly deviations. Adopting, for example, the MIC methodology under these conditions will reduce the accuracy due to non-linearities in the material behaviour. Söderberg et al. [8] also point out the importance of using non-linear material models in variation simulations and the need for incorporating new material models in current methodologies.

The contact in cutting tools between the insert and the tool body are surface-to-surface contacts. Dantan et al. present a skin model-based approach is used to define a coherent expression of Geometrical Product Specification (GPS) during tolerancing on isolated parts [9]. Schleich et al. extend the skin model approach by incorporating a framework that allows simulation of assembly and kinematic behaviours [10]. Schleich and Wartzack [11] validate the skin model approach in which they present a quantitative study of tolerance analyzes by comparing a skin model with three well-known methods: tolerance stacking, vector loops, and small displacement torsor. Schleich and Wartzack also highlight the importance of integrating deformation and thermal effects in the skin model approach. Garaizar et al. [12] present a framework for integrating thermal effects in skin models. The skin model is generated through a finite element mesh where geometric deviations, both systematic and random, are added to the nodes. The new mesh is then used to simulate thermal effects using finite element analysis (FEA). Using FEA, it is possible to calculate the thermal expansion of the skin model. Junnan et al. [13] take a similar approach, incorporating deformation due to static loads. Skin models with integrated effects will require numerous FE simulations in order to get statistical data. It is time-expensive and resource-heavy due to the non-linearity of the boundary conditions. Therefore, the number of simulations must be reduced without losing the accuracy of the results, keeping it possible to collect enough data for statistical assessments. To further improve the accuracy and time efficiency of the skin model approach, Liu et al. [14] developed a methodology that predicts assembly variations by accounting for the initial deformation of contacting surfaces. Instead of relying on time-intensive direct FEA, they implemented Herzian contact theory [15], which allows for a more efficient simulation of contact interactions. This approach significantly reduces simulation time while maintaining accuracy in predicting how the assembly will behave under different loading conditions.

Lorin et al. [16], [17] generate a design of experiments where process input parameters, such as mold temperature and cooling time, are varied. Each observation is simulated, and a regression model is created for each node on the surface and used for variation simulations. The approach is independent of the distribution of input parameters, as variation simulations are conducted prior to the FEA simulations. Using regression or meta-models also allows for various distributions of the input parameters in the variation simulations compared to the data collection. The accuracy of the variation simulations is therefore dependent on the coverage of nonlinear behaviours in the design of experiments and the FE-model.

The research on variation analysis within the machining industry has mainly focused on the fixturing of the workpiece and fixture design optimization and widely employs the 3-2-1 and N-2-1 positioning methods for fixture-workpiece alignment, where high fixture stiffness is crucial to minimize displacement during machining. The importance of these methods was demonstrated by Shawki and Abdel-Aal [18]–[20] through their investigation into the dimensional accuracy of fixturing under various working conditions and contact formulations. Hurtado and Melkote [21] further advanced this approach by integrating a tolerance budget for the machined part into the stiffness optimization of machining fixtures. Recent research in fixturing has increasingly focused on leveraging finite element methods, combined with neural networks and evolutionary algorithms, to optimize fixture layout designs [22]–[25], although these techniques often require time-intensive simulations.

Research on insert positioning variations is limited. Lopatukhin et al. [26] concluded that maintaining an even pressure distribution between the insert and tool holder is critical; failure to achieve this can reduce life expectancy at the cutting edge.

1.2 Scope

This research project aims to develop a methodological framework to assist engineers in the early design phases of indexable cutting tools, ensuring robust positioning of the insert within the tool holder. The framework should preferably consider and address the following elements when analyzing indexable cutting tool interfaces to ensure the formulation of a robust positioning system.

- Non-linear material behaviour
- Surface contact with friction
- External effects such as mechanical and thermal loads
- Transient analysis for operations such as drilling and milling

By fulfilling these requirements and addressing the associated research questions, the project will contribute to the advancement of the three intersecting research domains: Positioning, Variation Simulation, and Metal Cutting Mechanics, thereby bridging the identified knowledge gap illustrated in Fig. 1.1.

1.3 Delimitations

Deformations in the tool body will alter the positioning of the insert, thus changing the macro geometry. Changing the macro geometry will affect the forces generated from the cutting process. In this research, modelled cutting forces are kept constant throughout a simulation. Wear mechanisms on the insert due to the cutting conditions have also been neglected in this thesis. However, future simulation implementations should take consideration to variations in the cutting forces due to the cutting geometry.

1.4 Research Questions

From the introduction two research questions have been defined and will be answered in this thesis. They are as follows:

RQ I *How can external loads be handled in locating schemes for overdetermined indexable cutting tools?*

This research question addresses the issue of overdetermined locating schemes in cutting tools. The external thermomechanical loads can alter the positioning of an indexable carbide insert in the interface of a tool body and affect the overall quality of the cutting tool.

RQ II *How can nonlinear material behaviour be accounted for in variation simulations?*

Current variation simulation methodologies neglect the effect of plastic deformations, as solving nonlinear material behaviours require an iterative approach, which will increase computational time extensively. This research question addresses this issue and aims to incorporate nonlinear material behaviours in variation simulations.

RQ III *How can the insert in an indexable cutting tool be positioned to achieve maximum robustness?*

This research question explores the challenge of maintaining consistent pressure on all contact surfaces during operation and maximizing the robustness with respect to insert movement, as micro-movements of the insert during machining can lead to premature failure.

Chapter 2

Frame of Reference

This chapter will outline the foundation of the theoretical background and frame of reference used in this research project and give an overview of previous research conducted within this research field.

2.1 General Metal Cutting and Classifications

Metal cutting is a manufacturing process that removes excess material as chips from the workpiece. The objective is to get the workpiece to its desired dimensions and surface finish. The cutting edge of a wedge-shaped tool causes the workpiece to plastically deform, forming chips. This process generates large shear strains in the primary shear zone, see Fig. 2.1. There are two main deformation mechanisms associated with the secondary shear zone. The first mechanism is the chip rubbing against the surface of the rake face, generating heat and shear stresses that exceed the material yield limit. The second mechanism is the material flow over the stagnation point[1] that generates shear stresses. Friction between the flank surface of the insert and the machined surface generates shear stresses in the tertiary zone.

A machining system contains three major subsystems: the machine tool, the tool holder, and the cutting holder. A machine tool is a power-operated machine that cuts or shapes materials such as metal and wood. The most common practice is to distinguish machine tools by the type of machining operation they can perform, which are either rotation symmetric (Fig. 2.2(a)) or prismatic (Fig. 2.2(b)) [27]. Rotation symmetrical machines have a rotating workpiece and a stationary cutting tool, while prismatic machines have a stationary workpiece and a rotating cutting tool. However, there are hybrid machines that can both do rotation symmetric and prismatic machining. This allows for more operations per set-up, which reduces both lead time and variations induced by fixturing the workpiece.

The tool holder is the interface that connects the cutting tool to the machine

[1]The stagnation point is where the material meets the edge and either goes over or under it thus generating intense shear stresses.

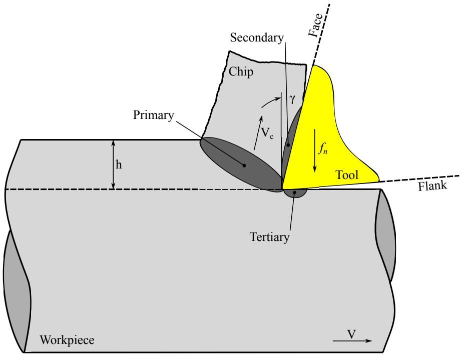

Figure 2.1: Deformation/shearing zones

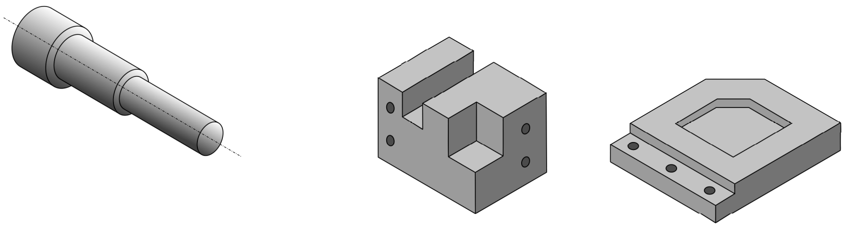

(a) Rotation symmetric (b) Prismatic

Figure 2.2: Machine tool operation classification [27]

tool, see Fig. 2.3. The design of the tool holder is dependent on the application. Tool holders are either made from one solid piece (monolithic) or as a mechanical modular system. Choosing the wrong type for an operation can result in a decrease in quality aspects such as accuracy, repeatability, rigidity and tool life.

The third subsystem is the cutting tool which is either a solid High-Speed Steel (HSS) tool or a cemented carbide tool. HSS tools are preferable for ductile materials and low-speed applications where a sharp cutting edge is required. Solid carbide tools consist essentially of a mix of tungsten and cobalt powder that is compressed in a die to form the tool shape. After that, the tool is sintered[2]. The result is a cemented carbide tool that has enhanced wear resistance and can withstand higher temperatures than HSS tools. This makes cemented carbide more suitable for machining tougher materials such as carbon - or stainless steel.

In this research project, indexable cutting tools are in focus. An indexable cutting tool consists of a tool body with a cemented carbide insert that is fixated on the tool body using either a screw, self-clamping mechanism or some other mechanical clamping mechanisms. The term ”indexable” refers to the interchangeability of the cutting edge (or insert), as an insert can have more

[2]Sintering is a process that uses heat and/or pressure to fuse masses together without reaching the liquefaction point, which is roughly 1400^oC for tungsten/cobalt mix

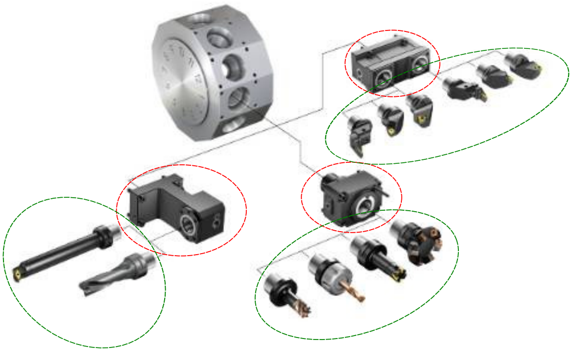

Figure 2.3: Tool holder; Cutting tools

than one cutting edge, Fig.2.4.

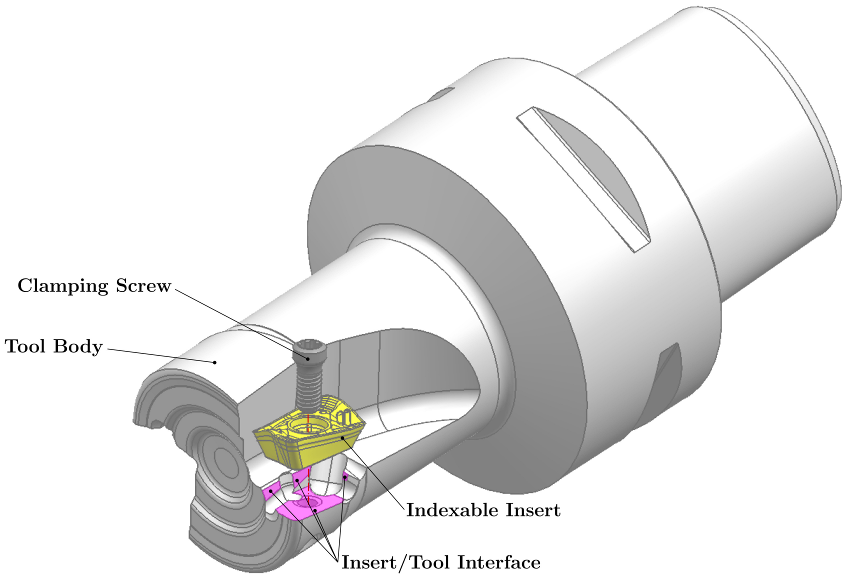

Figure 2.4: Illustration of an indexable cutting tool assembly

2.1.1 Cutting Tool Classification

Cutting tools can be classified in numerous ways. The most common classification is based on the number of cutting edges that are active during an operation: single point, double point and multi-point. Single point cutting tools have only one main cutting edge that is operational during the machining process for turning, boring, slotting, etc . Double point tools have two cutting edges that are active during for example drilling. Multi-point cutting tools have more than two main cutting edges that are active during an operation and that work simultaneously to remove material in a single pass during for example milling, broaching, gear hobbing, etc.

2.1.2 Mechanistic Models to Predict Cutting Forces

There are different approaches to model the cutting process and they can be divided into four categories: analytical, experimental, numerical and mechanistic models. This section will briefly outline the different models to predict cutting forces but will mainly focus on mechanistic models.

Analytical models predict the cutting forces based on physical mechanisms during machining. The models are either based on single shear plane theory [28]–[31], or shear zone theory [32]. However, analytical models do not consider high strain rates, temperature gradients and elasto-plastic material behaviours. This results in analytical models not accurately predicting the general case of machining.

Experimental models rely on empirical measurements and focus on collecting data through static and dynamic cutting tests. This information can be used to calculate cutting parameters to e.g. avoid chatter vibrations [33], which limits the productivity of the machining process.

Numerical models rely mainly on simulations of the cutting process using FEA to predict cutting forces. One of the major challenges within this field is to formulate the material models. Inaccurate material behaviour will give invalid predictions.

Mechanistic models are semi-analytical models that assume that the cutting forces are proportional to the uncut chip area. This means that the models are dependent on the cutting conditions, the cutting geometry and the material properties of the workpiece. These dependencies are referred to as cutting force coefficients or specific cutting forces in the mechanistic models. There are two main approaches to model the mechanistic cutting forces: First-Order Model and Kienzle's Model. For both approaches, the initial step is to conduct force measurements at different feed rates f_n using specialised cutting tools [33]. Both cutting depth a_p and cutting speed v_c are kept constant. The average forces determine the magnitude of the forces during a stable cut, see Fig. 2.5.

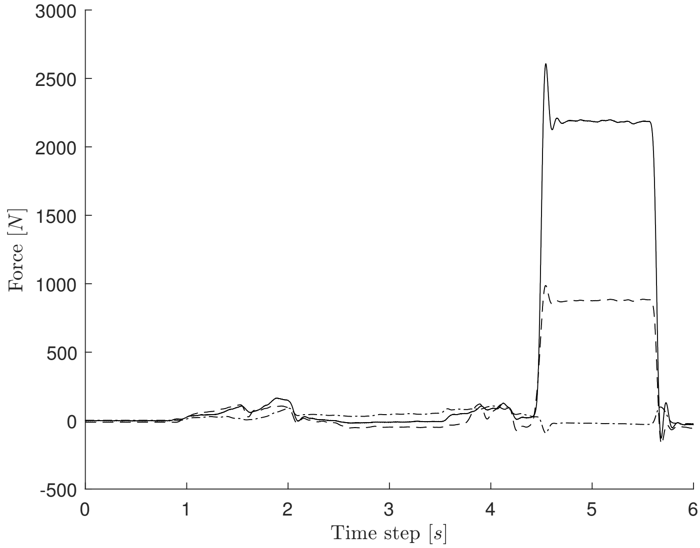

Figure 2.5: Orthogonal turning: — Tangential force (F_t); - - Normal force (F_n); -·- Radial force (F_r)

First-Order Models describe a linear relationship between the normalized cutting force and the uncut chip thickness, such as:

$$\frac{F_q}{b} = K_{qc}h + K_{qe} \tag{2.1}$$

Here, q denotes the cutting force direction, (t)angent or (n)ormal. The variable $h = f_n \sin(\kappa)$ is the uncut chip thickness, $b = \frac{a_p}{\sin(\kappa)}$ and κ is the major cutting angle, see Fig. 2.6. The specific cutting forces K_{qc} and K_{qe} are the only unknown parameters and are determined by the curve fitting equation (2.1) together with force measurements at different feeds (f_n), see Fig. 2.7.

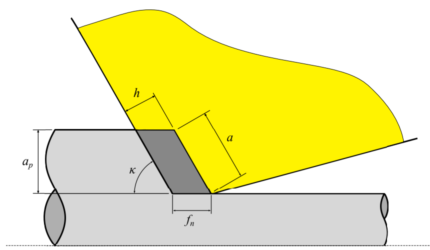

Figure 2.6: Uncut chip area of a sharp longitudinal turning tool (nose radius, $r_e = 0$)

The mechanistic model derived by [34] gives a better prediction for a large variation in chip thickness as the specific cutting forces are dependent on the chip thickness. For lower feed rates Kienzle's model tends to underpredict the cutting forces, while the linear model overpredicts. Therefore, Kienzle's model is most suitable for medium to large feed rates. It takes the effects from strain hardening of the workpiece material, induced in the previous revolution, into consideration. The model is also the most commonly used model to predict cutting forces and cutting energy. Kienzle's model for turning operations is derived as:

$$\frac{F_q}{b} = K_{q1} h^{1-m_q c}, \tag{2.2}$$

here K_{q1} is the specific cutting force at $h = 1$mm. The tool-workpiece dependent exponent, m_q, describes the behaviour of the cutting force in different materials. The specific cutting force and the dependent exponent are curve-fitted in the same way as for the linear model, see Fig. 2.7.

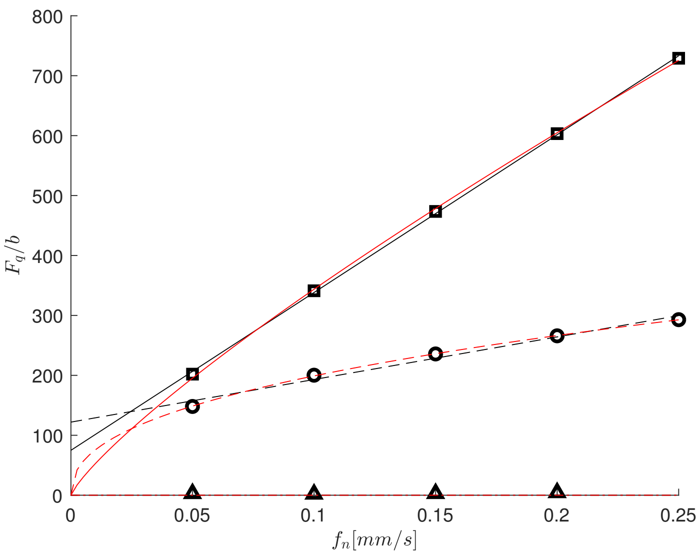

Figure 2.7: **First-Order Model** {— Tangential force (F_t); - - Normal force (F_n); -·- Radial force (F_r)} - **Kienzle's Model** {— Tangential force (F_t); - - Axial force (F_a); -·- Radial force (F_r)} - **Empiric data** {◘ Tangential force (F_t); ⚬ Normal force (F_n); ▲ Radial force (F_r)}

2.1.3 Modified Kienzle's Equation for Milling Operations with Noseradius Compensation

The term Modified Kienzle's equation is a broad concept that encompasses various compensations to enhance model accuracy under different cutting conditions. The applied compensations are most often based on observing physical behaviors of controlled experiments, for example there is a linear relationship between rake angle, γ, and the cutting forces as the tool/chip contact length is altered, increasing the rake angle decreases the cutting forces [35], Fig. 2.9(a).

Increasing the edge radius, e_r, will significantly impact cutting forces at lower feed rates due to the increased height of the ploughing zone. At higher feed rates this effect will be less impactful, Fig. 2.9(b). Therefore, an equation with an exponential component is applied to model the cutting forces. The modified Kienzle's equation with rake angle and edge radius compensation for the k^{th} step can hence be stated as follows:

$$\delta F_t = K_c \delta b h_k^{1-m_c} \tag{2.3}$$
$$\delta F_n = K_n \delta b h_k^{1-m_n} \tag{2.4}$$

compensate nose radius for each discrete area of the uncut chip area, forces in axial and radial direction

$$\delta F_t = K_c \delta b h_k^{1-m_c} \tag{2.5}$$
$$\delta F_r = K_n \delta b \sin(\kappa_k) h_k^{1-m_n} \tag{2.6}$$
$$\delta F_a = K_n \delta b \cos(\kappa_k) h_k^{1-m_n} \tag{2.7}$$

effect of rake angle is retrieved empirically and has a linear effect on the cutting forces

$$\delta F_t = K_c \delta b h_k^{1-m_c} \left(1 - p_c \gamma\right) \tag{2.8}$$
$$\delta F_r = K_n \delta b \sin(\kappa_k) h_k^{1-m_n} \left(1 - p_n \gamma\right) \tag{2.9}$$
$$\delta F_a = K_n \delta b \cos(\kappa_k) h_k^{1-m_n} \left(1 - p_n \gamma\right) \tag{2.10}$$

the effect of the edge radius is retrieved empirically, ploughing etc.

$$\delta F_t = K_c \delta b h_k^{1-m_c} \left(1 - p_c \gamma\right) \left(1 + \frac{h}{e_r}\right)^{m_{er|c}} \tag{2.11}$$
$$\delta F_r = K_n \delta b \sin(\kappa_k) h_k^{1-m_n} \left(1 - p_n \gamma\right) \left(1 + \frac{h}{e_r}\right)^{m_{er|n}} \tag{2.12}$$
$$\delta F_a = K_n \delta b \cos(\kappa_k) h_k^{1-m_n} \left(1 - p_n \gamma\right) \left(1 + \frac{h}{e_r}\right)^{m_{er|n}} \tag{2.13}$$

Where δb is the segment length as a function of the incremental depth of cut (δa_p) and approach angle ($\delta \kappa_k$) and h_k is the uncut chip thickness of the k^{th} segment as a function of immersion angle (Φ_k) and approach angle. The rake angle coefficient is denoted as $p_{(c,n)}$ and $m_{(er,c,n)}$ are the edge radius exponents.

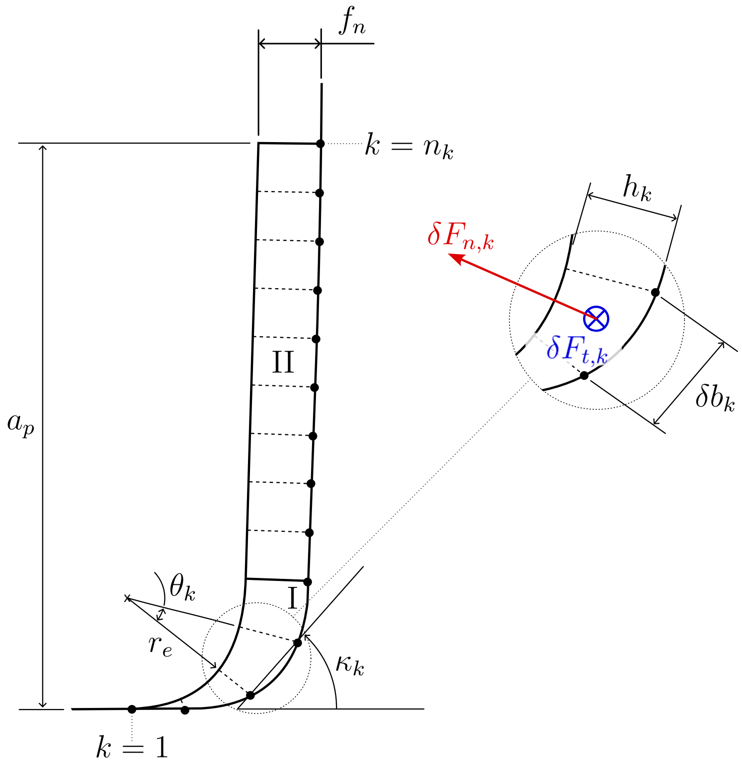

Figure 2.8: discrete, nose radius compensation

$$\delta b = \delta a_p / \sin \kappa_k \tag{2.14}$$

$$h_k = f_z \sin \phi_t \sin \kappa_k \tag{2.15}$$

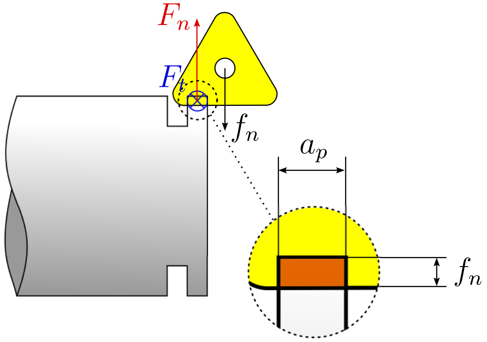

Figure 2.10: Orthogonal turning

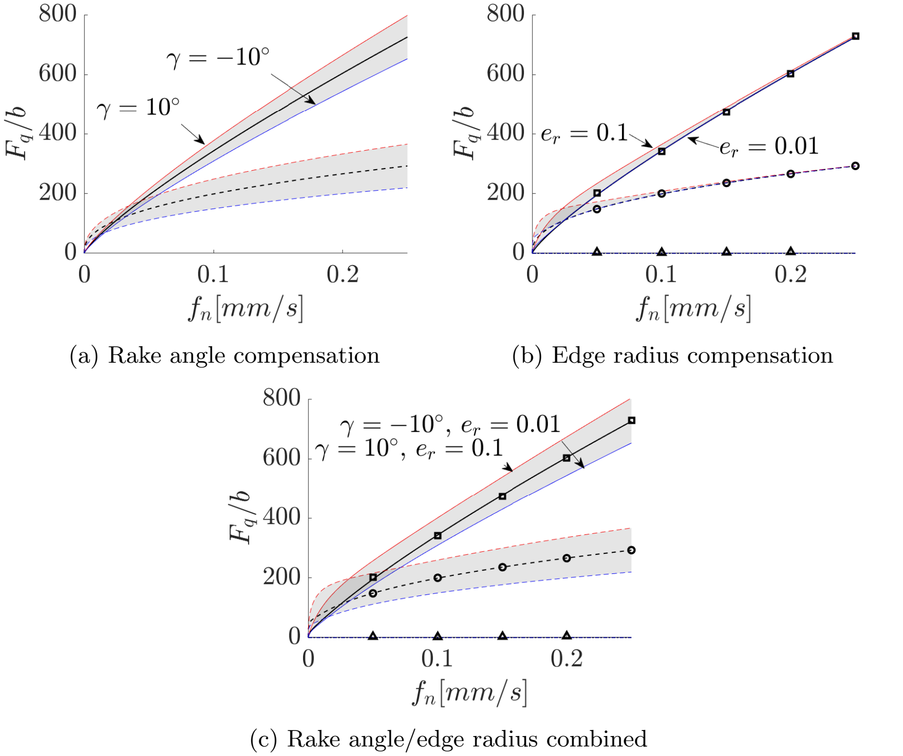

Figure 2.9: Modified Kienzle's Equation, —Nominal (tangential), - - Nominal (feed),—Upper limit (tangential), - - Upper limit (feed), —Lower limit (tangential), - - Lower limit (tangential)

2.2 Quality

The concept and the definition of quality will vary depending on whom you may ask and within what discipline they are active in. Walter Shewhart demonstrated in the late twentieth century that quality needs to be distinguished between measurable and subjective views on quality [36]. Shewhart highlighted that both views were important but the measurable view was more crucial for the producer. The subjective view is based on the customer experience and his or her point of view. However, they are interlinked, within the automotive industry perceived quality is the most important attribute that defines a successful automotive design [37], [38]. A measurable quality aspect within the automotive industry is the flush and gap between adjacent parts of the car body. This will trigger a customer's visual senses and direct their vision towards any inconsistencies of the car body [39].

A more holistic view on quality was presented in the U.S. by Bryne and Taguchi where they state that: "The quality of a product is the loss imparted by the product to the society from the time the product is shipped" [40]. However, Taguchi's view on quality was well-established in Japan during the 60's. What differentiates Taguchi's view on quality from others is that it involves the effect from the society and how poor quality will have an economic impact on the manufacturer. Taguchi presented together with his view on quality a whole concept and philosophy involving methodologies for increasing and analysing quality [41].

Quality could also be divided in two larger groups that consist of both measurable and subjective views on quality, goods and services. The quality concept of goods is presented in Fig. 2.11 and it can be separated into eight dimensions [42]:

- **reliability** measures how often problems occur and how severe they are
- **performance** is a measure on how well functions and key characteristics are fulfilled
- **maintainability** defines the accessibility, detectability and complexity of a problem
- **environmental impact** is the impact of the product on the environment from manufacturing to end-use
- **appearance** refers to the design and colour choices of the product
- **flawlessness** indicates that the product does not have defects or deficiencies at the time of purchase
- **safety** of the product is that it does not cause harm to persons or damage properties
- **durability** determines that the product can be used, stored and transported without being damaged

In this research project, the quality dimensions are viewed from a metal cutting perspective in the machining industry. The quality dimensions that are emphasized are durability, reliability and performance.The mentioned three dimensions are strongly correlated with each other, meaning the performance will affect the durability of the cutting tool [43]. The main effects for each quality dimension for cutting tools are presented in Fig. 2.12.

2.2.1 Durability

As mentioned before, the investigated quality dimensions within the metal cutting industry are correlated. Setting up a machining process involves determining the cutting speed, feed rate and cutting depth, which are dependent on the cutting geometry. In an optimized machine process, the durability is typically dependent on insert grade and coating. Meaning, the expected tool life or durability of a cutting tool is dependent on the wear rate and is only controllable by the coating and the grade of the cemented carbide.

In the concept and design phase of new cutting tools there are numerous controlled experiments. The experiments determine the cutting tools expected

Figure 2.11: Quality of goods

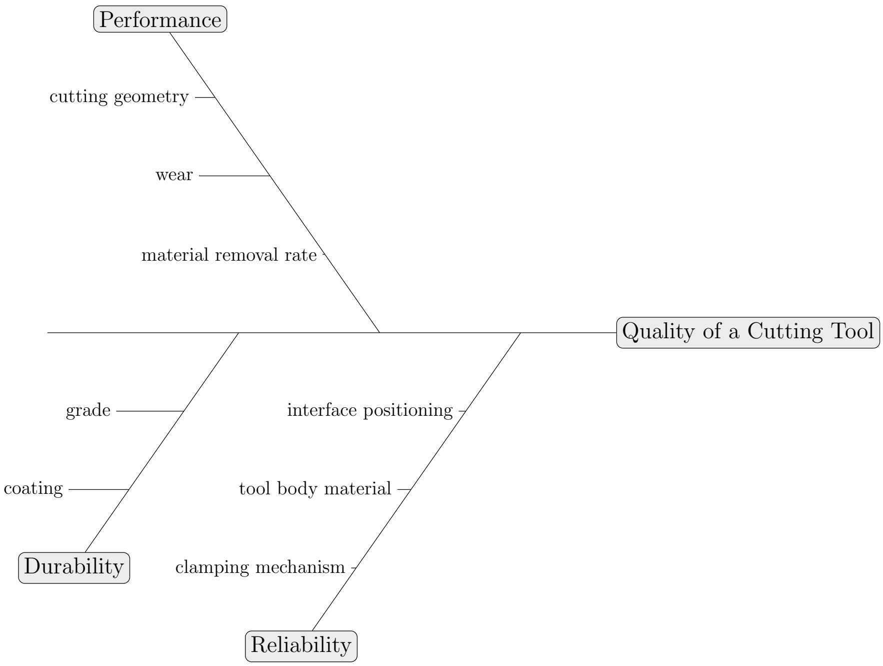

Figure 2.12: Cause and effect diagram of quality dimensions in cutting tools

tool life, performance and the optimum machine process parameters. As a new design is determined, it undergoes numerous on-site experiments to acquire relevant information that was left out during the controlled experiments. Deviations in the cutting tool interface are not considered and critical failures due to deviations in the interface are typically caught once the product is commercially available.

2.2.2 Reliability

Reliability is the cutting tool's ability to reproduce a consistent result, such as surface finish, throughout its tool life. Also, a carbide insert has a lower life expectancy than the tool body. For consistency, switching inserts should not affect the dimensional accuracy, the durability or the performance of the cutting tool.

The main affecting factors on the reliability of cutting tools, in this research project, are interface positioning, tool body material and the clamping mechanism. The tool body material will determine how much the interface plastically deforms, altering the interface positioning for the current insert and future inserts. The stiffness of the clamping mechanism determines the resistance to position changes during a cutting operation. However, too stiff clamping will break the insert.

2.2.3 Performance

The performance of a cutting tool is determined by its capabilities of productively removing metal from the workpiece. The assessment of performance also often involves an estimate of work spent determining optimum cutting conditions to avoid degenerative vibrations, also to increase the metal removal rate.

As mentioned, the main benchmark of the performance quality dimension is the metal removal rate. The metal removal rate is however dependent on the cutting geometry, as it determines the required feed rate and cutting depth for the machining process. The process parameters are set prior to the machining operation and in this research project, the cutting geometry is assumed to change during a cutting operation. Therefore, the cutting geometry is considered to be the main impacting factor on the performance quality dimension.

2.3 Locating Scheme

Locating schemes, or positioning systems, are used to: fixate parts during manufacturing operations, assemble multiple parts and lock parts for inspection. Variations induced by the fixture on the finished product need to be controlled to ensure that the product is within specified tolerances [3].

The most common locating scheme in various industries is the $3-2-1$ locating scheme for rigid assemblies or parts [3], see Fig. 2.13. A rigid part has six degrees of freedom that determine its position and orientation in space.

To lock all six degrees of freedom the part needs: three points $(A1, A2, A3)$ to describe a plane and thus locking the R_x, R_y, T_z[3] degrees of freedom, two points $(B1, B2)$ to describe a line and thus locking the R_z, T_x degrees of freedom and one point $(C1)$ to lock the last degree of freedom T_y.

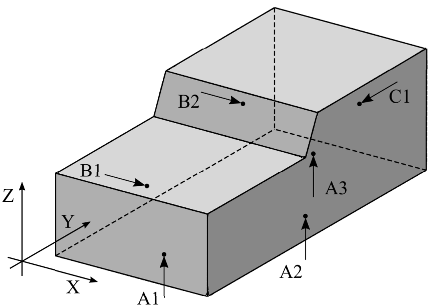

Figure 2.13: 3-2-1 Locating scheme for rigid parts

An issue with the $3-2-1$ positioning system is that it only applies to rigid parts and assemblies. This gives a poor correlation to reality as no parts or materials have infinite stiffnesses. To incorporate flexibility in the positioning system [4] presented the $N-2-1$ for compliant assemblies, especially to fixate sheet metal assemblies. In [5] the authors expanded the positioning systems further by incorporating orthogonal and non-orthogonal systems. Orthogonal positioning systems have all locator directions orthogonal to each other.

In the machining industry, much research has been conducted in order to optimize the fixture-workpiece design. Early research concluded that fixture-workpiece design within machining requires high stiffness of the locators to minimize dimensional errors caused by the machining processes [18]–[20]. Hurtado and Melkote presented an analytical contact elasticity model in order to predict the normal and the tangential reaction forces on the locators during machining for $3-2-1$ locating schemes [44]. This allows for the possibility to optimize fixture designs for machining processes to minimize its effect on dimensional errors caused by the fixturing of the workpiece. Hurtado and Melkote improved upon this concept by including stiffness optimization based on the specified tolerance limits of the machined part [21].

2.4 Variation Simulation

Variation simulation is a terminology for tools and methods used to calculate statistical variation on assembly level. Predicting the variation in the final product can ensure that the functional, aesthetic and assembly requirements are fulfilled. In this section, variation simulation methods used within this research are presented. The common denominator for all variation simulation methods is to simulate how the tolerances accumulate. Different approaches can be taken to model how tolerances accumulate through an assembly, each

[3] $R_{x,y,z}$ - Rotation around the x, y, z-axis; $T_{x,y,z}$ - Translation in the x, y, z-direction

with certain advantages and disadvantages [1]. The earliest models to predict the tolerance sum are Worst Case (WC) and Root Sum Squares (RSS) [45]. The WC model is based on the assumption that all component dimensions will occur simultaneously at their lower or upper bound limit. A problem that will occur with WC models is that the component tolerances will be reduced significantly as the number of components increases in an assembly, thus increasing the manufacturing cost for each component. The RSS model is a statistical model that allows for larger component tolerances compared to the WC model as it accumulates with the root sum squared. The WC model is described using the following equation:

$$dU = \sum \left(\left| \frac{\partial f}{\partial X_i} \right| T_i \right) \leq T_{asm} \tag{2.16}$$

Here, dU is the predicted assembly variation and $f(X_i)$ is the assembly function that describes the tolerance sum, such as gap or flush, as a function of the nominal component dimension X_i. T_i is the component tolerances and the tolerance sum limit is T_{asm}. The RSS model is described using the following equation:

$$dU = \left[\sum \left(\frac{\partial f}{\partial X_i} \right)^2 T_i^2 \right]^{\frac{1}{2}} \leq T_{asm} \tag{2.17}$$

Even though each component is within its dimensional specifications the accumulated tolerance sum may not be. Also, the interchangeability of components can be affected by poorly designed component dimension tolerances. A crucial step in tolerance analysis, is to determine the assembly function $f(X_i)$, which describes how each tolerance specification in a design affects the tolerance sum. The most common practices in tolerance analyses are tolerance chain loops (TCL), see Fig. 2.14. Relevant linear dimensions that stack in an assembly are represented as vectors for components that mate [46]–[48]. The TCL approach can be used for one-, two -and three-dimensional assemblies where the complexity of building the loops increases with the dimensions. An example for a 1D stack-up can be seen in Fig. 2.14 where the clearance gap, G, is of interest and can be described using the actual dimensions $L_1, \ldots, L_4$:

$$G = L_1 - L_2 - L_3 - L_4 \tag{2.18}$$

However, the actual dimensions $L_1, \ldots, L_4$ can vary from their nominal values $\lambda_1, \ldots, \lambda_4$ in such ways that the constraint on the clearance gap is not satisfied, $G < 0$. The main objective is to obtain a clearance gap that is non-negative and not too large. To this extent the gap is quantified as $G - \gamma$ where γ is the nominal clearance gap. Equation (2.18) can therefore be reformulated as:

$$G - \gamma = (L_1 - \lambda_1) - (L_2 - \lambda_2) - (L_3 - \lambda_3) - (L_4 - \lambda_4) \tag{2.19}$$

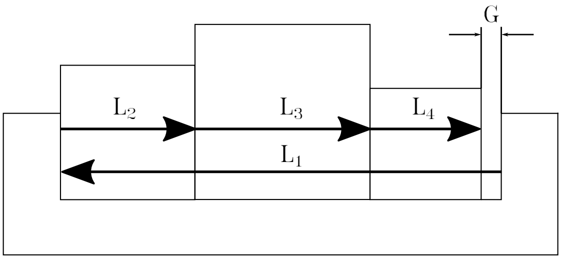

Figure 2.14: Example: 1D stack-up

A more generalised form of (2.19) is given by:

$$f(X_i) = G - \gamma = \sum_{i=1}^{N} a_i (X_i - \lambda_i) \tag{2.20}$$

Here X_i is the measured value of the i^{th} component in an assembly with N components. The effect and the direction of the stack-up are given by the coefficient a_i. In the given example the coefficients are $a_1 = 1, a_{2,\ldots,4} = -1$. It should be noted that the assembly function can be any black-box function that describes an input-output relation. For more complex assemblies it may prove to be difficult to apply conventional stack-up methods, and new approaches for complex non-trivial contacting interfaces may be needed.

2.4.1 Non-rigid Variation Simulation of Sheet Metal Assemblies

Variation simulation of deformable, i.e. non-rigid, sheet metal assemblies is a common industrial application of variation simulation. Here the material model is typically assumed to be within the elastic region of its material properties. The desired output is to calculate or predict the spring-back variation after the assembly of two or more sheet metal plates. The most common approaches for this use Method of Influencing Coefficients (MIC) [2] or Direct Monte Carlo Simulations (DMCS).

The DMC approach is straightforward and calculates the spring-back variation by using FEA. The first step is to add deviations to the nominal part. The second step is to clamp the parts to its nominal positions in a fixture using FEA thus forming the unwelded assembly. The third step is to weld the parts together and is calculated using FEA. This will also change the overall stiffness of the assembly which will affect the spring-back once the clamps of the welded assembly are released in the fourth step. However, this approach is time-consuming and requires the algorithm to call for an FE-solver twice during one simulation step and numerous iterations are required in order to gather any statistical data of the spring-back variations.

To this extent, [2] proposed an approach using MIC where a linear relationship is formed between part deviations and the spring-back deviations of the spot welded assembly. The sheet metal assembly and plates are assumed to be within the linear region of the material properties. This gives that the forces required to clamp the unwelded assembly are equal to the forces generated due to the spring-back of the welded assembly.

$$F_w = F_u \iff K_w U_w = K_u V_u \tag{2.21}$$

Here, F_w and F_u are the forces required to clamp the assembly and the forces generated from the spring-back. K_w is the assembled stiffness matrix of the welded structure and K_u is the unwelded stiffness matrix of each individual part. Spring-back deviations are given by U_w and the part deviations by V_u [2]. By simple linear algebra, the relationship between spring-back deviations and part deviations can be found as:

$$U_w = K_w^{-1} K_u V_u = S_{wu} V_u \tag{2.22}$$

Here, S_{wu} is referred to as the sensitivity matrix. This approach will require that FEA is performed to calculate the stiffness matrices. However, since the behaviour of the assembly processes is assumed to be linear, the stiffness matrices only need to be calculated once to form the sensitivity matrix. Then, the only form of variations that can occur are part deviations generated from the forming process and the fixturing of the sheet metal parts. The MIC approach allows for a great reduction in CPU time compared to DMCS where the full FEA model is solved at each randomly generated disturbance.

The MIC methodology within variation simulations laid the basis for continued development of the methodology and the field of variation simulations. Robustness evaluation and locating schemes for variation simulations was presented by creating a variation simulation software RD&T [3]. An approach of implementing a contact search algorithm in the MIC methodology to avoid penetration of contacting surfaces was presented by [6]. The implementation shows great significance in reducing computational time with limited loss in accuracy.

2.4.2 Meta-Model

A meta-model is a model of a model and is not bound to any specific type of field. Typically within engineering, it is a simplified model of a complex physical behaviour. In this section, the meta-modelling process that has been used within this thesis project is presented. The conducted research is based on finite element simulations, where meta-models are used to simulate variations of the controllable parameters in order to reduce the simulation time for variation simulations. The meta-model describes the relationship between geometric deviations and stress magnitudes of each individual node on the tool-body interface. The problem definition defined earlier states that the interface is over-determined, meaning that the contact locations will vary depending on the input. As a result, the stress magnitudes for the nodes will exponentially decrease or increase depending on the geometric deviation. The issue is resolved by forcing the response in each node to be linear by taking the logarithm of the response. This gives the general function that is used to model the impact of geometric deviations on contact location in the interface of cutting tools.

$$\ln(\mathbf{Y}_i^{(s)}) = \boldsymbol{\beta}_0^{(s)} + \sum_{j=1}^{r} \boldsymbol{\beta}_j^{(s)} \mathbf{X}_{i,j}^{(s)} + \epsilon_i^{(s)}, \quad \text{for } i \leq r \tag{2.23}$$

The nodal response, $\mathbf{Y}^{(s)} \in \mathbb{R}^{r \times n^{(s)}}$, is, as mentioned, logarithmic where r is the number of design points or observations and $n^{(s)}$ is the number of nodes for the surface s. The matrix $\mathbf{X} \in \mathbb{R}^{r \times (1+m)}$ is a matrix containing all terms of a polynomial with an arbitrary[4] order where m is the number of independent variables, and a column of ones to give the β_0 terms for each observation. The matrix $\boldsymbol{\beta}^{(s)} \in \mathbb{R}^{(1+m) \times n^{(s)}}$ is a matrix of the coefficients in the meta-model and $\epsilon^{(s)} \in \mathbb{R}^{r \times n^{(s)}}$, defined by $\epsilon^{(s)} = \mathbf{Y}^{(s)} - \hat{\mathbf{Y}}^{(s)}$, is the matrix of residuals between the true response and the predicted response [49]. The model is then fitted by using least squares and finding the minimum vertical distance between the data points and the polynomial line.

2.5 Design Optimization

Design optimizations can be divided into two sub-groups, deterministic or probabilistic, referring to the constraints of the problem definition. A deterministic approach does not take consideration to any production or manufacturing uncertainties that exist, [50], [51]. This means that the most probable point (MPP) is most likely at a peak or a valley depending on the problem definition. A general deterministic constrained minimization problem with an objective function $f(\mathbf{x})$ can be formulated as:

$$\begin{aligned} &\min_{\mathbf{x}} \; f(\mathbf{x}) \\ &\text{subjected to} \; \begin{cases} g(\mathbf{x}) = c \\ h(\mathbf{x}) \geq d \end{cases} \end{aligned} \tag{2.24}$$

Here, $g(\mathbf{x})$ is called an equality constraint, $h(\mathbf{x})$ is called an inequality constraint and the constants c and d are arbitrary deterministic values or limits. By finding the MPP at a peak or valley in a sensitive system, any uncertainties in the input variables $\mathbf{x}$ can have a significant impact on the response $f(\mathbf{x})$ and all industrial applications have uncertainties.

Probabilistic optimization methods can be further separated into two groups, robust design optimization (RDO) and reliability based design optimization (RBDO). Robust design optimization aims at finding a local optimum that is insensitive to noise. This is most commonly done by adding variations to the input variables $\mathbf{x}$ for a found deterministic optimum. The second probabilistic approach, RBDO, uses probabilistic constraints instead of deterministic

[4] The order of the polynomial is determined for each case study separately

constraints to take account for any uncertainties on x by finding an optimum design at a sufficient distance[52]–[56] from the deterministic optimum, see Fig 2.15.

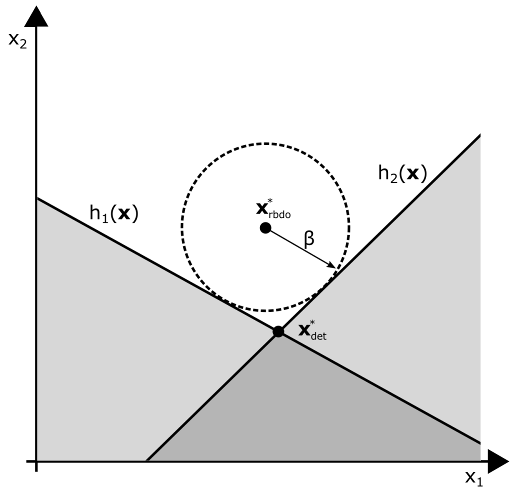

Figure 2.15: Deterministic optimum $\mathbf{x}^*_{det}$, probabilistic optimum $\mathbf{x}^*_{rbdo}$

The general RBDO problem definition can be written as:

$$\begin{aligned} &\min_{\mathbf{x}} \; f(\mathbf{x}) \\ &\text{subjected to } \begin{cases} P_f[h(\mathbf{x})] \geq 0 \\ \mathbf{x}^l \leq \mathbf{x} \leq \mathbf{x}^u \end{cases} \end{aligned} \tag{2.25}$$

Here, $P_f[h(\mathbf{x})]$ is the reliability constraint and can be formulated as:

$$P_f[h(\mathbf{x})] = P_{allow} - p_f \tag{2.26}$$

Here, p_f is failure limit of the system and P_{allow} is the allowable probability of failure and is estimated using various approaches such as the first order reliability method, which is used in this research project for its capabilities and robustness of approximating the reliability.

2.5.1 First Order Reliability Method (FORM)

FORM is a method to predict the reliability of a system by approximating the probability integration of the joint probability density function. The definition of reliable in FORM is that the probability of the performance function $g(\mathbf{X})$ being greater than zero [57], $P\{g(\mathbf{X}) > 0\}$ where $\mathbf{X} = (X_1, X_2, \ldots, Xn)$ are the normally distributed random variables. It can also be seen as the stable region, while $P\{g(\mathbf{X}) < 0\}$ is the unstable region, or failure region. The performance function, $g(\mathbf{X})$, is a black-box model which can be built using various kinds of data. These models often involve higher dimensions, which may mean that a direct evaluation of the probability integration of failure

$$p_f = P\left\{g(\mathbf{X}) < 0\right\} = \int_{g(\mathbf{X})<0} f_x(\mathbf{x})\mathrm{d}\mathbf{x} \tag{2.27}$$

can prove very difficult to solve. Here $f_x(\mathbf{x})$ is the joint probability density function of $\mathbf{X}$. Using FORM or other approximation methods, the probability integration can be approximated with good coherence. The derivation of FORM is divided into two basic steps [57]:

1. Simplify the integrand

2. Approximate the integration boundary

By simplifying the integrand the random variables in the original space, X-space are transformed, using the Rosenblatt transformation [58], to the U-space. The U-space is a standard normal space with a mean of 0 and a standard deviation of 1.

$$U = \Phi^{-1}\left[F_x(X)\right] = \Phi^{-1}\left[\Phi\frac{X-\mu}{\sigma_{std}}\right] = \frac{X-\mu}{\sigma_{std}} \tag{2.28}$$

By transforming to the U-space, the contours of the integrand become concentric circles without any loss of accuracy. This provides a probability integration that is less complicated to solve than in the original, X-space.

The joint probability density function (pdf) in the U-space is the product of each individual pdf of the normal standard distribution, due to the fact that the random variables are independent. The probability integration of failure in the transformed U-space becomes

$$p_f = \underset{g_(u_i)<0}{\int\cdots\int} \prod_{i=1}^{n} \frac{1}{\sqrt{2\pi}} \exp\left(-\frac{1}{2}u_i^2\right)\mathrm{d}u_i, \quad i \in n. \tag{2.29}$$

To simplify the integration boundary further, the performance function for the integration boundary, $g(\mathbf{U}) = 0$, is approximated using first-order Taylor expansion.

$$g(\mathbf{U}) \approx \mathbf{u}^* + \nabla g(\mathbf{u}^*)(\mathbf{U} - \mathbf{u}^*)^T \tag{2.30}$$

This allows that the following optimization problem can be formulated:

$$\begin{aligned} &\min_{u} ||\mathbf{u}|| \\ &\text{subject to } \; g(\mathbf{u}) = 0 \end{aligned} \tag{2.31}$$

By solving the optimization formulation given in (2.31), one will find the MPP, u^*. The MPP describes the minimal Euclidean distance from a starting point to the limit state $g(\mathbf{U}) = 0$. The reliability or the probability of failure are given in each iteration i as.

$$\Phi(-\beta_i) = \Phi\left(-\left[\beta_{i-1} + \frac{\nabla g}{||\nabla g||}\right]\right) \tag{2.32}$$

Here Φ is the normal cumulative density function. A FORM based approach will only find the closest point to the linearized limit-state function based on its starting origin point, design point, in the standard space. However, more than one design point may exist that satisfies the limit-state function and other constraints. To handle the existence of multiple design points a ”bulge” or a restricted area is created around a found solution, and integrated it into the limit-state function as [59]:

$$g_{m-1}(\mathbf{u}) = g_{m-2}(\mathbf{u}) + B_{m-1}(\mathbf{u}) = g(\mathbf{u}) + \sum_{i=1}^{m-1} B_i(\mathbf{u}) \tag{2.33}$$

Here B_i is the ”bulge” of the i-th design point. This continues until all the m design points are found.

2.5.2 Genetic Algorithm

Genetic Algorithm (GA) is based on evolutionary progress by slowly, gradually improving its population; it is also a stochastic optimization approach, meaning that variables are randomly generated and use a randomized search method, which can improve issues such as converging to a local optimum. The standard GA approach has eight steps: 1) creating a starting population, Fig. 2.16, of binary individuals (chromosomes). 2) For numerical interpretations of the individuals, it can prove beneficial to use Gray code encoding to allow for incremental changes. For example, to go from a value 5 (101) to 6 (110) in binary would require both the first bit (gene) and the second bit to mutate; in Gray code, this translates to (111) $\rightarrow$ (101), which means that only the second bit needs to mutate from 1 to 0 for an incremental increase from 5 to 6.

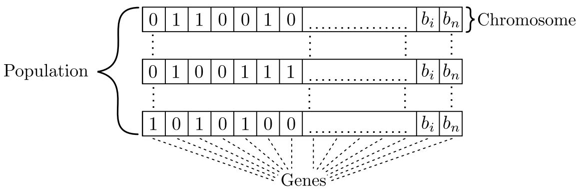

Figure 2.16: Genetic Algorithm Population

3) The goodness of the chromosome is evaluated with a fitness function, describing how well it fits with the sought-after output. Once the population

evaluation process is finished, the selection process starts; a common approach is using a 4) random tournament selection, where two individuals are selected randomly and chosen to "mate" to produce new individuals by randomly selecting a 5) crossover point and exchanging a part of their chromosome with each other, Fig. 2.17. Once the whole population has mated, a 6) mutation process starts; each gene in the chromosome has a chance to mutate, changing its 0 to 1 and vice versa; a typical mutation rate is 5%. 7) The individual with the highest fitness score from the evaluation process is inserted into the modified population, and this step is referred to as Elitism; this helps with maintaining a direction for the optimization process, but it can also increase the likeliness of finding local optimums. 8) The last step is to generate a new population for the next generation, and the evolutionary process starts again.

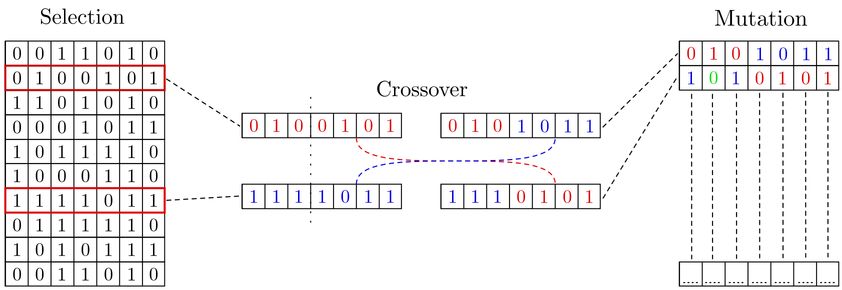

Figure 2.17: Genetic Algorithm Tournament-Crossover-Mutation

2.5.3 Desirability Function

A common approach for multiple response optimization routines is to use the desirability function methodology as an objective function. The method is conceptualized by [60] for use in the quality aspects of a product with multiple quality characteristics. The authors [61] expanded the methodology further. They introduced two desirability function types, one-sided (smaller-the-better (STB) 2.34, larger-the-better (LTB) 2.35) for either minimum or maximum and two-sided (nominal-the-better (NTB) 2.36) for nominal is the best type of problem statement.

$$d_{STB}(x) = \begin{cases} 1, & y(x) < y_{min} \\ \left(\frac{y(x)-y_{max}}{y_{min}-y_{max}}\right)^s, & y_{min} < y(x) < y_{max} \\ 0, & y(x) > y_{max} \end{cases} \tag{2.34}$$

$$d_{LTB}(x) = \begin{cases} 0, & y(x) < y_{min} \\ \left(\frac{y(x)-y_{min}}{y_{max}-y_{min}}\right)^s, & y_{min} < y(x) < y_{max} \\ 1, & y(x) > y_{max} \end{cases} \tag{2.35}$$

$$d_{NTB}(x) = \begin{cases} 0, & y(x) < y_{min} \\ \left(\frac{y(x)-y_{min}}{y_{nom}-y_{min}}\right)^{s}_{1}, & y_{min} < y(x) < y_{nom} \\ \left(\frac{y(x)-y_{max}}{y_{nom}-y_{max}}\right)^{s}_{2}, & y_{nom} < y(x) < y_{max} \\ 0, & y(x) > y_{max} \end{cases} \tag{2.36}$$

The methodology converts and normalizes a function response to a subset where $y(x) \longrightarrow d(x) \in (0,1) \subset \mathbb{R}$ by setting simple limits to the responses where a function $d(x) \longrightarrow 1$ is nearing its target value, and $d(x) \longrightarrow 0$ when it is moving away from its target. The exponent $s_i \in (0.1, 10) \subset (R)$ is the weighting parameter and determines the rate at which the function grows towards the limit, see Fig.2.18.

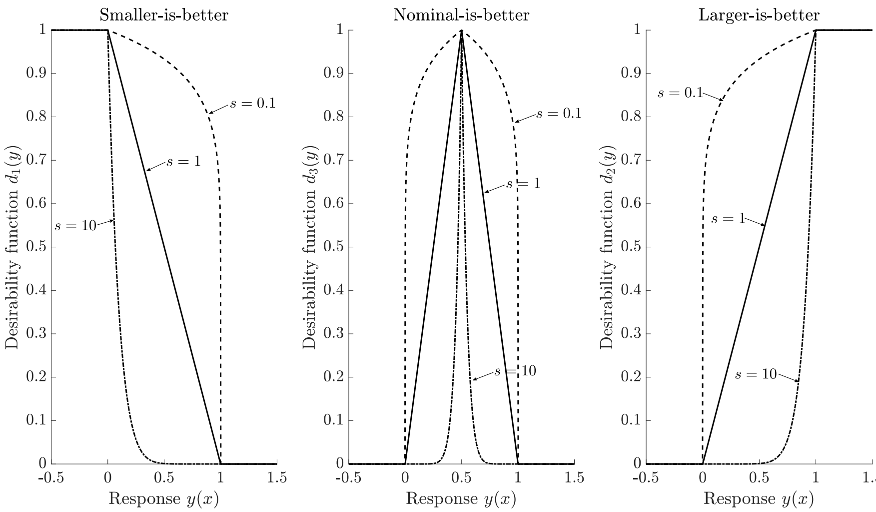

Figure 2.18: Desirability functions

For a given set of n_d multiple desirability functions $\{d_1, d_2, \ldots, d_{n_d}\}$, the overall desirability is calculated by using the geometric mean:

$$D = \prod_{i=1}^{n_d} d_i(x) = (d_1 d_2 \dots d_{n_d})^{\frac{1}{n_d}} \tag{2.37}$$

The objective of the optimization process is to find a set of independent variables, x, that maximize the overall desirability 2.37. It is important to note that the overall desirability does not necessarily go to 1 as it depends on the limit constraints. The overall desirability does not have any physical meaning, e.g., if $D(x_1) > D(x_2)$, then x_1 is a better design point than x_2 [62] and two different models are incomparable to each other.

2.6 Research Approach

This chapter briefly outlines different approaches for conducting quantitative research, mainly describing Mitroff's quantitative research cycle which was used within this research project.

2.6.1 Qualitative and Quantitative Research

Scientific research is distinguished between two sub-groups, qualitative and quantitative research. Qualitative research approaches focus particularly on discovering underlying meanings and interrelating phenomena and entities, without involving mathematical modelling. Quantitative research methodologies use statistics, mathematical or computational techniques on empirical observations, to form theories or draw conclusions. Even though there is a clear distinction between the two research methodologies, they are not inseparable. For example, case research can often combine both qualitative and quantitative methods in its research design. A method in this sense refers to the technique of data collection and analysis rather than how data is interpreted and presented. Meredith et al. proposed a generic framework for the classification of a research method [63]. The framework is not intended to guide a researcher to choose what method to use, e.g. case study or action research, but to visualize the paradigmatic influence upon different methods [64].

2.6.2 Methods and Methodologies in Quantitative Research

Methods, as mentioned, are the tools or techniques that we use in order to collect data for the research. A methodology is how we conduct our research. Quantitative model-based research is quantified according to [63] as a rational knowledge generation method. This is based on the assumption that it is possible to construct objective models that describe operational processes. Relationships between the variables are described as causal, which indicates that a change of a in a variable x will lead to a change of $f(a)$ in another variable y. For causal and quantitative relationships it is possible to predict future states of the modelled process rather than being bound to the observations made. This requires all claims that are made within the modelled process to be unambiguous and verifiable. Quantitative modelling can therefore be categorized into two classes: axiomatic quantitative modelling research and empirical quantitative modelling research. Axiomatic research is primarily driven by an idealized model [64]. Idealized models will tend to simplify the problem to such an extent that relevant information could be lost. For empirical research, the main issue of the practitioner is to make certain that there is coherence between a model and observations from reality or simulations. Empirical research can be both descriptive and prescriptive. Descriptive empirical research mainly aims at creating a model that sufficiently describes the causal relationship. Prescriptive empirical research tends to create policies, strategies and actions to improve the processes. In this research project, a prescriptive empirical research approach is conducted to create a framework with a set of tools to handle robust positioning of cutting tool interface designs.

2.6.2.1 Mitroff's Model

Mitroff and Sagasti presented a research methodology for studying science from a holistic or systems point of view in [65], [66] because anything less will fail to pick up certain aspects of science's most essential characteristics [66]. This is one of the earliest contributions to the field of quantitative research methodologies. The model is referred to as the Mitroff's Cycle, see Fig.2.19. The model consists of four phases (**I**) conceptualization, (**II**) modelling, (**III**) model solving and (**IV**) implementation.

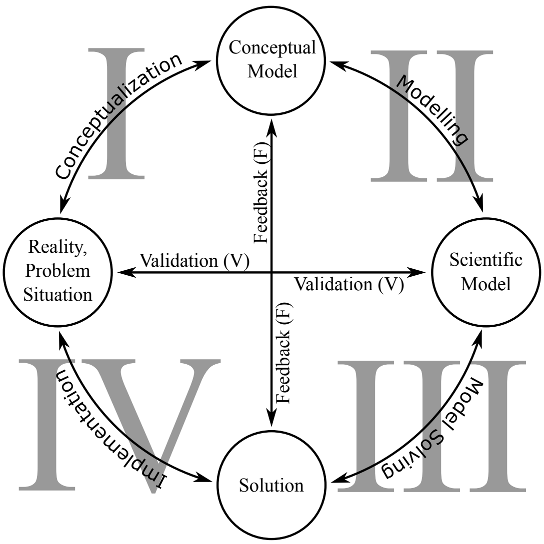

Figure 2.19: Mitroff's Cycle [66]

The conceptualization phase consists of the researcher building a conceptual model of the system of interest. This usually specifies which variables should be addressed and the aim and scope of the model. Previous studies and literature reviews are often used to build upon. In the modelling phase the quantitative model is built which defines the causal relationships between the independent variables. In the next phase, the model is solved and finalized by implementing its results in the implementation phase. However, Mitroff et al. state that a research cycle can begin and end in any of the four phases if the practitioner is aware of the conclusions that can be made based on the results of the research. Mitroff et al. also discuss the shortcuts, (**F**) narrow feedback and (**V**) validation, which practitioners can use and which are often applied in research projects. This tends to lead to less desirable research designs. The authors also adress the **II-III-(F)** cycle that many practitioners following the cycle tend to mistake the model solving phase for implementation of the model. Also, practitioners following the **I-(F)-IV** cycle tend to misinterpret conceptualization for modelling. The Mitroff's cycle is an essential tool to identify methodological paths that certain work follow in order to relate the validity of the claims that were made.

Axiomatic research can, as empirical, be both descriptive and prescriptive. For axiomatic descriptive (AD) research, the central part of the cycle is the modelling. The practitioner most often takes a conceptual model from literature and creates a scientific model of it. Typically in axiomatic descriptive research, the practitioner does not move to the model solving phase thus giving a **I-II-(V)** cycle. However, for axiomatic prescriptive (AP) research, the practitioner enters the model solving phase, which will lead to the practitioner taking the narrow feedback shortcut. The results of the model are then feedback to the conceptual model, which can be confused with implementation. This is often mistaken for implementation and most often claims are made in that sense [64].

The typical empiric descriptive (ED) research practitioner tends to follow a **I-II-(V)** and is someone who is over-concerned with the validation of the model [66]. For example, the practitioner is trying to overfit the model with respect to reality. This typically leads to a noisy model that only describes the observations made. Empiric prescriptive (EP) research usually follows the complete cycle, **I-II-III-IV**, and in many cases, empiric prescriptive research is based on earlier published research from the axiomatic descriptive research approach [64].

2.6.3 Verification and Validation

The definition of verification and validation varies and is dependent on the subject. In this research, the objective is to create a functional framework that employs multiple simulation models to analyze tolerance in cutting tool tip seat designs.

From a manufacturing perspective, [67] states that verification defines how the model corresponds to its specifications and defines validation as to how well the model describes its intended purpose. The following questions are stated by [67] to clarify the definitions further. **Validation:** Are we building the right product? **verification:** Are we building the product right?

Verification and validation of simulation models are slightly different in definition. The authors in [68] state that model verification is to ensure that the programmed model and its implementation are correct. Model validation ensures that a model holds a satisfactory range of accuracy for its intended field of application [68]. When developing a model it has to be for a specific purpose or application. The validity of the model is therefore determined depending on its purpose. If a model has to answer multiple questions, then the validity needs to be determined for each question [68].

[69] presents a simplified version of the model development process (MDP) in Fig. 2.20, based on standards set by [70]. The MDP involves three main phases:

- **Problem entity** is the phenomena to be modelled.
- **Conceptual model** is the mathematical/logical/graphical representation of the problem entity and is developed through analysis and modelling.
- **Computerized model** is the conceptual model implemented on a computer.

For each step in the MDP, it is possible to relate model verification and validation, dashed lines in Fig. 2.20. Conceptual model validation establishes that the assumptions and hypotheses underlying the conceptual model are correct and reasonable for the intended purpose of the model. The conceptual model validation process typically involves ensuring that assumptions on, for example, linearity and variable reductions are correct. Computerized model verification is to ensure that the implementation and programming of the conceptual model are correct. An example of computerized model verification can be ensuring that adding variation to the mesh in an FEA will not cause surface penetrations between contacting surfaces. Operational validation refers to the process of establishing that the response of the model is within a satisfactory range of accuracy for the intended purpose of the model. Operational validation can be performed for both observable system and non-observable systems. The creator of the model needs to decide what approach is required, subjective or objective, for operational validation of the system, see Tab. 2.1 [68], [69].

Table 2.1: Operational validity classification [68]

Decision approach	Observable system	Non-observable system
Subjective	- Comparison using graphical displays	- Explore model behaviour
	- Explore model behaviour	- Comparison to other models
Objective	- Comparison using statistical tests and procedures	- Comparison to other models using statistical tests

Data validity ensures that any data, such as material models, are sufficient and correct. Data validity is typically not considered due to the fact that it is usually difficult, time-consuming and costly to obtain appropriate, accurate and sufficient data [68]. Verification and validation of the framework presented in this research mainly focus on the outer circle of Fig. 2.20, conceptual model validation and computerized model verification. Operational model validation is neglected as the system is non-observable, and therefore it is not likely to obtain a high confidence in the model. The overall validity of the results is dependent on each method used within the framework. As the research, in its current state, is concentrating on method development the validation of the models is subjective. Furthermore, each appended paper state under what circumstances the models are valid and their limitations.

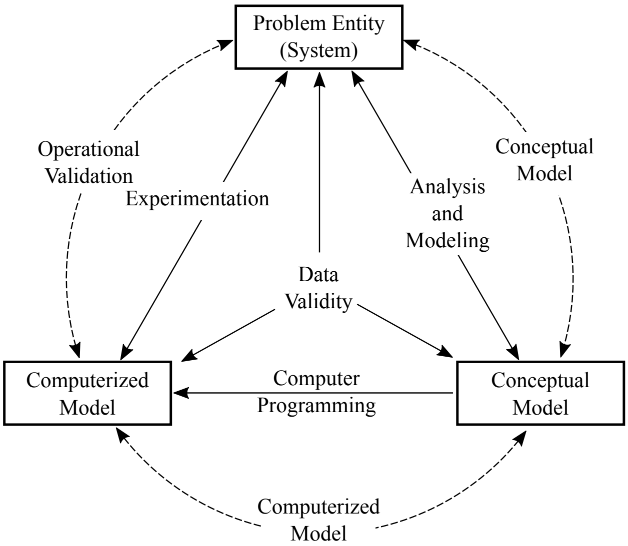

Figure 2.20: Simplified version of the model development process [68]

Chapter 3

Summary of Appended Papers

This chapter will present a summary of the results in the appended papers.

3.1 Paper I: Tolerance Analysis of Surface-to-Surface Contacts Using Finite Element Analysis

In this paper, an approach to analyze tolerances of surface-to-surface contacts subjected to external loads such that elastic and plastic deformations occur in the contact zones was suggested. In the case study a Corocut QD parting tool was used. The effect of the tool body geometry on the stress distributions in the interface was studied using a parametric CAD model. After simplifications it was assumed that 10 parameters, defining the contacting surfaces in the tool body, would affect the positioning of the insert in the tip seat, see Fig. 3.1. Both the translational[1] and rotational[2] degrees of freedom were assigned with uniformly distributed values within ± 0.01 mm and ± 1 deg.

[1]Subscript TX, TY or TZ
[2]Subscript RX, RY or RZ

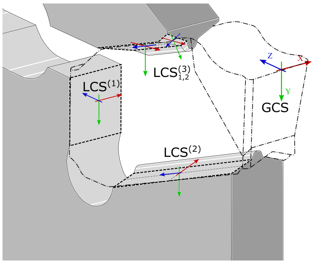

(a) Contact surfaces of the tool body

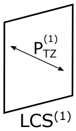

(b) Translation in Z

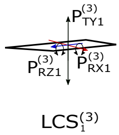

(c) Translation in Y - Rotation around X and Y

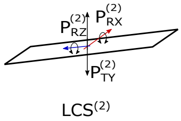

(d) Translation in Y - Rotation around X and Y

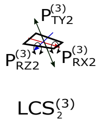

(e) Translation in Y - Rotation around X and Y

Figure 3.1: Contact surface degree of freedom

A meta-model was built for each individual node in the contacting surface between the insert and the cutting tool body. Creating a meta-model of the contacting surface allowed for visualization and optimization of the contact stress distribution, see Fig. 3.2, for any distribution of the input parameters within the simulated parameter space.

Paper I also incorporates a simplified cutting force model and considers how the contact variation affects the cutting forces as a result of variations in the rake angle.

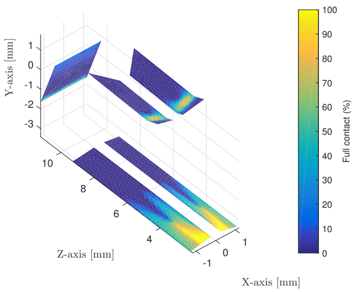

(a) Variational model for 1000 DMC iterations using the meta-model

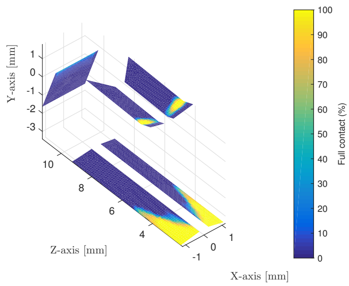

(b) Minimization of the distributed stress and rake angle variation

Figure 3.2: Probability of full contact on the tip seat

Paper I concludes that it is possible to analyze the effect of tolerances on the contact variation and and to analyse the impact of contact variation on cutting forces as a result of rake angle variations.

3.2 Paper II: Reliability based design optimiz ation of surface-to-surface contact for cutting tool interface designs

In this paper, a methodology for reliability based design optimization of overdetermined surface-to-surface contacts for cutting tools is presented. The reliability based design optimization uses a genetic algorithm with an implemented first order reliability method (FORM) approach to approximate the reliability of the performance functions. The performance functions are based on the percentage of contact in the preferred contact zones (PCZ) and can be retrieved through sensitivity analyses. The PCZ in this paper are chosen such that the leverage load acting on the insert due to the positioning of the insert on the tool body is minimized in order to avoid breaking the inserts. The methodology is presented through calculations on assemblies, containing two individual parts for different surface geometries found within the field of metal cutting tools. One part is defined as flexible (grey), see Fig. 3.3, with a linear material model which will represent the tool body. The other part is seen as rigid (white) which represents a cemented carbide insert. The flexible body rests on a frictionless surface. This allows translation in x,y-directions while prohibiting translation in the z-directions. A distributed load is acting on the rigid body that will compress the flexible body.

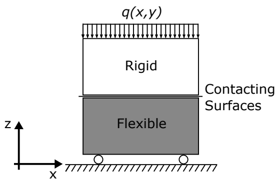

Figure 3.3: Illustration of the FE models used in the case studies

The results of Paper II is presented in four case studies. The first case study shows the validity of using a FORM based approach to calculate reliability using numerical data. The second case study presents the validity of the calculated reliability by comparing the results to direct Monte Carlo simulations. The third case study expands the complexity of the interface further with a two-dimensional serrated surface which can be described using four separately interfering surfaces. The fourth case study uses a three-dimensional serrated surface which can be described using eight separately interfering surfaces. The geometries of case studies three and four are chosen to resemble the interfaces of modern cutting tools out in the market today. The contact variation optimization algorithm is applied for case studies II-IV.

Paper II concludes that a FORM based approach on predicting the reliability of design variables with respect to a performance function can be used to define contact zones where contact is preferred. The FORM based approach on numerical data reduces computational time of the reliability with limited loss on the accuracy.

3.3 Paper III: Non-Linear Material Model in Part Variation Simulations of Sheet Metals

In Paper III an adaptation of the MIC for non-linear material models is presented and is referred to as the non-linear MIC method (NLMIC). The NLMIC approach incorporates an elasto-plastic material model with isotropic hardening through a first order Taylor expansion of the primary variable around a nominal load. The derivative of the primary variable is identified as the Newton step and can be retrieved from the FE formulation. An elasto-plastic material model with isotropic hardening was used for demonstration purposes. For highly non-linear material models, it is expected that the error will increase as the distance from the nominal load increases. The presented case studies show that it is possible to incorporate plastic strains for single and multiple loads in variation simulations with limited effect on accuracy.

In the first case, the same load deviation vector was applied for both the proposed method and FEA with 1,000 generated numbers with a normal distribution $u_y \sim N(6.15, 0.2)$[3]. The primary variables for the nominal prescribed displacement can be seen in Fig. 3.4 and the L^2 normalization of the residual between FEA and NLMIC. Results are presented in Fig. 3.5. This indicates that the correlation between the simulated and the approximated solution are coherent.

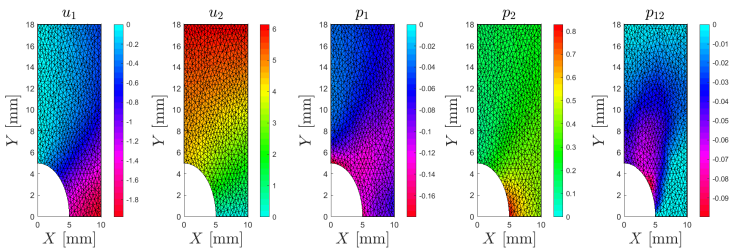

Figure 3.4: Nominal prescribed displacement $u_{y|\Gamma_3} = 6.15$ [mm]

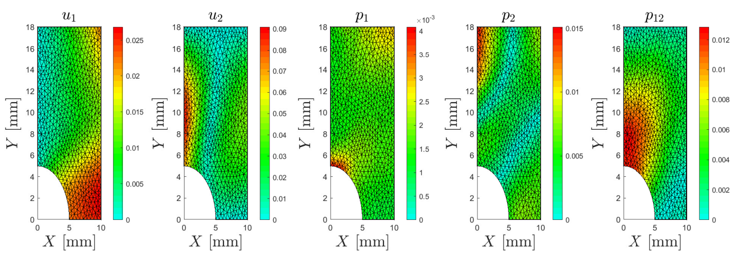

Figure 3.5: L^2 normalization of the residual between FEA and NLMIC, uni-axial

[3]Normal distribution of a variable x, $x \sim N(\mu, \sigma)$, where μ is the mean of the variable x and σ is the standard deviation

The second case is intended to show the validity of the superposition principle assumption. The quarter symmetric plate is subjected to a uniformly distributed prescribed displacement $u_x \sim U(5, 0.2)$ on Γ_2 and $u_y \sim U(6.15, 0.2)$ on Γ_3. A FE simulation is conducted with the mean prescribed displacements, where the components in the energy functional are obtained for the NLMIC. The assumption of superposition requires that the affected degrees of freedom due to the prescribed displacement are decoupled, for each load case. Once the components of the matrices are decoupled, the load deviation vector is applied and the primary variables can be calculated. A 2-level full factorial test space was created to validate the NLMIC for multiple boundary conditions. The primary variables, with nominal prescribed displacement applied to the boundaries, are presented in Fig. 3.6 and the L^2-normalization of the residuals is presented in Fig. 3.7.

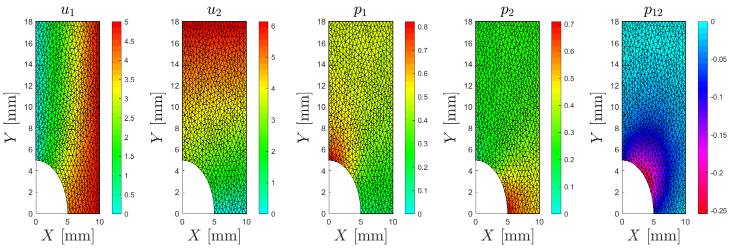

Figure 3.6: Nominal prescribed displacement $u_{x|\Gamma_2} = 5$ [mm] and $u_{y|\Gamma_3} = 6.15$ [mm]

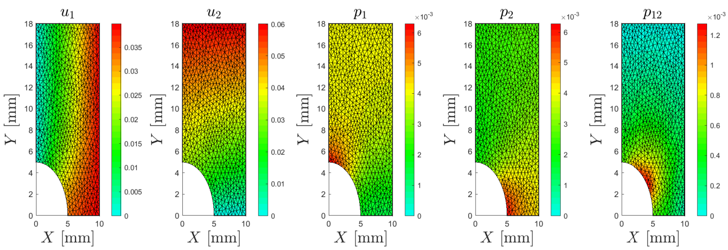

Figure 3.7: L^2 normalization of the residual between FEA and NLMIC of the 2-level full factorial test space

Paper III concludes that for small variations in a prescribed displacement it is possible to use Taylor's expansion to linearize the effect of plasticity on a sheet metal part. Paper C also concludes that the principle of superposition is valid as the model is linearized making it possible to apply the approach for assemblies in future research.

3.4 Paper IV: Algorithm for Detecting Load-Carrying Regions Within the Tip Seat of an Indexable Cutting Tool

Paper IV presents a methodology for detecting load-carrying surfaces in homogenous elastic cutting tool interfaces to assist engineers in early product design phases. In the finite element analysis, linear elastic springs suspend the object of interest to satisfy the Dirichlet boundary condition, ensuring the analysis finds a unique solution. Assuming material linearity, the principle of superposition applies, enabling separate simulations for each load case.

The methodology consists of three steps, with the first step calculating the surface normal vectors of the body of interest and aligning them to point outwards from the mass center using the two-argument arctangent.

A moving object's only possible contact is on surfaces where the surface normal vector is in the same direction as the displacement vector. Therefore, the second step involves determining the object's movement direction using the displacement vector retrieved from the finite element analysis. Predicting the movement direction consists of calculating the projection of the normalized displacement vector onto the surface normal vector. If the scalar value is negative, the object moves in the opposite direction; if positive, the object moves in the same direction, which indicates that contact is plausible.

It is essential to consider potential reaction forces to determine if the surface is suitable for contact. A higher reaction force suggests that support in this area is more advantageous than in areas with lower reaction forces. Therefore, the third step is calculating the reaction forces for each node using Hooke's Law's constitutive relationship, where the reaction force in a spring is linearly dependent on its displacement. The reaction forces are normalized against the highest linear spring reaction force, meaning each nodal displacement is divided by the maximum nodal displacement.

To demonstrate the methodology's effectiveness, we conducted three case studies: 1) unidirectional movement with a static load, 2) rotational movement with a static load, and 3) cutting tool insert subjected to a time-dependent load. The first case study shows the algorithm for a uniaxial static load to validate the magnitude of the contact index for different shapes and angles. The second case study, similar to the first case study, verifies that the magnitude of the contact index is predicted even for torsional static loads.

The third case study increases the complexity by combining time-dependent loads with static loads featuring a statistical distribution. In this scenario, the contact index algorithm updates the contact index at node j at timestep t only if it exceeds the value from the previous timestep $t-1$. This approach helps determine the highest achievable contact index for the surface, accounting for any outliers that could potentially lead to catastrophic failure of the cutting tool insert.

Paper IV concludes that it is possible to identify surface regions where contact is essential, thereby assisting engineers in the early stages of product design to optimize support for objects subjected to mechanical loads.

3.5 Paper V: Robustness Optimization of the Tip Seat of an Indexable Cutting Tool

Paper V introduces a methodology for optimizing the positioning of an insert within an indexable cutting tool body by considering the full spectrum of cutting forces and variations in insert clamping. The approach aims to account for all operational conditions that the tool might encounter, ensuring that the insert remains securely positioned despite changing forces and clamping conditions. This comprehensive consideration enhances the reliability and performance of the cutting tool under diverse machining scenarios. A prototype is created based on the results of the proposed optimization routine and validate its durability, performance, and reliability by comparing it to a similar, existing tool upon which the prototype is modelled. The validation process will ensure that the optimized prototype improves upon the existing tool's design and performs reliably under real-world cutting conditions, maintaining its durability and performance throughout its operational life.

The first step in the optimization process is to identify the support surfaces based on the 3-2-1 positioning methodology. This involves defining three points on the A-surface, two points on the B-surface, and one point on the C-surface. To achieve this, density-based cluster analysis is used to group surface normal vectors, and the surfaces are ranked by size to establish the A, B, and C surfaces. Once the support surfaces are defined, a stability analysis is performed using the commercially available software, RD&T. The analysis is combined with a genetic algorithm in Matlab to optimize the 3-2-1 positioning system. The optimization aims to minimize the cutting point's root mean square (RMS) value, ensuring the insert's most stable and robust positioning in the cutting tool body is found such that a normalized value could be used in the next step of the methodology.

The positioning system optimization follows a process similar to the previous step but introduces three essential desirability functions to achieve the desired outcome. These functions aim to:

1. Minimize the cutting point's root mean square (RMS) value, ensuring alignment with the global minimum to reduce deviations.

2. Maximize the overall contact index, enhancing stability and ensuring optimal load distribution across the contact surfaces.

3. Enforce the $A1$, $A2$, and $A3$ points to form a prescribed triangle around the clamping screw hole, ensuring that these three critical contact points provide consistent and reliable support.

This multi-objective optimization approach ensures that the positioning system is stable and precise and maintains contact to handle operational forces efficiently. The validation process includes:

1. FEA to predict the insert movement and estimate the stresses on the insert to avoid fractures.

2. Fatigue tests to measure the insert movement under a cutting force load of $2940N$ and clamping screw fatigue.

3. Conduct machining tests to measure flank wear and identify any other potential failure modes.

The FEA revealed maximum tensile stresses of 625 MPa on the insert's bottom surface, close to the 0.1% percentile failure threshold of $632MPa$ for uncoated grades of a spectrum of hardness levels. In fatigue tests, the prototype displayed insert movement comparable to the reference positioning, with no observed clamping screw fatigue. In contrast, the chamfered tool, designed to simulate a heavily deformed tip seat, exhibited significantly higher insert movement. The clamping mechanism in the chamfered tool began to fail after $35,000$ to $125,000$ cycles under a load of $2940N$. The results from Paper V demonstrate that it is feasible to optimize the robust positioning of an insert within the cutting tool body, leading to improvements in key quality aspects such as durability and reliability for the entire indexable cutting tool.

Chapter 4

Discussion

In this chapter, the answering of the research questions and the relevance of the used research methodology are discussed. The contribution this work makes to new knowledge is also considered.

4.1 Answering the Research Questions

The research questions will be answered one question at a time.

RQ I *How can external loads be handled in locating schemes for overdetermined indexable cutting tools?*

This question is addressed in Paper I, II and IV where methods to

1. simulate overdetermined surface-to-surface contact assemblies with mechanical loads,
2. detect critical areas, w.r.t geometric variations, on the contacting surface,
3. define and optimize an overdetermined locating schemes for surface-to-surface contact designs using a first order reliability based approach, and
4. identify load-carrying regions on a surface

were suggested. Those four methods together form a framework to handle positioning and tolerance analysis of surface-to-surface contact conditions with external loads.

RQ II *How can non-linear material behaviour be accounted for in variational simulations?*

An approach is suggested in Paper III that incorporates non-linear material behaviour in the MIC methodology and was given the name NLMIC. The NLMIC shows great potential and applicability to take in to account material hardening effects and plastic strains with greatly reduced simulation times, compared to direct Monte Carlo simulations with a FE-solver.

RQ III *How can the insert in an indexable cutting tool be positioned to achieve maximum robustness?*

Papers IV and V introduce optimization techniques to ensure a robust distribution of the insert's positioning within the tool-insert interface. These methods focus on optimizing surface interactions to enhance stability and performance under varying load conditions. These methods ensure contact in predefined areas, as outlined in the results from Paper V. The methods presented in Paper V can also be applied independently to single-point contacts, such as half-spheres, to ensure that all six degrees of freedom are constrained.

Figure 4.1: Research question and the publications connection to the research fields Positioning, Variation Simulation and Metal Cutting Mechanics

4.2 Scientific Contribution

Contributions to the scientific community can be considered in light of the difficulties the cutting tool industries are facing regarding insert positioning in the interface designs. In Section 1.2 the requirements on a robust design framework for cutting tool interface designs were outlined. Through extensive literature review it was found that two of the points were lacking in scientific publications, (1) non-linear material models in variation simulations and (2) surface-to-surface contact positioning. The contribution to the scientific community is summarized as:

- New knowledge and a method for variation simulation of sheet metal parts with nonlinear material models

- A reliability-based optimization methodology to position surface-to-surface contacts

- An approach to optimize robustness in the positioning of insert in the tool body interface based on mechanical loads

- Increased knowledge of robust insert positioning in cutting tool interface designs

4.3 Industrial Contribution

The primary industrial contribution is a robust design framework for indexable cutting tool designs, or similar products facing comparable challenges. This framework enables the transformation of an indexable insert concept into a reliable tool holder design, offering greater time and cost efficiency compared to traditional product design methods within AB Sandvik Coromant. This research also contributes to advancing knowledge in tolerance analysis and robust design optimization for cutting tool interface designs.

4.4 Applied Research Approach

This research project aims to develop a framework for engineers and researchers to transition from a carbide insert design concept to a fully supported and robust indexable cutting tool interface design. Given the absence of existing frameworks or methodologies that fully address the identified gap in this field, the initial iteration of the framework begins in phase one (**conceptualization**) of the Mitroff Cycle, starting with the problem situation:

> *There is an absence of methodologies to analyze tolerances that affect the positioning of the insert within the interface.*

The conceptualization in phase one outlines the set of tools, based on existing methods, necessary to develop the framework. The required steps, in subsequent order, are:

- Create a design of experiments
- Run simulations
- Build a model of the results
- Find an optimum set of input variables
- Visualize the results

Phase two (**modeling**) defines the Design of Experiments (DOE) type and specifies the appropriate simulation model. Phase three focuses on solving each step outlined in phases one and two, forming the initial iteration of the framework needed to address the defined problem situation.

The defined problem situation provides a holistic view of the current state of research in this field. Upon completing the first cycle, the problem situation evolves, reflecting the new reality. Additionally, analyzing feedback from the previous cycle enables the formulation of new realities and problem situations. Based on the results of Paper I, two key problem situations emerge: (1) *finding an optimal set of design variables lacks robustness*, and (2) *FEA is excessively time-consuming*. The new problem situations outline the problem definitions of Papers II and III where Mitroff's Cycle initiates the second iteration of the framework.

The first problem situation identified after Paper I—*finding an optimal set of design variables that lack robustness*—was addressed in Paper II, where a first-order reliability-based method to manage surface-to-surface contact positioning in cutting tool interface designs was developed. Paper II follows a complete Mitroff cycle (**I-II-III-IV**), with the final phase involving the implementation of the algorithm into the framework and two new problem situations could be defined as (II.1) *implementing an adaptive DOE to reduce simulation time* and (II.2) *implementing a sensitivity analysis on where to place the preferred contact zones.*

The second problem definition, *FEA is too time-consuming*, was partially addressed in Paper III and followed a typical prescriptive axiomatic research cycle (**I-II-III-(F)**). Common pitfalls in prescriptive axiomatic research, defined by [63], [65], [66], include a danger of getting stuck in a continuous loop of constantly improving the conceptual model as not enough knowledge exists about the goal. Therefore, the model-solving phase results are validated with related research, which is discussed further in section 4.4.1. The feedback path gave additional problem situations that need to be considered. The problem situations are defined as sub-problems and involve (III.1) *expanding the NLMIC to multiple sheet metal parts*, (III.2) *verifying and validating the NLMIC method*, and (III.3) *expanding the material linearization to solid-type elements in the FEA.*

For the third research iteration, the focus shifted to the problem situation (II.2), aiming to implement a sensitivity analysis to determine the contact placement based on the acting loads on the indexable insert addressed in Papers IV and V. Paper IV, similar to Paper III, also followed the typical prescriptive axiomatic research model by continuously updating the conceptual model (II-III-(F)) with newly found knowledge or methods to improve its results to approximate the expected outcome. However, Paper V implements the model from Paper IV to optimize the positioning of an indexable insert in the tool holder interface and follows a partially empiric prescriptive research model (I-II-III-IV) where machine tests, verifies, and validates the scientific model developed in Paper IV. The framework can now be presented in its final, condensed form for this research project, as illustrated in Fig. 4.2.

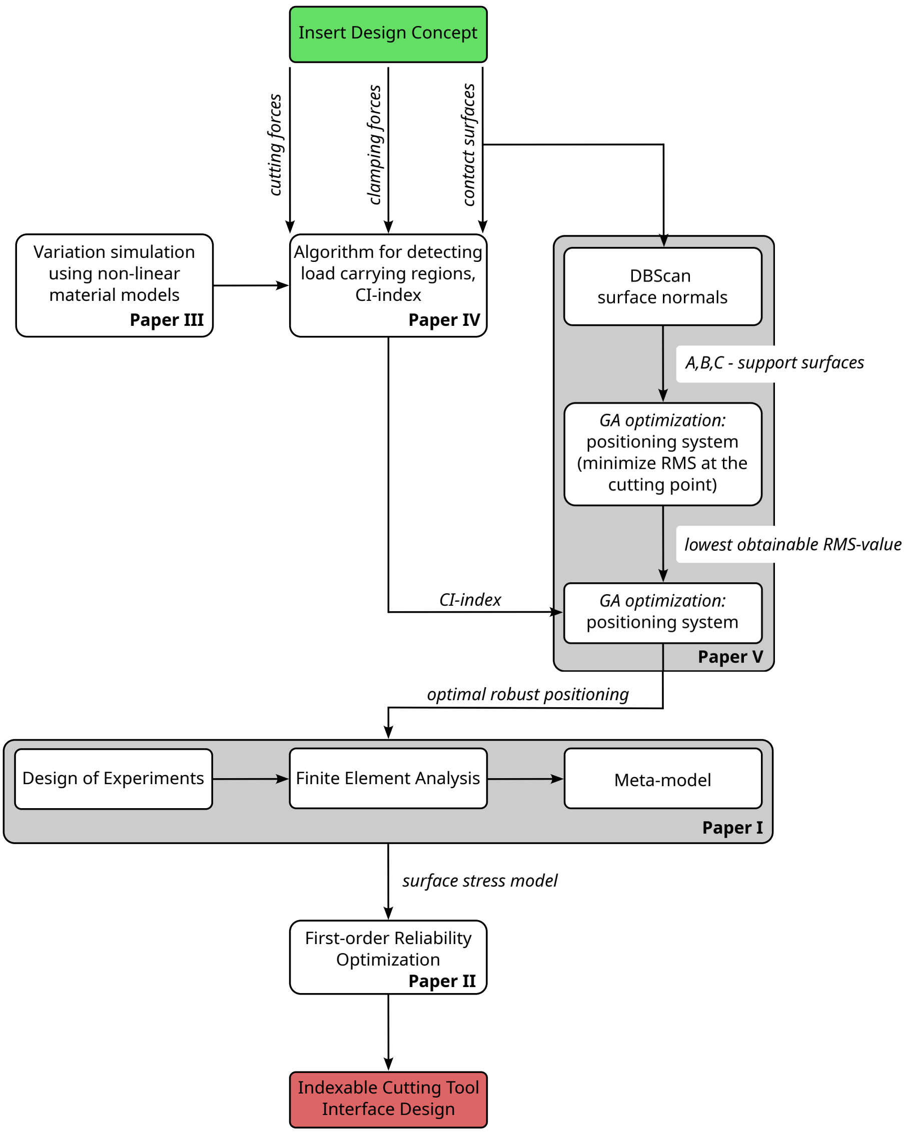

Figure 4.2: Robust design framework for positioning of inserts in indexable cutting tool bodies

4.4.1 Verification and Validation of the Results

This section discusses the verification and validation of the results and how it affects the validity of the framework.

The results in Paper I and Paper II have undergone multiple procedures to collect necessary data for the final results. The first step was to generate a sufficient test space using LHS. For linear regression, it is recommended to use $15-20$ observations per variable [71]. In Paper I, approximately 30 observations per variable were assumed necessary for constructing the simulation model.

The second step is to build the mesh, add boundary conditions, run the FE simulations and export the nodal responses in the contacting surfaces. Building the mesh for each observation can result in that the node positions are adjusted. Constructing the meta-model requires that the nodes in the mesh do not alter its position. Therefore, the third step is to interpolate the nodal responses in observation to a nominal mesh. The interpolation error is calculated using L^2 normalization and since linear element shape functions were used the interpolation error was negligible.

In the fourth step, a meta-model is built for each node on the contacting surfaces. The verification of meta-models is quantified using the R^2-value. A genetic algorithm is utilised to remove irrelevant predictors to avoid overfitting the meta-model to ensure that subsequent predictions do not have random variations [72].

To conclude the data collection in Paper I and Paper II, the number of observation per variable for an acceptable meta-model matches the literature. The interpolation error is negligible as the simulations use linear element shape functions. The verification of the meta-model relies on the R^2-value and on reducing irrelevant predictors. Paper I and Paper II are both non-observable systems and will rely on a subjective validation of the model behaviour in the FE simulation.

In Paper II the validity of the results is divided into four case studies. The first case study shows a negligible loss in accuracy when numerical data is used compared to analytical data. This allows for more complex models to be analyzed. The reliability of the found optimum was validated in the second case study by comparing the results to DMC simulations of the performance function. The third and fourth case study expand the complexity of the interface further and show the effectiveness of the presented approach with regards to restricting the contact variations to the PCZ.

The methodology and results in Paper III are validated using an objective decision approach. The implementation of the conceptual model is validated with known research of a deterministic case and is extended to a non-deterministic case.

The verification and validation of the algorithm to predict load-bearing surfaces presented in Paper IV mainly involves the two presented case studies. The equations for calculating the contact index and the conditions needed to achieve a specific outcome are provided. These conditions are tested and presented in the two case studies to verify the prediction, while the third case study shows the results of implementing the algorithm on an indexable insert.

Paper V uses the output and the contact index algorithm to determine the optimal positioning for the indexable insert within the tool body interface. The optimization results are validated and verified by manufacturing a prototype with the optimal positioning and testing it through physical experiments with machining and fatigue tests, comparing its performance to that of an unmodified tool holder.

4.5 Discussion of Limitations

The current state of the framework relies heavily on Finite Element Analysis (FEA) to simulate the assembly process and the impact of cutting forces on the interface. However, these simulations are computationally intensive, and the time required increases exponentially with the addition of controllable parameters. This presents a limitation as the complexity of the model grows, leading to longer computational times and reduced efficiency in the simulation process. Future implementations need to handle the stated issue and limit the number of simulations necessary to increase the number of parameters to study.

Sometimes, a small number of data points within a dataset may disproportionately influence the slope, commonly called outliers. However, in an overdetermined system, an outlier may arise from legitimate factors, such as introducing a new set of contact points. While deterministic simulation models inherently avoid the generation of outliers, meta-models often only capture the general trend of the dataset, thereby overlooking significant outlier effects. The omission of these outliers can lead to a meta-model that fails to reflect the overdetermined system's entire behavior accurately. Consequently, a new approach to constructing meta-models is required to incorporate the influence of outliers without overfitting the meta-model.

The proposed framework requires practitioners to possess expertise in several advanced topics, including FEA, geometry assurance, and optimization methodologies. This requirement poses a significant challenge, as the steep learning curve associated with mastering these techniques may deter engineers from incorporating the framework into their development processes. To address this limitation, future work should prioritize the development of a user-friendly interface and integrate the various algorithms and software tools into an unified software.

Chapter 5

Conclusion and Future Work

In this chapter, the results are summarized and future work is outlined.

RQ I *How can external loads be handled in locating schemes for overdetermined indexable cutting tools?*

The first research question addresses the challenge of positioning indexable cutting tools by incorporating external loads in the positioning methodology. Based on the literature and research findings, it is evident that movements in the insert positioning are critical to the cutting tool's life expectancy. Using First-Order Reliability Optimization methods, meta-models of the contact pressure, and identifying load-carrying regions on a surface, it is possible to design a robust positioning of the insert in early concept design phases with improved reliability.

RQ II *How can non-linear material behaviour be accounted for in variational simulations?*

The second research question addresses a common issue within variation simulations: non-linear material behavior, assuming small variations around a nominal displacement, and incorporating Taylor's expansion of the primary variable. Results indicate that it can be incorporated into the MIC methodology and used in sheet-metal assemblies with limited effect on accuracy while drastically decreasing computational time.

RQ III *How can the insert in an indexable cutting tool be positioned to achieve maximum robustness?*

The third research question focuses on identifying a robust design methodology for analyzing and optimizing the positioning of an insert within the tool-body interface. The methodology utilizes the algorithms and results from the research leading up to Paper IV to perform a robust design optimization to find an optimal positioning of the insert. The methodology was validated and verified by developing a prototype and comparing it to a reference and a deformed tool holder, where results indicate that clamping screw fatigue was reduced. At the same time, no significant increase in insert flank wear was found.

5.1 Conclusion

The research and framework presented in this work address cutting tool manufacturers' challenges in enhancing product reliability. By providing engineers and practitioners with tools to design indexable cutting tools that ensure robust insert positioning. The framework helps improve the overall quality such as performance, durability, and reliability of the tools. The presented framework also optimizes the design process by reducing the need for costly iterations typically encountered during the product development process of cutting tools. By incorporating reliability-based optimization methods and FEA simulations, the framework enables a more precise understanding of the interaction between the insert and tool body, ensuring optimal performance under varying mechanical loads. Furthermore, it supports engineers in identifying key parameters that influence insert positioning, improving the overall robustness and longevity of the tool design. However, the framework's methodologies present a steep learning curve, requiring hands-on experience to integrate fully into new product designs. Practitioners will need to invest time in familiarizing themselves with the intricacies of the framework to effectively apply them in the design and development of robust cutting tools. Despite these challenges, the potential long-term benefits of improved tool reliability and reduced design iterations make this investment worthwhile.

5.2 Future work

Typically, the tool body functions as a heat sink for the insert, helping to lower the insert's temperature and reducing wear mechanisms like flank wear. Future work should optimize the contact area between the insert and the tool body to enhance heat transfer, ensuring more efficient thermal regulation. By doing so, the framework could further improve tool longevity and performance, as better heat dissipation can directly impact wear rates and operational efficiency under high-temperature conditions.

Enhancing usability without compromising the framework's precision and effectiveness will be crucial for ensuring its practical application in industry settings. Therefore, future work should also simplify the framework to make it more accessible and user-friendly. Streamlining the interface and reducing the complexity of incorporating the methodologies would encourage wider adoption among engineers and designers, enabling them to integrate the proposed robust design techniques into new cutting tool designs.

Bibliography

[1] Z. Shen, G. Ameta, J. J. Shah, and J. K. Davidson, "A comparative study of tolerance analysis methods," *Journal of Computing and Information Science in Engineering*, vol. 5, no. 3, pp. 247–256, 2005, ISSN: 15309827. DOI: 10.1115/1.1979509 (cit. on pp. 4, 22).

[2] S. Charles Liu and S. Jack Hu, "Variation simulation for deformable sheet metal assemblies using finite element methods," *Journal of Manufacturing Science and Engineering, Transactions of the ASME*, vol. 119, no. 3, pp. 368–374, 1997, ISSN: 15288935. DOI: 10.1115/1.2831115 (cit. on pp. 5, 23, 24).

[3] R. Söderberg and L. Lindkvist, "Computer aided assembly robustness evaluation," en, *Journal of Engineering Design*, vol. 10, no. 2, pp. 165–181, 1999, ISSN: 09544828. DOI: 10.1080/095448299261371 (cit. on pp. 5, 20, 24).

[4] W. Cai, S. J. Hu, and J. X. Yuan, "Deformable sheet metal fixturing: Principles, algorithms, and simulations," *Journal of Manufacturing Science and Engineering, Transactions of the ASME*, vol. 118, no. 3, pp. 318–324, 1996, ISSN: 15288935. DOI: 10.1115/1.2831031 (cit. on pp. 5, 21).

[5] R. Söderberg, L. Lindkvist, and S. Dahlström, "Computer-aided robustness analysis for compliant assemblies," *Journal of Engineering Design*, vol. 17, no. 5, pp. 411–428, 2006, ISSN: 09544828. DOI: 10.1080/09544820500275800 (cit. on pp. 5, 21).

[6] S. Dahlstrom and L. Lindkvist, "Variation simulation of sheet metal assemblies using the method of influence coefficients with contact modeling," *Journal of Manufacturing Science and Engineering*, vol. 129, no. 3, pp. 615–622, 2007, ISSN: 10871357. DOI: 10.1115/1.2714570 (cit. on pp. 5, 24).

[7] S. Moos and E. Vezzetti, "An integrated strategy for variational analysis of compliant plastic assemblies on shell elements," *International Journal of Advanced Manufacturing Technology*, vol. 69, no. 1-4, pp. 875–890, 2013, ISSN: 14333015. DOI: 10.1007/s00170-013-5080-0 (cit. on p. 5).

[8] R. Söderberg, L. Lindkvist, K. Wärmefjord, and J. S. Carlson, "Virtual Geometry Assurance Process and Toolbox," *Procedia CIRP*, vol. 43, pp. 3–12, 2016, ISSN: 22128271. DOI: 10.1016/j.procir.2016.02.043 (cit. on p. 5).

[9] J. Y. Dantan, A. Ballu, and L. Mathieu, “Geometrical product specifications - model for product life cycle,” *CAD Computer Aided Design*, vol. 40, no. 4, pp. 493–501, 2008, ISSN: 00104485. DOI: `10.1016/j.cad.2008.01.004` (cit. on p. 5).

[10] B. Schleich, N. Anwer, L. Mathieu, and S. Wartzack, “Contact and Mobility Simulation for Mechanical Assemblies Based on Skin Model Shapes,” *Journal of Computing and Information Science in Engineering*, vol. 15, no. 2, 2015, ISSN: 15309827. DOI: `10.1115/1.4029051` (cit. on p. 5).

[11] B. Schleich and S. Wartzack, “A Quantitative Comparison of Tolerance Analysis Approaches for Rigid Mechanical Assemblies,” *Procedia CIRP*, vol. 43, pp. 172–177, 2016, ISSN: 22128271. DOI: `10.1016/j.procir.2016.02.013` (cit. on p. 5).

[12] O. R. Garaizar, L. Qiao, N. Anwer, and L. Mathieu, “Integration of Thermal Effects into Tolerancing Using Skin Model Shapes,” *Procedia CIRP*, vol. 43, pp. 196–201, 2016, ISSN: 22128271. DOI: `10.1016/j.procir.2016.02.079` (cit. on p. 5).

[13] Z. Junnan, C. Yanlong, L. Fan, L. Ting, and Y. Jiangxin, “Tolerance analysis of an assembly by considering part deformation,” *Procedia CIRP*, vol. 92, pp. 81–87, 2020, ISSN: 2212-8271. DOI: `10.1016/J.PROCIR.2020.05.167` (cit. on p. 6).

[14] J. Liu, Z. Zhang, X. Ding, and N. Shao, “Integrating form errors and local surface deformations into tolerance analysis based on skin model shapes and a boundary element method,” *Computer-Aided Design*, vol. 104, pp. 45–59, 2018, ISSN: 0010-4485. DOI: `10.1016/J.CAD.2018.05.005` (cit. on p. 6).

[15] S. Ma, T. Hu, and Z. Xiong, “Precision Assembly Simulation of Skin Model Shapes Accounting for Contact Deformation and Geometric Deviations for Statistical Tolerance Analysis Method,” *International Journal of Precision Engineering and Manufacturing*, vol. 22, no. 6, pp. 975–989, 2021, ISSN: 20054602. DOI: `10.1007/S12541-021-00505-1/FIGURES/15` (cit. on p. 6).

[16] S. Lorin, R. Söderberg, J. Carlson, and F. Edelvik, “Simulating geometrical variation in injection molding,” in *Proceedings of NordDesign 2010, the 8th International NordDesign Conference*, vol. Aug. 25-27, Göteborg, 2010, pp. 395–406 (cit. on p. 6).

[17] S. Lorin, L. Lindkvist, and R. Söderberg, “Simulating part and assembly variation for injection molded parts,” in *Proceedings of the ASME Design Engineering Technical Conference*, vol. 5, Chicago, 2012, pp. 487–496, ISBN: 9780791845042. DOI: `10.1115/DETC2012-70659` (cit. on p. 6).

[18] G. S. Shawki and M. M. Abdel-Aal, “Effect of fixture rigidity and wear on dimensional accuracy,” *International Journal of Machine Tool Design and Research*, vol. 5, no. 3, pp. 183–202, 1965, ISSN: 00207357. DOI: `10.1016/0020-7357(65)90025-9` (cit. on pp. 6, 21).

[19] G. S. Shawki and M. M. Abdel-Aal, "Rigidity considerations in fixture design-contact rigidity at locating elements," *International Journal of Machine Tool Design and Research*, vol. 6, no. 1, pp. 31–43, 1966, ISSN: 00207357. DOI: 10.1016/0020-7357(66)90005-9 (cit. on pp. 6, 21).

[20] G. S. Shawki and M. M. Abdel-Aal, "Rigidity considerations in fixture design-rigidity of clamping elements," *International Journal of Machine Tool Design and Research*, vol. 6, no. 4, pp. 207–220, 1966, ISSN: 00207357. DOI: 10.1016/0020-7357(66)90011-4 (cit. on pp. 6, 21).

[21] J. F. Hurtado and S. N. Melkote, "Improved algorithm for tolerance-based stiffness optimization of machining fixtures," *Journal of Manufacturing Science and Engineering, Transactions of the ASME*, vol. 123, no. 4, pp. 720–730, 2001, ISSN: 15288935. DOI: 10.1115/1.1403446 (cit. on pp. 6, 21).

[22] G Prabhaharan, P Asokan, P Ramesh, and S Rajendran, "Genetic-algorithm-based optimal tolerance allocation using a least-cost model," *Int J Adv Manuf Technol*, vol. 24, pp. 647–660, 2004. DOI: 10.1007/s00170-003-1606-1 (cit. on p. 6).

[23] G. Prabhaharan, K. P. Padmanaban, and R. Krishnakumar, "Machining fixture layout optimization using FEM and evolutionary techniques," *International Journal of Advanced Manufacturing Technology*, vol. 32, no. 11-12, pp. 1090–1103, 2007, ISSN: 02683768. DOI: 10.1007/S00170-006-0441-6/METRICS (cit. on p. 6).

[24] K. A. Sundararaman, S. Guharaja, K. P. Padmanaban, and M. Sabareeswaran, "Design and optimization of machining fixture layout for end-milling operation," *International Journal of Advanced Manufacturing Technology*, vol. 73, no. 5-8, pp. 669–679, 2014, ISSN: 14333015. DOI: 10.1007/S00170-014-5848-X/METRICS (cit. on p. 6).

[25] D. Wu, B. Zhao, H. Wang, K. Zhang, and J. Yu, "Investigate on computer-aided fixture design and evaluation algorithm for near-net-shaped jet engine blade," *Journal of Manufacturing Processes*, vol. 54, pp. 393–412, 2020, ISSN: 1526-6125. DOI: 10.1016/J.JMAPRO.2020.02.023 (cit. on p. 6).

[26] I. Lopatukhin, A. Ber, and J. Rotberg, "Analysis and Optimization of the Contact Pressure Distribution Between an Insert and its Pocket Due to the Clamping and the Cutting Action," *Journal for Manufacturing Science and Production*, vol. 2, no. 1, pp. 17–26, 2011, ISSN: 0793-6648. DOI: 10.1515/ijmsp.1999.2.1.17 (cit. on p. 6).

[27] P Mikell, *Groover Fundamentals of Modern Manufacturing Materials, Processes, and Systems*, 5th. Upper Saddle River, N.J: Prentice Hall, 2016, p. 1028 (cit. on pp. 9, 10).

[28] H. Ernst and M. Merchant, "Chip formation, friction and high quality machined surfaces," *Surface Treatment of Metals, ASM*, vol. 29, pp. 299–378, 1941 (cit. on p. 12).

[29] M. E. Merchant, “Mechanics of the metal cutting process. I. Orthogonal cutting and a type 2 chip,” *Journal of Applied Physics*, vol. 16, no. 5, pp. 267–275, 1945, ISSN: 00218979. DOI: 10.1063/1.1707586 (cit. on p. 12).

[30] M. E. Merchant, “Mechanics of the metal cutting process. II. Plasticity conditions in orthogonal cutting,” *Journal of Applied Physics*, vol. 16, no. 6, pp. 318–324, 1945, ISSN: 00218979. DOI: 10.1063/1.1707596 (cit. on p. 12).

[31] E. H. Lee and B. W. Shaffer, “The Theory of Plasticity Applied to a Problem of Machining,” *Journal of Applied Mechanics*, vol. 18, no. 4, pp. 405–413, 1951, ISSN: 0021-8936. DOI: 10.1115/1.4010357 (cit. on p. 12).

[32] P. L. Oxley and A. P. Hatton, “Shear angle solution based on experimental shear zone and tool-chip interface stress distributions,” *International Journal of Mechanical Sciences*, vol. 5, no. 1, pp. 41–55, 1963, ISSN: 00207403. DOI: 10.1016/0020-7403(63)90038-9 (cit. on p. 12).

[33] Y Altintas and A. Ber, *Manufacturing Automation: Metal Cutting Mechanics, Machine Tool Vibrations, and CNC Design*, 2nd. New York: Cambridge University Press, 2001, vol. 54, B84–B84. DOI: 10.1115/1.1399383 (cit. on p. 12).

[34] O Kienzle and H Victor, “Spezifische Schnittkraefte bei der Metallbearbeitung,” *Werkstattstechnik und Maschinenbau*, vol. 47/5, no. 7, pp. 224–225, 1957 (cit. on p. 13).

[35] H. Saglam, F. Unsacar, and S. Yaldiz, “Investigation of the effect of rake angle and approaching angle on main cutting force and tool tip temperature,” 2005. DOI: 10.1016/j.ijmachtools.2005.05.002 (cit. on p. 15).

[36] J. O. I. and W. A. Shewhart, *The Economic Control of Quality of Manufactured Product.* American Society for Quality (ASQ), 1932, vol. 95, p. 546. DOI: 10.2307/2342413 (cit. on p. 17).

[37] B. Falk, K. Stylidis, C. Wickman, R. Söderberg, and R. Schmitt, “Shifting paradigm: Towards a comprehensive understanding of quality,” *Proceedings of the International Conference on Engineering Design, ICED*, vol. 9, no. DS87-9, 2017, ISSN: 22204342 (cit. on p. 17).

[38] K. Stylidis, C. Wickman, and R. Söderberg, “Perceived Quality Attributes Framework and Ranking Method. Perceived Quality Attributes Framework and Ranking Method,” *Journal of Engineering Design*, vol. 31, no. 1, pp. 31–67, 2019. DOI: 10.17605/OSF.IO/P5YTR (cit. on p. 17).

[39] O. Wagersten, B. Lindau, L. Lindkvist, and R. Sooderberg, “Using morphing techniques in early variation analysis,” *Journal of Computing and Information Science in Engineering*, vol. 14, no. 1, p. 011 007, 2014, ISSN: 15309827. DOI: 10.1115/1.4025719 (cit. on p. 17).

[40] D. M. Byrne and S. Taguchi, “Taguchi Approach To Parameter Design.,” in *Quality Progress*, vol. 20, Anaheim, CA, 1987, pp. 19–26 (cit. on p. 17).

[41] W. C. Parr and G. Taguchi, *Introduction to Quality Engineering: Designing Quality into Products and Processes.* Asian Productivity Organization, 1989, vol. 31, p. 255. DOI: 10.2307/1268824 (cit. on p. 18).

[42] J. D. Barrett, *Quality From Customer Needs to Customer Satisfaction*, 3rd. Malmö: Studentlitteratur, 2004, vol. 46, pp. 118–118, ISBN: 9789144059426. DOI: 10.1198/tech.2004.s752 (cit. on p. 18).

[43] B. Denkena and D. Biermann, "Cutting edge geometries," *CIRP Annals - Manufacturing Technology*, vol. 63, no. 2, pp. 631–653, 2014, ISSN: 17260604. DOI: 10.1016/j.cirp.2014.05.009 (cit. on p. 18).

[44] J. F. Hurtado and S. N. Melkote, "A model for the prediction of reaction forces in a 3-2-1 machining fixture," *Technical Paper - Society of Manufacturing Engineers. MS*, vol. 98, no. 264, pp. 335–340, 1998, ISSN: 01616382 (cit. on p. 21).

[45] E. T. Fortini, *Dimensioning for Interchangeable Manufacture.* Industrial Press, 1967, p. 276 (cit. on p. 22).

[46] K. W. Chase and A. R. Parkinson, "A survey of research in the application of tolerance analysis to the design of mechanical assemblies," *Research in Engineering Design*, vol. 3, no. 1, pp. 23–37, 1991, ISSN: 09349839. DOI: 10.1007/BF01580066 (cit. on p. 22).

[47] K. W. Chase, J. Gao, and S. P. Magleby, "General 2-D Tolerance Analysis of Mechanical Assemblies with Small Kinematic Adjustments," *J Des Manuf*, vol. 5, pp. 263–274, 1995 (cit. on p. 22).

[48] J. Gao, K. W. Chase, and S. P. Magleby, "Generalized 3-D tolerance analysis of mechanical assemblies with small kinematic adjustments," *IIE Transactions (Institute of Industrial Engineers)*, vol. 30, no. 4, pp. 367–377, 1998, ISSN: 15458830. DOI: 10.1080/07408179808966476 (cit. on p. 22).

[49] L. J. Bain, *Applied Regression Analysis*, 3rd ed. New York: John Wiley and Sons, INC, 1967, vol. 9, pp. 182–183. DOI: 10.1080/00401706.1967.10490452 (cit. on p. 25).

[50] J. S. Aror, *Introduction to Optimum Design, Third Edition.* 2011, pp. 1–880, ISBN: 9780123813756. DOI: 10.1016/C2009-0-61700-1 (cit. on p. 25).

[51] R. T. Haftka and Z. GurdalL, *Elements of Structural Optimization: Third Edition (Google eBook)* (Solid Mechanics And Its Applications). Dordrecht: Springer Netherlands, 1992, vol. 11, p. 481, ISBN: 0792315049. DOI: 10.1007/978-94-011-2550-5 (cit. on p. 25).

[52] L. B. Enevoldsen, "Reliability-Based Optimization as an Information Tool*," *Mechanics of Structures and Machines*, vol. 22, no. 1, pp. 117–135, 1994, ISSN: 08905452. DOI: 10.1080/08905459408905207 (cit. on p. 26).

[53] I. Enevoldsen and J. D. Sørensen, "Reliability-based optimization in structural engineering," *Structural Safety*, vol. 15, no. 3, pp. 169–196, 1994, ISSN: 01674730. DOI: 10.1016/0167-4730(94)90039-6 (cit. on p. 26).

[54] S. V. Chandu and R. V. Grandhi, "General purpose procedure for reliability based structural optimization under parametric uncertainties," *Advances in Engineering Software*, vol. 23, no. 1, pp. 7–14, 1995, ISSN: 09659978. DOI: 10.1016/0965-9978(95)00049-W (cit. on p. 26).

[55] X. Yu, K. H. Chang, and K. K. Choi, "Probabilistic structural durability prediction," *AIAA Journal*, vol. 36, no. 4, pp. 628–637, 1998, ISSN: 00011452. DOI: 10.2514/2.415 (cit. on p. 26).

[56] R. V. Grandhi and L. Wang, "Reliability-based structural optimization using improved two-point adaptive nonlinear approximations," *Finite Elements in Analysis and Design*, vol. 29, no. 1, pp. 35–48, 1998, ISSN: 0168874X. DOI: 10.1016/S0168-874X(98)00007-9 (cit. on p. 26).

[57] M. W. Lu and M. D. Forrest, "Probabilistic engineering design," in *International Journal of Vehicle Design*, 1, vol. 23, Missouri, 2000, ch. First Orde, pp. 68–77. DOI: 10.1504/ijvd.2000.001883 (cit. on pp. 26, 27).

[58] M. Rosenblatt, "Remarks on a Multivariate Transformation," *The Annals of Mathematical Statistics*, vol. 23, no. 3, pp. 470–472, 1952, ISSN: 0003-4851. DOI: 10.1214/aoms/1177729394 (cit. on p. 27).

[59] A. Der Kiureghian and T. Dakessian, "Multiple design points in first and second-order reliability," *Structural Safety*, vol. 20, no. 1, pp. 37–49, 1998, ISSN: 01674730. DOI: 10.1016/S0167-4730(97)00026-X (cit. on p. 28).

[60] E. Harrington, "The desirability function," *Industrial quality control*, vol. 21, no. 10, pp. 494–498, 1965 (cit. on p. 29).

[61] G. Derringer and R. Suich, "Simultaneous Optimization of Several Response Variables," *Journal of Quality Technology*, vol. 12, no. 4, pp. 214–219, 1980, ISSN: 0022-4065. DOI: 10.1080/00224065.1980.11980968 (cit. on p. 29).

[62] K. J. Kim and D. K. Lin, "Simultaneous optimization of mechanical properties of steel by maximizing exponential desirability functions," *Journal of the Royal Statistical Society. Series C: Applied Statistics*, vol. 49, no. 3, pp. 311–325, 2000, ISSN: 00359254. DOI: 10.1111/1467-9876.00194 (cit. on p. 31).

[63] J. R. Meredith, A. Raturi, K. Amoako-Gyampah, and B. Kaplan, "Alternative research paradigms in operations," *Journal of Operations Management*, vol. 8, no. 4, pp. 297–326, 1989, ISSN: 02726963. DOI: 10.1016/0272-6963(89)90033-8 (cit. on pp. 31, 48).

[64] C. Karlsson, *Researching operations management*, 1th ed. New York, NY: Routledge, 2008, pp. 1–322, ISBN: 020388681X. DOI: 10.4324/9780203886816 (cit. on pp. 31–33).

[65] F. R. Sagasti and I. I. Mitroff, "Operations research from the viewpoint of general systems theory," *Omega*, vol. 1, no. 6, pp. 695–709, 1973, ISSN: 03050483. DOI: 10.1016/0305-0483(73)90087-X (cit. on pp. 32, 48).

[66] I. I. Mitroff, F. Betz, L. R. Pondy, and F. Sagasti, "On Managing Science in the Systems Age: Two Schemas for the Study of Science as a Whole Systems Phenomenon," *Interfaces*, vol. 4, no. 3, pp. 46–58, 1974, ISSN: 0092-2102. DOI: 10.1287/inte.4.3.46 (cit. on pp. 32, 33, 48).

[67] B. W. Boehm, *Guidelines for Verifying and Validating Software Requirements and Design Specifications*, P. Samet, Ed. North Holland Publishing Company, 1979, vol. 79, pp. 711–719 (cit. on p. 33).

[68] S. J. Aboud, M. Al Fayoumi, and M. Alnuaimi, "Verification and validation of simulation models," *Handbook of Research on Discrete Event Simulation Environments: Technologies and Applications*, vol. 7, pp. 58–74, 2009. DOI: 10.4018/978-1-60566-774-4.ch004 (cit. on pp. 33–35).

[69] R. G. Sargent, "An assessment procedure and a set of criteria for use in the evaluation of computerized models and computer-based modeling tools," Final Technical Report RADC-TR-80-409, U.S. Air Force, Tech. Rep., 1981 (cit. on p. 34).

[70] SCS Technical Committee on Model Credibility, "Terminology for model credibility," Tech. Rep. 3, 1979, pp. 103–104. DOI: 10.1177/003754977903200304 (cit. on p. 34).

[71] S. B. Green, "How Many Subjects Does It Take To Do A Regression Analysis?" *Multivariate Behavioral Research*, vol. 26, no. 3, pp. 499–510, 1991, ISSN: 15327906. DOI: 10.1207/s15327906mbr2603_7 (cit. on p. 50).

[72] D. M. Hawkins, "The Problem of Overfitting," *Journal of Chemical Information and Computer Sciences*, vol. 44, no. 1, pp. 1–12, 2004, ISSN: 00952338. DOI: 10.1021/ci0342472 (cit. on p. 51).

Part II

Appended Papers

Paper I

Tolerance Analysis of Surface-to-Surface Contacts Using Finite Element Analysis

S. Camuz, R. Söderberg, K. Wärmefjord, M. Lundblad

15th CIRP Conference on Computer Aided Tolerancing (Apr 2018), Vol. 75, p.250-255

https://doi.org/10.1016/j.procir.2018.04.029

Available online at www.sciencedirect.com

ScienceDirect

Procedia CIRP 75 (2018) 250–255

www.elsevier.com/locate/procedia

15th CIRP Conference on Computer Aided Tolerancing – CIRP CAT 2018

Tolerance Analysis of Surface-to-Surface Contacts Using Finite Element Analysis

Soner Camuz[a], Rikard Söderberg[a], Kristina Wärmefjord[a], Mikael Lundblad[b]

[a]Dept. Industrial and Materials Science, Chalmers University of Technology, Göteborg, Sweden
[b]Metal Cutting Technology, AB Sandvik Coromant, Sandviken, Sweden

* Soner Camuz Tel.: +46-72-981-99-94.; *E-mail address:* soner@chalmers.se

Abstract

The accuracy of a cutting tool is dependent on the surface-to-surface contact between the tool body and the insert. Depending on the application, the forces generated during a cutting operation will change in both magnitude and direction. This will alter the contact locations between the tool body and carbide insert thus affecting on both tool life and key characteristics such as cutting performance and productivity. In this article, a methodology is presented to analyse contact variation in the interface between the tool body and the carbide insert. Results presented in this paper can be used for tolerance allocation of surface-to-surface contacts.

© 2018 The Authors. Published by Elsevier B.V.
Peer-review under responsibility of the Scientific Committee of the 15th CIRP Conference on Computer Aided Tolerancing - CIRP CAT 2018.

Keywords: Variation simulation; Machining tool; Tolerances; Contact prediction; Tolerance analysis

1. Introduction

Assembly deviations caused by part variations, fixture variations and external effects such as temperature and mechanical loads are inevitable to avoid and need to be statistically controlled. During the past decades numerous of approaches have been developed in order to handle these type of problems, different approaches for different industries. Within the machining industry research as mainly focused upon fixture design due to the direct response on the produced quality [1]. The most common type of rigid locating method is the $3-2-1$ locating scheme [2] and *N-2-1* for compliant assemblies [3, 4] but it implies that the locators are known and pre-defined. The authors in [5] describe a method using skin-models to address this issue, however, this is purely a rigid assembly variation simulation, which is not applicable for cutting tool assemblies.

Conventional variation simulation of deformable sheet metal assemblies uses Method of Influencing Coefficients (MIC), where a linear relationship between part deviations and the springback deviations is formed [6]. Finite element analysis (FEA) is used on assembly level to calculate springback deviations and extract the stiffness matrix. A novel approach is presented in [7, 8] where a regression model is created for each node of a finite element mesh of an injection moulded plastic part, in order to see the effects of process input parameters, such as mould temperature and cooling time. In [9] a tolerance optimization routine is presented that uses finite element analysis and neural networks to optimize a set of tolerances for a mechanical motor assembly, with respect to manufacturing cost, quality loss and deformation due to inertia effect.

For metal cutting, the locating scheme is given by the contacts between the tool body and insert and the position of the contact points are not always fully constrained. This means that a change of cutting direction or surface topology can affect the contacts between the two bodies. During a cutting operation, depending on the cutting process, the cutting force will change both in magnitude and direction. This will alter the cutting point which will resolve in movements in the carbide insert, thus altering the location and contacts in between the tool body and insert, see Fig. 1a. This can lead to a change in the rake angle, see Fig. 1b, which in a metal removal process can have a dramatical effect on tool life and productivity.

For parting operations there are high demands on the robustness and performance of parting tools due to the fact that during a cut there will be material on both sides of the tool, meaning that chip clearing is crucial. Failure in chip clearing will lead to poor surface qualities and chip jamming that will break the tool. As the tool reaches the center of the work piece the axial forces will drastically increase due to the tangential force going towards zero and the tool is pushing instead of cutting. In [10] the author calculates the cutting forces using finite elements during orthogonal cutting conditions. It is found that a change in the positive direction of α_r gives a reduction of the cutting forces. This was also shown by experimental measurements in [11]. Both results from finite elements and experiments show that the analytical expressions derived from mechanistic models [12, 13, 14] are valid for orthogonal cutting conditions. There-

2212-8271 © 2018 The Authors. Published by Elsevier B.V.
Peer-review under responsibility of the Scientific Committee of the 15th CIRP Conference on Computer Aided Tolerancing - CIRP CAT 2018.
10.1016/j.procir.2018.04.029

fore it is crucial to control any geometric variation in the interface between the tool body and carbide insert, that can affect key characteristics of the cutting tool such as cutting point, rake angle and tool life.

An approach is needed to identify sensitive contact areas on a surface between two or more contacting bodies with respect to any systems key characteristics. In this paper a methodology will be presented on a industrial application using a parting tool in orthogonal cutting conditions, Corocut QD tool and QD-NE-0200-0502-CM carbide insert. The proposed method is divided in two separate parts, FEA and variational simulation. In the FEA part a test space is created using design of experiments, where the independent variables are geometric variations of the contact surface and the response is the stress magnitude in each individual node in the contact surface. Each observation is simulated and the results from the contact surfaces are extracted. In order to perform the variational simulation a meta-model is created for each individual node of the contact surface. This allows for a larger data set to be simulated within the boundaries of the test space also the independent variables are not bound to a specific distribution.

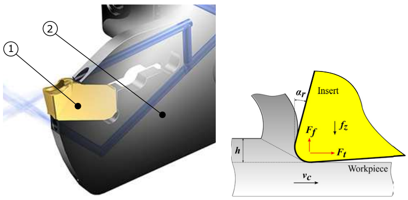

(a) Cutting tool assembly [15], **1** - carbide insert, **2**-tool body

(b) Illustration of the cutting process

Fig. 1: Corocut QD cutting tool

1.1. Scope of Paper

The aim of this paper is to present an approach that can handle contact variation in surface-to-surface contacts with external loads. The methodology will be presented using an industrial case from the machining industry where these conditions are common. The relationship between contact variation and the rake angle of the cutting tool is investigated and the goal is to minimize its impact on the rake angle. The main approach of the methodology is to create a sample space of geometric variations on the tool body in the interface to the carbide insert. Output from this paper will be the effect from geometric variations in the contact surface on cutting forces. One may decide tolerances based on minimizing the variation of the cutting forces due to geometric variations in the interface during a metal removal process or similar problem definitions. Results based upon the presented methodology are valuable input for tolerance allocation of both the surface geometry and functional requirements such as rake angle.

In Section 2.1 the industrial case is presented and the input parameters for the meta-model that are described in Section 2.4. The FE model is presented in Section 2.3 and the analysed rake angle variation and how it effects the cutting forces are modelled in Section 2.2. The results of the methodology are presented in Section 3 and conclusions are drawn in Section 4.

2. Methodology

The aim of the methodology is to create a set of tools in order to set suitable functional tolerance requirements for surface-to-surface contacts under external loads. The main activities are presented in a flowchart, see Fig. 6.

The first step is to create a test space to cover all possible combinations of the input variables. Afterwards FEA is used to simulate the cutting process during steady state conditions, meaning, the entry and exit from the workpiece are neglected and the cutting forces are stable. The variational simulations are performed by building meta-models of the stress distributions in the contacting surfaces. This allows for faster simulations outside the FE environment.

2.1. Generation of the Test Space

To create the test space Latin Hypercube Sampling (LHS) [16, 17] with a uniform distribution is used. A uniform LHS partitions the parameters evenly into Latin squares, where the parameter can only take a value once within a Latin square. One draw back of using LHS is that extreme values, on parameter limits, will most likely not be captured. To resolve this issue the LHS is combined with a 2-level full factorial sampling. In [18] the author suggests that $15-25$ observations per variable are needed for a linear regression model. For this paper, 30 observations per variable are used. This is done because some design points may not converge due to the complex contact formulation and to pick up any non-linear behaviours.

The interface between the tool body and insert contains eight surfaces that are in contact, each surface has six degrees of freedom, see Fig. 2a - 2e. This means that the assembly has 48 degrees of freedom (24 for the insert, 24 for the tool). In order to get a reliable meta-model, according to [18], a total of 1440 design points need to be simulated. This requires an excessive amount of computer resources, therefore the model needs to be reduced without loosing valuable information.

The tool body has three separate contact surfaces, $s = 1, 2, 3$, and each surface has its own local coordinate system ($LCS^{(s)}$), see Fig. 2a. The insert is assumed to be nominal and rigid since not enough information exists on how the surfaces vary in the insert. It is also assumed that the tool is symmetric in the YZ-plane and that the back support, in the local coordinate system $LCS^{(1)}$, only translates along its y-axis.

With these simplifications, the model now has 10 input parameters, which will give 300 design points to simulate. In Fig. 2 each contacting surface and its degrees of freedom are visualised. The parameters are also presented in Table 1 together with their lower and upper tolerance limits. The superscript of the parameters in the first column of Table 1 denotes which surface it belongs to ($s = 1, 2, 3$), see Fig. 2a. The first value of the subscript denotes if it is a translational (T) degree of freedom or rotational (R) degree of freedom. The second value of the subscript denotes around or along which local coordinate axis it is bound to, see Fig. 2b. - 2e. It should be noted that due to confidentiality the used tolerances are arbitrary and are not representing the real variation.

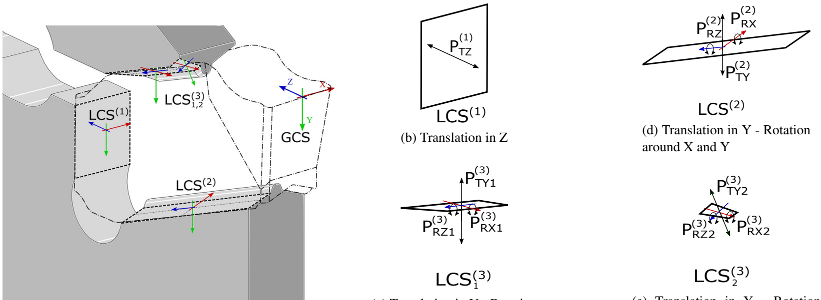

(a) Contact surfaces of the tool body

(b) Translation in Z

(c) Translation in Y - Rotation around X and Y

(d) Translation in Y - Rotation around X and Y

(e) Translation in Y - Rotation around X and Y

Fig. 2: Contact surface degree of freedom

Table 1: Parameters with nominal value and variation

Parameter	Lower boundary	Nominal	Upper Boundary	Unit	DOF	
$P^{(1)}_{TZ}$	−0.01	0	0.01	mm	Translation	$Z^{(1)}$-axis
$P^{(2)}_{RX}$	−1	0	1	deg	Rotation	$X^{(2)}$-axis
$P^{(2)}_{RZ}$	−1	0	1	deg	Rotation	$Z^{(2)}$-axis
$P^{(2)}_{TY}$	−0.01	0	0.01	mm	Translation	$Y^{(2)}$-axis
$P^{(3)}_{RX1}$	−1	0	1	deg	Rotation	$X^{(3)}$-axis
$P^{(3)}_{RZ1}$	−1	0	1	deg	Rotation	$Z^{(3)}$-axis
$P^{(3)}_{TY1}$	−0.01	0	0.01	mm	Translation	$Y^{(3)}$-axis
$P^{(3)}_{RX2}$	−1	0	1	deg	Rotation	$X^{(3)}$-axis
$P^{(3)}_{RZ2}$	−1	0	1	deg	Rotation	$Z^{(3)}$-axis
$P^{(3)}_{TY2}$	−0.01	0	0.01	mm	Translation	$Y^{(3)}$-axis

2.2. Cutting Force Model

The empirical model derived by Kienzle [19] is chosen to model the tangential force, F_t, and the axial feed force, F_f, since it gives a good prediction for large variation in chip thickness, see Fig 1b. The model takes the effects from strain hardening of the workpiece material, induced in the previous revolution, into consideration. It is also the most commonly used model to predict cutting forces and cutting energy. Kienzle introduced the specific cutting coefficients (m_c, K_{c1}, m_f and K_f) which describes the amount of force required to remove material from the workpiece with a specific insert geometry. The forces are given by:

$$F_t = K_{c1} a_p h^{1-m_c} \tag{1}$$

$$F_f = K_f a_p h^{1-m_f} \tag{2}$$

where K_{c1} is the specific cutting force in tangential direction. The tool-workpiece dependent exponent of the tangential force, m_c, describes the behaviour of the cutting force in different materials. K_f is the specific feed force and m_f is the tool-workpiece dependent exponent of the feed force. The cutting forces are measured empirically at different feed rates, f_z. The cutting depth h is in the same direction as the feed and therefore it is directly connected to the feed and can be formulated as $h = f_z$, where f_z is the feed in axial direction. For an arbitrary parting operation the feed f_z is chosen as 0.2 mm/rev. The cutting width a_p is determined by the width of the insert and for the chosen tool the cutting width is 3 mm. The numerical values for the modelled cutting coefficients for the combination of $SS2541$ workpiece material and Corocut QD – NE – 0200 – 0502 – CM insert are $m_c = 0.22$, $K_{c1} = 1745\text{N/mm}^2$, $m_f = 0.47$ and $K_f = 605\text{N/mm}^2$. From empirical studies done by AB Sandvik Coromant it is found that 1° change in the rake angle give 1% change in the tangential force F_t and a 4% change in the feed force F_f. Assuming that this relationship is reasonable a linear variation term $\{1 - p_{t,f}\delta_{\alpha_r}\}$ is added to the Kienzle's force model Eqn.(1)-(2). Where p_t and p_f are amplification constants ($p_t = 0.01$ and $p_f = 0.04$) for the rake angle variation δ_{α_r}:

$$F_t = K_{c1} a_p f_z^{1-m_c}\{1 - p_t\delta_{\alpha_r}\} \tag{3}$$

$$F_f = K_f a_p f_z^{1-m_f}\{1 - p_f\delta_{\alpha_r}\} \tag{4}$$

Sign convention of δ_{α_r} gives that a $\delta_{\alpha_r} < 0$ results in a more negative rake angle which increases cutting forces, while $\delta_{\alpha_r} > 0$ gives an increased positive rake angle and reduced cutting forces [10, 11].

2.3. Finite Element Model

The finite element analysis is done with the commercial software Ansys®. The entire tool model consists of linear solid elements (*SOLID185*), with contact elements (*CONTA174*) on the contact surfaces (tool body) where the insert has *TARGE170* target elements, meaning that the contact methodology is surface-to-surface which is solved with an unsymmetric Newton-Raphson method. The insert is assumed to be rigid in relation to the tool body, since Corocut QD – NE – 0200 – 0502 – CM has a grade 1125 and is PVD-coated (Physical Vapor Deposition) with a $(Ti, Al)N$ composition. This gives a compressive yield strength significantly higher than the tool material ($SS\,2541$). A friction coefficient for contact between carbide and steel is chosen according to [20] as $\mu = 0.5$ in order to give a more realistic movement of the insert in the tip seat. The used material model for the tool body is a linear in-built steel model with Young's modulus given as $E = 200$ GPa and Poisson's ratio as $\nu = 0.3$.

For each observation and simulation a CAD (Computer Aided Design) model is generated where the geometry of the interface deviate from its nominal values. This will cause the contacting surfaces $LCS^{(3)}_{1,2}$, Fig. 2c - 2e, to penetrate the insert surface. The contact search algorithm adds a displacement in the normal direction of the contact elements, allowing the tool to open. Only the self clamping finger ($LCS^{(3)}_{1,2}$) is allowed to move in order to avoid any unrealistic deformations due to the contact search algorithm. Once all contacts are found with no penetration, the rigidity in the finger pushes the carbide insert down, locking it in place.

In the simulations the adaptor connecting the tool to machine is neglected. The interface between the adaptor and tool body is seen as rigid with no flexibility thus locking all degrees of freedom with an overhang of 50 mm. The cutting force is applied on the tip of the insert at $(0, 0, 0) \in GCS$, see Fig. 2a, in over the whole width with a depth of 0.2 mm corresponding to a feed of 0.2 mm/rev. The magnitude of the cutting forces are found to be $F_y = 1493$ N, $F_z = 773$ N and are experimentally retrieved by Sandvik Coromant. The carbide insert is prohibited to translate in the X-direction and rotate around Y and Z axes , meaning it can only translate in the YZ-plane of the global coordinate system GCS, see Fig. 2a.

2.4. Meta-Model

To analyse variation a meta-model relating tolerances to stress concentrations is designed with a second-order function with interaction terms.

$$\ln(\mathbf{Y}^{(s)}_i) = \boldsymbol{\beta}^{(s)}_0 + \sum_{j=1}^{r} \boldsymbol{\beta}^{(s)}_j \mathbf{X}^{(s)}_{i,j} + \epsilon^{(s)}_i, \text{ for } i \leq r \tag{5}$$

The function is built in such that each node on the contact surface has its own meta-model. Due to the over-constrained assembly, some design points may have one node with equivalent stresses around 1 GPa and in the next design point it is 0. The variation in the stress magnitudes can cause a poor fit between the simulated data and the meta-model. Therefore the nodal response, $\mathbf{Y}^{(s)} \in \mathbb{R}^{r \times n^{(s)}}$, is logarithmic, where r is the number of design points or observations and $n^{(s)}$ is the number of nodes for the surface s. The matrix $\mathbf{X} \in \mathbb{R}^{r \times (1+m)}$ is a matrix containing all terms of the 2^{nd}-order polynomial where m is the number of independent variables, and a column of ones to give the β_0 terms for each observation. The matrix $\boldsymbol{\beta}^{(s)} \in \mathbb{R}^{(1+m) \times n^{(s)}}$ is a matrix of the coefficients in the regression model and $\epsilon^{(s)} \in \mathbb{R}^{r \times n^{(s)}}$, defined by $\epsilon^{(s)} = \mathbf{Y}^{(s)} - \hat{\mathbf{Y}}^{(s)}$, is the matrix of residuals between the true response and the predicted response [21]. The model is then fitted by using least squares and finding the minimum vertical distance between the data points and polynomial line.

2.5. Variation Simulation Using a Meta-Model

The variation simulations are conducted using Direct Monte Carlo (DMC) simulations with the nodal meta-model, Eqn. 5. The input variables, Table 1, are randomly generated for each monte carlo simulations. In order to achieve a contact the magnitude of the stress in a node needs to be equal or exceed the compressive yield stress, $\sigma_c = 250$ [MPa], so called full contact. This gives the expression of the probability of full contact for a node i on the contacting surfaces of the tool body.

$$p_{fc}{}^{(s)}_i = \sum_{k}^{N} \frac{(\phi_i)^{(s)}_k}{N} \tag{6}$$

$$\phi^{(s)}_i = \begin{cases} 1 & \text{if } \hat{Y}^{(s)}_i \geq 250\text{MPa} \\ 0 & \text{else} \end{cases} \tag{7}$$

The number of DMC simulations is $N = 1000$ and the number of nodes on a contacting surface. $s = 1, 2, 3$, is given by $n^{(s)}$.

3. Results

To illustrate the application of the methodology a parting tool from the machining industry is used thus it fulfils the sought requirements of surface-to-surface contacts and an external load. In order to define a contact, the concept of full contact has been used. In order to minimize the computer resources used, the number of independent variables was reduced as described in Section 2.1. This resulted in four surfaces moving independent of each other thus giving an indirect effect on the rake angle dependent on the contact variation. The geometric variations are controlled through the CAD software where each surface is seen as a plane with at maximum six degrees of freedom.

3.1. Comparison Between Variation in the Fitted Model and the FE-model

The variation simulation is done by DMC with a randomly distributed sample space within the specified boundaries given in Table 1 for the fitted model. The surface plots in Fig. 3 show the probability of a full contact in a particular region for the

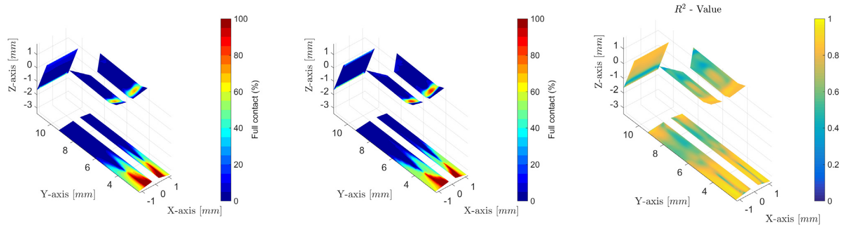

(a) Variational model for 1000 DMC iterations using the meta-model

(b) FE-model with r observations

(c) R^2-value plotted over the surfaces of the tip seat

Fig. 3: Probability of full contact on the tip seat

Table 2: Maximum and minimum values of the variation due to the rake angle variation, δ_{α_r}

Parameter			**Unit**
δ_{α_r}	−0.55	1.32	deg
$F_f(\delta_{\alpha_r})$	791	732	N
$F_t(\delta_{\alpha_r})$	1500	1472	N

meta-model and for the FEA. Here, full contact is equivalent to stresses equal to, or exceeding the compressive yield strength. This means that for the bottom surface, roughly 40% of the production outcomes will have contact close to the YZ-plane or close to the sides of the parting tool. Where the contact is located will have an effect on the deformation of the surface which in turn will affect the rake angle of the insert under operation.

3.2. Correlation Between Tolerances and Responses

In Fig. 4 a correlation between the input tolerances and the response, the effective stress, is shown over the surfaces of the tip seat. It can be seen that parameter $P^{(2)}_{RZ}$ has the most influence on the stress in the bottom surface (s = 2). On the back surface (s = 1) there is a field where the most significant parameter is $P^{(3)}_{TY1}$, which is unlikely. By observing the R^2-value in Fig. 3c the same field has a R^2-value of approximately 0.3 which shows a poor correlation with the FE-data. Therefore $P^{(3)}_{TY1}$ is not taken in to consideration for the adjustment of tolerances. It should be noted that there can exist cases where one parameter can have a 51% influence while another parameter have 49% and these are not taken into consideration. .

3.3. Variation Simulation with Adjusted Tolerances

It was found that $P^{(2)}_{RX}$ and $P^{(2)}_{RZ}$ and $P^{(3)}_{RZ1}$ had the most influence on the stress location and magnitude. By looking at their definition in the CAD-model, one can see that by changing the parameters from symmetric to positive asymmetric tolerances, contact variation is localized as seen in Fig. 3. The parameters are presented in Table 3 and the remaining parameters are kept the same. The probability for full contact can be seen in Fig. 5 for the tolerances defined in Table 3. In Table 4 the rake angle

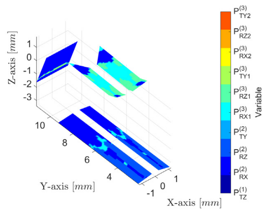

Fig. 4: Parameters with most correlation to the surface stresses

variation and force variation are presented with the new set of tolerances.

Table 3: Parameters with nominal value and upper/lower limits

Parameter	**Lower boundary**	**Nominal**	**Upper Boundary**	**Unit**
$P^{(2)}_{RX}$	0	0.5	1	deg
$P^{(2)}_{RZ}$	−0.8	−0.65	−0.5	deg
$P^{(3)}_{RZ1}$	0	0.5	1	deg

Table 4: Maximum and minimum values of the variation due to the rake angle variation, δ_{α_r}, with adjusted tolerances

Parameter			**Unit**
δ_{α_r}	−0.42	−0.08	deg
$F_f(\delta_{\alpha_r})$	787	776	N
$F_t(\delta_{\alpha_r})$	1498	1493	N

4. Conclusion

The proposed methodology was proven to be very successful in redefining the tolerances within the test space and finding the most influential parameters. Due to the factt that the method is based on FEA it can be applied on any situation where a finite element model can be provided and operational conditions are known, though further case studies needs to be done to confirm this. The methodology can be divided into four major steps (1) create a sample space using design of experiments, (2) simulate the test space using FEA, (3) build the meta-model for each node on the contacting surfaces and (4) optimize the contact variation.

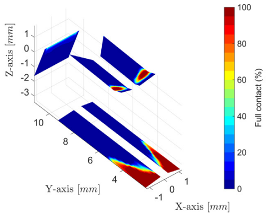

Fig. 5: Probability of full contact on the tip seat

A more detailed work process can be seen in Fig. 6 in the form of a flow chart. By following the developed methodology it was found that (1) three parameters had significant effects on the contact variations, see in Table 3 and (2) the rake angle was only dependent on $P_{RZ}^{(2)}$, the rotation of the bottom surface around its z-axis.

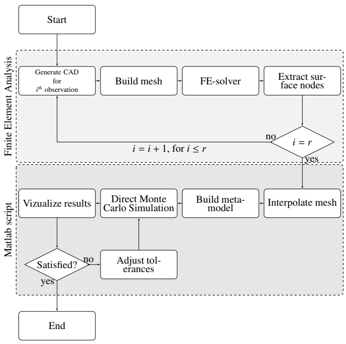

Fig. 6: Flow chart for the presented methodology to determine tolerances in early product development

The obtained results imply that variation simulations can be conducted for complex geometries where contact points are not known for systems under external forces, for example metal cutting operations. The finite element model and its surfaces variations have not been validated against physical experiments with respect to geometric variations, however for this paper the presented finite element model should be seen as a proof of concept. It is shown in Fig. 3c, that the meta-model was able to pick up and replicate the significant areas. This is assumed to be where the majority of the contact is located. The downside of using meta-models fitted with least squares is that it does not take outliers into consideration which can be of importance for over-constrained assemblies.

For future work it might be interesting to consider (1) validation of the finite element model, (2) how to optimize contact location with respect to robustness and key characteristics and (3) how to incorporate time variant deviations in the cutting process.

5. Acknowledgement

This work was carried out at the Wingquist Laboratory within the Area of Advance Production at Chalmers, supported by the Swedish Governmental Agency for Innovation Systems (VINNOVA). The support is gratefully acknowledged. A deep gratitude goes towards the department of Metal Cutting Modelling at AB Sandvik Coromant for the help and support.

References

[1] Wang, H., Rong, Y.K., Li, H., Shaun, P.. Computer aided fixture design: Recent research and trends. Computer-Aided Design 2010;42(12):1085–1094.
[2] Söderberg, R., Lindkvist, L.. Computer Aided Assembly Robustness Evaluation. Journal of Engineering Design 1999;10(2):165–181.
[3] Cai, W., Hu, S.J., Yuan, J.X.. Deformable Sheet Metal Fixturing: Principles, Algorithms, and Simulations. Journal of Manufacturing Science and Engineering 1996;118(3):318.
[4] Söderberg, R., Lindkvist, L., Dahlström, S.. Computer-aided robustness analysis for compliant assemblies. Journal of Engineering Design 2006;17(5):411–428.
[5] Schleich, B., Wartzack, S.. A discrete geometry approach for tolerance analysis of mechanism. MAMT 2014;77:148–163.
[6] Liu, S.C., Hu, S.J.. Variation Simulation for Deformable Sheet Metal Assemblies Using Finite Element Methods. Journal of Manufacturing Science and Engineering 1997;119(3):368.
[7] Lorin, S., Söderberg, R., Carlson, J., Edelvik, F.. Simulating Geometrical Variation in Injection Molding. In: International Conference on Methods and Tools for Product and Production Development; vol. Aug. 25-27. Göteborg; 2010,.
[8] Lorin, S., Lindkvist, L., Söderberg, R.. Simulating Part and Assembly Variation for Injection Molded Parts. In: International Design Engineering Technical Conferences & Computers and Information in Engineering Conference. Chicago; 2012,.
[9] Jayaprakash, G., Sivakumar, K., Thilak, M.. Parametric Tolerance Analysis of Mechanical Assembly Using FEA and Cost Competent Tolerance Synthesis Using Neural Network. J Software Engineering & Applications 2010;3:1148–1154.
[10] Shih, A.J.. Finite element analysis of the rake angle effects in orthogonal metal cutting. International Journal of Mechanical Sciences 1995;38(1):1–17.
[11] Günay, M., Korkut, I., Aslan, E., Seker, U.. Experimental investigation of the effect of cutting tool rake angle on main cutting force. Journal of Materials Processing Technology 2005;166(1):44–49.
[12] Altintas, Y.. Manufacturing Automation: Metal cutting mechanics, machine tool vibrations, and CNC design. 2nd ed.; New York: Cambridge University Press; 2012.
[13] Shaw, M.C.. Metal Cutting Principles. Oxford: Claredon Press; 1989.
[14] Stephenson, D.A., Agapiou, J.S.. Metal Cutting Theory and Practice. New York: Marcel Dekker; 1997.
[15] CorocutQD, . AB Sandvik Coromant. 20180306. URL: `https://www.sandvik.coromant.com/en-us/products/corocut-qd`.
[16] Stein, M.. Large Sample Properties of Simulations Using Latin Hypercube Sampling. Techometrics 1987;29(2).
[17] Mckay, M.D., Beckman, R.J., Conover, W.J.. A Comparison of Three Methods for Selecting Values of Input Variables in the Analysis of Output from a Computer Code. Techometrics 1979;21(2):239–245.
[18] Green, S.. How Many Subjects Does It Take to Do a Regression Analysis? MULTIVARIATE BEHAVIORAL RESEARCH 1991;26(3).
[19] Kienzle, O., Victor, H.. Spezifische Schnittkrafte bei der Metallbearbeitung. Werkstofftechnik und Machinenbau 1957;45(7):224–225.
[20] Holmberg, K., Matthews, A.. Coatings Tribology: Properties, Mechanisms, Techniques and Applications in Surface Engineering. Elsevier; 2009.
[21] Draper, N.R., Smith, H.. Applied Regression Analysis. 3rd ed. ed.; New York: John Wiley & Sons, INC; 1998.

Paper II

Reliability-Based Design Optimization of Surface-to-Surface Contact for Cutting Tool Interface Designs

S. Camuz, M. Bengtsson, R. Söderberg, K. Wärmefjord

Journal of Manufacturing Science and Engineering (Feb 2019), Vol. 141, Issue 4, p.141(4)

https://doi.org/10.1115/1.4042787

Soner Camuz[1]
Geometry Assurance,
Department of Industrial and Materials Science,
Chalmers University of Technology,
Göteborg, Sweden
e-mail: soner@chalmers.se

Magnus Bengtsson
Product Development,
Department of Industrial and Materials Science,
Chalmers University of Technology,
Göteborg, Sweden
e-mail: magnus.bengtsson@chalmers.se

Rikard Söderberg
Geometry Assurance,
Department of Industrial and Materials Science,
Chalmers University of Technology,
Göteborg, Sweden
e-mail: rikard.soderberg@chalmers.se

Kristina Wärmefjord
Geometry Assurance,
Department of Industrial and Materials Science,
Chalmers University of Technology,
Göteborg, Sweden
e-mail: kristina.warmefjord@chalmers.se

Reliability-Based Design Optimization of Surface-to-Surface Contact for Cutting Tool Interface Designs

In recent years, cutting tool manufacturers are moving toward improving the robustness of the positioning of an insert in the tool body interface. Increasing the robustness of the interface involves designs with both chamfered and serrated surfaces. These designs have a tendency to overdetermine the positioning and cause instabilities in the interface. Cutting forces generated from the machining process will also plastically deform the interface, consequently, altering the positioning of the insert. Current methodologies within positioning and variation simulation use point-based contacts and assume linear material behavior. In this paper, a first-order reliability-based design optimization framework that allows robust positioning of surface-to-surface-based contacts is presented. Results show that the contact variation over the interface can be limited to predefined contact zones, consequently allowing successful positioning of inserts in early design phases of cutting tool designs. [DOI: 10.1115/1.4042787]

1 Introduction

The durability of a cutting tool is dependent on different aspects such as insert grade and the positioning of the insert. Effects that will alter the positioning involve cutting force direction/magnitude and the stiffness in the interface, as well as geometric deviations of the interface, which is a result of manufacturing process variations [1–4]. Therefore, methodologies for reducing variational effects in the positioning of the insert are necessary to ensure durable cutting tool designs. In recent years, efforts in improving the robustness of the positioning of an insert in the tool body have been in focus. These efforts have involved both chamfered and serrated interfaces which have a tendency to overdetermine the positioning in the interface. With current tolerance analysis and allocation methodologies, it is near impossible to ensure the expected robustness due to the sheer complexity of the interface. It is also necessary to take plastic deformations in the interface into consideration. As the forces generated from the cutting process will not only affect the positioning but also plastically deform the interface, which can lead to altered cutting geometry for future operations with new inserts.

To model how variations propagate through an assembly, different approaches can be used, each with its advantages and disadvantages [5]. The most common approaches in various industries are the 3-2-1 locating scheme for rigid assemblies [6] and N-2-1 for compliant assemblies [7,8]. Research within variation analysis and fixturing in machining processes has mainly focused on workpiece fixturing and optimal fixture design layout [9–11]. These approaches, however, require that the positioning between two or more parts is point-based, resulting in unrealistic boundary conditions for cutting tools. The main contact in cutting tools between the insert and the tool body (which will be referred to as the interface from this point and on) are surface-to-surface contacts. For such contacts, a skin model [12] approach can be used. Schleich and Wartzack [13] present a quantitative study on tolerance analyses by comparing a skin model to three well-known methods: tolerance stack up, vector loops, and small displacement torsor. The authors also highlight the importance of integrating deformation and thermal effects in the skin model approach. Garaizar et al. [14] present a framework for integrating thermal effects in skin models by generating a finite element mesh of a CAD (Computer Aided Design) model. The mesh is updated by adding systematic and random variations to the nodes. The new mesh is then used to simulate thermal effects using finite element analysis (FEA). However, this approach does not take contact boundary conditions into consideration, which would require an additional static FEA after the variations have been added. Skin models with integrated effects will require numerous FE simulations for obtaining statistical data. This will be time expensive and resource heavy due to the nonlinearity of the boundary conditions. Therefore, the number of simulations must be minimized while not losing accuracy or the ability to collect enough data for statistical assessments.

A common method used within the automotive industry is method of influencing coefficients (MICs) [15] where a linear relationship between part deviations and the springback deviations is built for compliant sheet metal assemblies. Dahlström and Lindkvist [16] present an approach of implementing a contact search algorithm in the MIC methodology to avoid penetration of contacting surfaces. The implementation shows great significance in reducing computational time with limited loss in accuracy. MIC in its current state does not take material nonlinearity into consideration. Therefore, it is not suitable when stresses between a carbide insert and tool body will be equal to or exceed the yield limit of the material. Yu et al. [17] proposes an irregular quadrilateral plate element based on absolute nodal coordinate formulation (ANCF) to discretize scalloped segment plates with good coherence with physical experiments. However, ANCF approaches are typically designed for sheet metal assemblies with large deformations and rotations [18].

In this paper, the aim is to create a framework for reliability-based design optimization of surface-to-surface contacts for cutting tools and related products using a skin model approach. It is necessary

[1]Corresponding author.

Manuscript received May 28, 2018; final manuscript received January 23, 2019; published online February 27, 2019. Assoc. Editor: Radu Pavel.

Copyright © 2019 by ASME

Downloaded From: https://manufacturingscience.asmedigitalcollection.asme.org on 04/02/2019 Terms of Use: http://www.asme.org/about-asme/terms-of-use

to minimize the contact variation in order ensure robustness in the positioning of cutting tools. The framework for reliability-based design optimization uses a genetic algorithm with an implemented first-order reliability method (FORM) approach. The performance functions are based on the percentage of contact in the preferred contact zones (PCZs) and can be retrieved through sensitivity analyses. In cutting tool interface designs, it is necessary to reduce the distance between the supporting contacts to not break the inserts due to tensile loads. Closer contacts contradict fundamental principles within geometry assurance [8] and can result in a positioning that is sensitive to geometric variations. Using a reliability-based design optimization ensures that the found optima are robust and fulfills specified sigma criterion. Results from the framework can be used for GD&T specifications later in the design process.

The paper is organized as follows. In Sec. 2, the steps of the framework is presented. The results are presented in Sec. 3 for four case studies where the framework was applied. Case study I, Sec. 3.1, validates the use of FORM on a numerical data set. Case study II, Sec. 3.2, is an industrial application where three variables are used to describe the interface surface of the tool body, and the results are compared to direct Monte Carlo simulations (MCSs) of the performance function. Case studies III and IV, Secs. 3.3 and 3.4, expand the problem definition further by increasing the number of interfering surfaces in the interface. In Sec. 5, the conclusions are presented along with possible future work that can be implemented in the framework. Additional results from the genetic algorithm are presented in Appendices A–C.

2 Method

The framework uses a FORM-based approach for design optimization of surface-to-surface contacts. The objective function is to minimize and localize contact variations between two solid bodies. The PCZ is retrieved from sensitivity analyses prior to this framework.

The first step of the framework is to collect data and create a metamodel of the data. Data are collected by creating a design of experiments using Latin hypercube sampling, and each observation is simulated using FEA. The metamodel is built such that it describes the stress magnitudes of each node on the interface of the tool body, see more details in Ref. [19]. This will be the input to the genetic algorithm that optimizes the interface design of the tool body with respect to a 3σ criterion, meaning 89% of the generated products will satisfy the PCZs.

2.1 Data Collection and Metamodeling. The effectiveness of the framework will be presented on assemblies containing two individual parts for different surface geometries found within the field of metal cutting tools [20]. One part is defined as flexible (gray), see Fig. 1, with a linear material model, which will represent the tool body. The other part is seen as rigid (white) which represents a cemented carbide insert. The flexible body rests on a frictionless surface to avoid interference of boundary conditions. This allows translation in x and y directions while prohibiting translation in the z-direction. A distributed load $q(x, y)$ is acting on the rigid body that will compress the flexible body. The commercial FEA software, ANSYS® 16.2, is used for all FE simulations. The simulation process divides into three steps to help the model converge: (1) add a rigid translation to the rigid part in the z-direction to a certain point, (2) remove the rigid translation to let gravity and the springback of the flexible part adjust the initial position, and (3) add the distributed load $q(x, y)$. The entire tool model consists of linear solid elements (SOLID185), using contact element (CONTA174) and target elements (TARGE170) on the contact (tool body) and insert surfaces, respectively. The contact methodology is surface-to-surface solved with an unsymmetric Newton–Raphson method. A friction coefficient for contact between carbide and steel is chosen according to Ref. [21] as $\mu = 0.5$ to give a realistic movement of the insert in the tip seat. The material model for the tool body is a linear built-in steel model with Young's modulus given as $E = 200$ GPa and Poisson's ratio as $\nu = 0.3$.

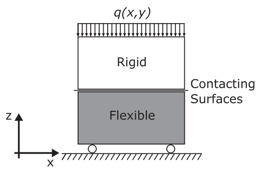

Fig. 1 Illustration of the FE models used in the case studies

Inputs to the FEA are design variables, controlling the geometric properties of the interface and altering the contact locations. The outputs from the FEA parametric study are the stresses and deformations in the nodes of the interface. The interface is further discretized to define the PCZs that are retrieved from various sensitivity analyses. The discretization is carried out by dividing the surface $\{n_x, n_y, n_z\} \in \mathbb{N}^+$ times, where the subscript determines the direction with respect to the local coordinate system. The surface discretization in the x-direction can be formulated as

$$\mathbf{Xd}_{ij_x} = \begin{cases} 1, & \text{if } \mathbf{N}_i^x < j_x \frac{L_x}{n_x} \\ 0, & \text{otherwise} \end{cases} \tag{1}$$

Here, $\mathbf{N}_i^x$ is a vector containing x-coordinates to the ith node. The total length in x-direction is given by the scalar L_x where $j_x = 1, \ldots, n_x$. The binary matrices for $\mathbf{Yd}_{ij_y}$ and $\mathbf{Zd}_{ij_z}$ are obtained in the same way. Each row corresponds to a node number and the columns are the discretized regions in the direction in either x, y, or z. The binary matrices given by Eq. (1) will contain a 1 for each node in a discretized region or a zero, 0, if it is not in the region. This allows the nodal positions of a discretized region to be obtained by element-wise multiplication of the matrices $\mathbf{Xd}$, $\mathbf{Yd}$, and $\mathbf{Zd}$. For example, to find the first discretized region in x-direction and the third in y direction, the notation would be $\zeta_i^{13} = \mathbf{Xd}_{i1} \odot \mathbf{Yd}_{i3}$.

2.2 First-Order Reliability Method. FORM is a semiprobabilistic approach that approximates the reliability of the system. A more direct approach to calculate the reliability is to use MCS; however, MCS is limited by the complexity of the problem definition. Larger systems tend to require more and more computational resources and are therefore not suitable in design optimization algorithms.

The definition [22] of reliability in FORM is the probability of the performance function $g(\mathbf{X})$ being greater than zero, $P\{g(\mathbf{X}) > 0\}$ where $\mathbf{X} = (X_1, X_2, \ldots, Xn)$ are the normally distributed random variables. It can also be seen as the stable region while $P\{g(\mathbf{X}) < 0\}$ is the unstable region or failure region. The performance function $g(\mathbf{X})$ is a black-box model which can be built using various kinds of data. These models often have high dimensions, leading to that a direct evaluation of the probability integration of failure

$$p_f = P\{g(\mathbf{X}) < 0\} = \int_{g(\mathbf{X})<0} f_x(\mathbf{x})\mathrm{d}\mathbf{x} \tag{2}$$

can prove to be very difficult to solve. Here, $f_x(\mathbf{x})$ is the joint probability density function of $\mathbf{X}$. Using FORM or other approximation methods, the probability integration can be approximated with good coherence. The derivation of FORM is divided into two basic steps [22]:

(1) simplify the integrand
(2) approximate the integration boundary

By simplifying the integrand, the random variables in the original X-space are transformed, using the Rosenblatt transformation [23] to the U-space. The U-space is a standard normal space with a

Downloaded From: https://manufacturingscience.asmedigitalcollection.asme.org on 04/02/2019 Terms of Use: http://www.asme.org/about-asme/terms-of-use

mean of 0 and a standard deviation of 1.

$$U = \Phi^{-1}[F_x(X)] = \Phi^{-1}\left[\Phi \frac{X-\mu}{\sigma_{std}}\right] = \frac{X-\mu}{\sigma_{std}} \tag{3}$$

By transforming to the U-space, the contours of the integrand become concentric circles without any loss of accuracy. This provides a probability integration that is less complicated to solve than in the original X-space.

The joint probability density function (PDF) in the U-space is the product of each individual PDF of the normal standard distribution, due to the fact that the random variables are independent. The probability integration of failure in the transformed U-space becomes

$$p_f = \int \ldots \int_{g(u_i)<0} \prod_{i=1}^{n} \frac{1}{\sqrt{2\pi}} \exp\left(-\frac{1}{2}u_i^2\right) \mathrm{d}u_i, \quad i \in n \tag{4}$$

To simplify the integration boundary further, the performance function for the integration boundary, $g(\mathbf{U}) = 0$ is approximated using first-order Taylor expansion.

$$g(\mathbf{U}) \approx \mathbf{u}^* + \nabla g(\mathbf{u}^*)(\mathbf{U} - \mathbf{u}^*)^T \tag{5}$$

This allows the following optimization problem to be formulated:

$$\begin{aligned} &\min_u \|\mathbf{u}\| \\ &\text{subject to} \quad g(\mathbf{u}) = 0 \end{aligned} \tag{6}$$

The solution to the optimization formulation given in Eq. (6) gives the most probable point (MPP) u^*. The MPP describes the minimal Euclidean distance from a starting point to the limit state $g(\mathbf{U}) = 0$. The reliability and probability of failure are given in each iteration i as

$$\Phi(-\beta_i) = \Phi\left(-\left[\beta_{i-1} + \frac{\nabla g}{\|\nabla g\|}\right]\right) \tag{7}$$

Here, Φ is the normal cumulative density function. For a more detailed derivation and step-by-step explanation, the Refs. [22,24] are suggested for the interested reader. A flowchart of the algorithm is presented in Fig. 2 together with the design optimization routine.

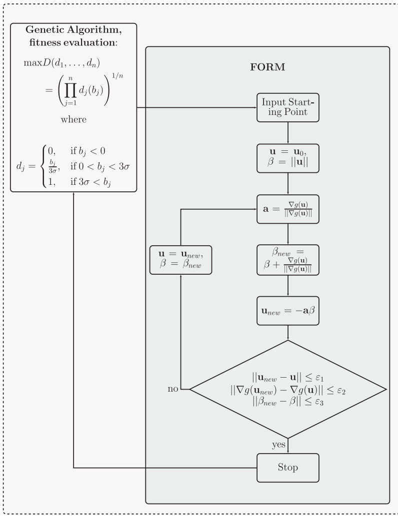

Fig. 2 Objective function algorithm for finding the most probable point

2.3 Surface-to-Surface Contact Location Optimization.

The problem definition of the optimization is to find a set of design variables that minimize the contact variation over the interface to a predefined set of zones, PCZ. As mentioned, the PCZs are retrieved from sensitivity analyses with the condition to not exert any excessive stresses on the cemented carbide, modeled as a rigid body. With this formulation, it is inevitable that numerous local optima be found. This is why it is necessary to approach the optimization problem using a stochastic method instead of a gradient-based approach.

A standard genetic algorithm is used with an implemented correlation factor, which is retrieved from the correlation matrix of the design variables and the response. The correlation factor allows for faster convergence and a reduced likelihood for finding a local optimum. The genetic algorithm follows a standard procedure and uses the gray encoder to retrieve corresponding design variables from the randomly generated binary strings, the chromosomes. Tournament selection is used to determine which chromosomes generate new individuals. The genetic algorithm also uses an elitism selection to allow for the best individual to reproduce regardless of the results from the crossover and mutations. A more detailed explanation of the genetic algorithm can be found in Ref. [25].

The correlation factor allows for the decoded variables to move faster toward an overall solution. By using the correlation matrix, the effect of each variable on the response can be retrieved. The step size is determined by the distance from an individual to its corresponding limit value with respect to the sign convention of the correlation, which means lower design limit for negative correlation and upper design limit for positive correlation. The significance of a correlation is determined by the p-value, a p-value of $p \leq 0.05$ is deemed to be a significant correlation. The correlation factor for a single-variable correlation is formulated as

$$c_j = \Delta d^{\pm} C(x, y_j) \tag{8}$$

Here, $\Delta d^{\pm}$ is the distance from the decoded chromosome to its corresponding upper (+) or lower (−) design limit and C is a matrix containing significant correlations of the x variable on the y_j response. The effect on a response is rarely dependent on only one variable. Each variable correlation must be weighted. The correlation factor for multiple variable correlations is formulated as

$$c_{i,j} = \sum_{k=1}^{n} \Delta d^{\pm} C_k(x_i, y_j) w_{i,k} \tag{9}$$

Here, $w_{i,k} = |C_k(x_i, y_j)| / \sum |C_k(x_i, y_j)|$ is the weight of each variable's effect on the response, for $k = 1, \ldots, n$ correlating variables, where n is the number of variables. As mentioned, the correlation factor is added to the corresponding design variables after the gray decoder, such that $x_{dn} = x_d + c_{i,j}$, for each individual in the population.

2.4 Fitness Function.

The FORM-based approach is incorporated in the fitness function when evaluating each individual in the population. The performance functions are defined as the ratio of stress to full contact stress within a PCZ compared to the whole contacting surface. Full contact refers to the stress magnitude in a single node exceeding the compressive yield strength of the material. The limit state is based on the number of defined PCZs and the geometry of the interface. The performance function is formulated as

$$g_j(\mathbf{X}) = \frac{\sigma_{\Omega_j}(\mathbf{X})}{\sigma_{\Sigma}} - (g_s)_j \tag{10}$$

Downloaded From: https://manufacturingscience.asmedigitalcollection.asme.org on 04/02/2019 Terms of Use: http://www.asme.org/about-asme/terms-of-use

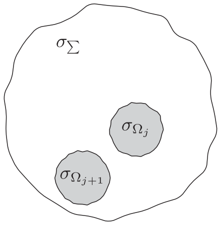

Fig. 3 PCZs, Ω_j, on the interface, Σ

Here, σ_{Ω_j} is the full contact stress in the jth PCZ, Ω_j, and σ_Σ is the full contact stress of the interface, see Fig. 3. The reliability index, b_j, for each response is calculated according to Eq. (7), and the fitness of an individual is based on the desirability approach.

$$\max D(d_1, \ldots, d_n) = \left(\prod_{j=1}^{n} d_j(b_j)\right)^{1/n} \tag{11}$$

where

$$d_j = \begin{cases} 0, & \text{if } b_j < 0 \\ \dfrac{b_j}{3\sigma}, & \text{if } 0 < b_j < 3\sigma \\ 1, & \text{if } 3\sigma < b_j \end{cases} \tag{12}$$

3 Results

The results of the proposed surface-to-surface contact location optimization methodology will be presented in four case studies. It is shown that a FORM-based approach can be used to optimize design variables to minimize variation in contact location for surface-to-surface contacts. The first case study shows the validity of using a FORM-based approach to calculate reliability using numerical data. The second case study presents the validity of the calculated reliability by comparing the results to direct Monte Carlo simulations. The third case study expands the complexity of the interface further with a two-dimensional serrated surface, which can be described by using four separately interfering surfaces. The fourth case study uses a three-dimensional serrated surface which can be described using eight separately interfering surfaces. The geometry of case studies III and IV are chosen to resemble the interface of modern cutting tools out in the market today. The contact variation optimization algorithm is applied for case studies II–IV.

3.1 Case Study I: Cantilever Beam. A uniform cantilever beam, see Fig. 4, with a rectangular cross section with width $w = 2$ in. and height $t = 4$ in. is used to validate the use of numerical data in a FORM-based approach. The beam is of length $L = 100$ in. and is subjected to the normally distributed loads $P_x \sim N(500, 100)lb$ and $P_y \sim N(1000, 100)lb$ at its tip. The failure mode is when the tip displacement exceeds the allowable value $D_0 = 3$ in. [22]. The performance function can now be formulated as

$$g(P_x, P_y) = D_0 - \frac{4L^3}{Ewt}\sqrt{\left(\frac{P_y}{t^2}\right)^2 + \left(\frac{P_x}{w^2}\right)^2} \tag{13}$$

Where the modulus of elasticity is $E = 30 \times 10^6$ psi. The example is solved by the proposed approach. Even though there exists an analytical expression, the gradients are solved numerically with small steps. A solution is found at $\mathbf{u}^* = (1.72,\ 0.28)$ with a reliability index of $\beta = 1.7429$, after 38 iterations. The MPP search history can be seen in Fig. 5. This can be compared with the results in Ref. [22], $\mathbf{u}^{*e} = (1.74,\ 0.16)$ with a reliability index of $\beta^e = 1.7444$, which is found after three iterations. Even though the MPP between them are somewhat different, the reliability index β differs with less than 0.1%. It is assumed that the found MPP is a valid optimum for the performance function equation (13), which also validates the use of FORM for numerical data.

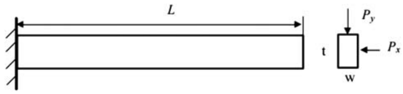

Fig. 4 Cantilever beam, subjected to horizontal and vertical loads [22]

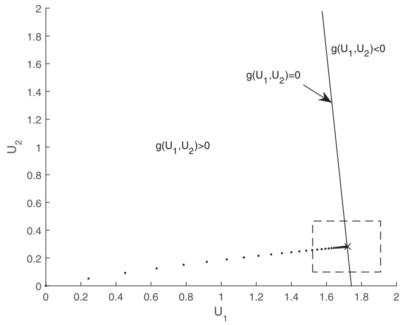

Fig. 5 MPP search history in U-space

3.2 Case Study II: Industrial Application, Three Variables. The second case study implements the proposed optimization routine in an industrial case. The investigated geometry is the bottom surface of a CoroCut QD parting tool, see Fig. 6(*a*). The PCZs are chosen such that the distance between them is minimized, see Fig. 6(*b*). For illustrative purposes, the presented approach for contact location optimization of surface-to-surface contacts is presented using three variables that will control the bottom surface $LCS^{(2)}$ of the tool body, see Fig. 6(*a*).

The presented approach finds a nominal set of design variables for a given normal distribution with a standard deviation σ that fulfills the performance function. For the case of a parting tool,

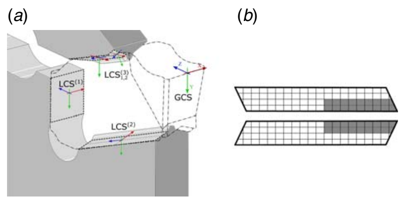

Fig. 6 Case study II Illustration, Corocut QD: (*a*) illustrated model and (*b*) PCZs (grayed) in the interface

Downloaded From: https://manufacturingscience.asmedigitalcollection.asme.org on 04/02/2019 Terms of Use: http://www.asme.org/about-asme/terms-of-use

Corocut QD, it is said that at least $\mathbf{g}_s^{II} = [0.3, 0.3]^T$ of the full contact stresses should be inside the PCZ, Fig. 6(*b*). The performance function is stated as described in Eq. 10 with the normally distributed design variables $X_{rx} \sim N(0, \sigma_{std})$, $X_{ry} \sim N(70.75, \sigma_{std})$, and $X_{rz} \sim N(0, \sigma_{std})$. The standard deviation is arbitrarily chosen as $\sigma_{std} = 0.1$. Variation simulations of the interface is seen in Figs. 7(*a*) and 7(*b*) for design variables before and after optimization, respectively. Due to the stochastic nature of the GA, it was run ten times in order to affirm a valid optimum. The correlating variables are presented in Table 1 and result for each run is presented in Table 2 in Appendix A. The optimum set of design variables is chosen as the point closest to the mean of the results, marked with a *.

The optimum that satisfies the objective function is found at X (-0.05, 69.87, 0.45) with a reliability that satisfies 3σ criteria ($\beta =$ 0.067). The reliability was validated with MCS running 100, 000 simulations where the performance function equation (10) is used and what is sought is the $P[g(X) < 0]$. The MCS is visualized in Fig. 8, where light dots represent points in the stable region $g(\mathbf{X}) > 0$ and dark dots the unstable region $g(\mathbf{X}) < 0$. It was found that the probability of failure is 0.06865, which is roughly a 2% difference between the approximated reliability using FORM. The simulation time for100, 000 simulations using MCS was 7.8 s where the FORM-based approach is almost instantaneous at 0.31 s. The time difference is assumed to increase exponentially for larger cases with more design variables. The MCS also validates the performance function used in the FORM-based approach.

3.3 Case Study III: 3D Serration, Four Variables.

The third case study has a 2D serrated surface, see Fig. 9(*a*) which is described using four rotational degrees of freedom $(x_1, \ldots, x_4) \sim N$ (0, 0.1). The limit states of the third case study are set to $\mathbf{g}_s^{III} = [0.45, 0.45]^T$, which indicates that in order for the MPP to be in a safe region at least 45% of the total stresses should be above or equal to $\sigma_{c,y}$ for each PCZ, see Fig. 9(*b*). The PCZs are placed on the peaks of the jagged interface in order to minimize the distances between contacting points and to reduce the reaction forces acting on the insert.

Variation simulations of the nominal design variables are shown in Fig. 10(*a*). It can be observed that for the majority of generated samples the contacts are within the PCZ. However, for approximately 20% of the generated samples, there is contact at either $x = 0$ and/or $x = 30$. The correlating variables are presented in Table 3 and result for each run is presented in Table 4 in Appendix B. Performing a variation simulation of the found optima X(1.58, $-$0.48, 1.03, $-$1.04), it is evident in Fig. 10(*b*) that the contact location variation has been minimized to the PCZ and satisfies 3σ conditions.

3.4 Case Study IV: 3D Serration, Eight Variables.

The fourth case study expands the complexity further by investigating a 3D-serrated surface, see Fig. 11(*a*). The surface variations are determined by eight design variables, $(x_1, \ldots, x_8) \sim N(0, 0.1)$, which define rotation around certain axes on the interface. The PCZs are placed, as in previous cases, at the peaks of the jagged interface in order to reduce reaction forces on the insert, see Fig. 11(*b*). The limit state for the fourth case study is set to $\mathbf{g}_s^{IV} = [0.15, 0.15, 0.15, 0.15]^T$.

The optimum set of design variables that minimize the contact location variation to the PCZ and satisfies the 3σ criteria is found at $X(-0.36, 1.06, -1.24, 1.03, -1.09, 0.46, -0.79, 0.36)$. Variation simulations before and after the proposed optimization routine can

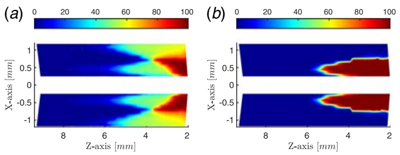

Fig. 7 Variation simulation, Corocut QD: (*a*) surface variation, using three variables, before contact location optimization and (*b*) optimized set of design variables

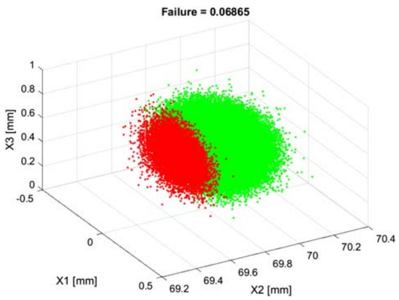

Fig. 8 Monte Carlo simulation for $g(\mathbf{X}) < 0$, failure $= 0.06865$

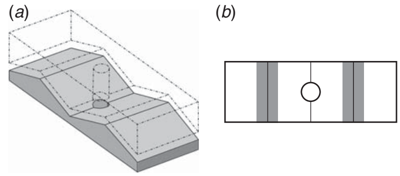

Fig. 9 Case study III illustration, 2D serration: (*a*) illustrated model and (*b*) PCZs (grayed) in the interface

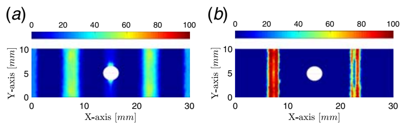

Fig. 10 Variation simulation 2D serration: (*a*) surface variation, using four variables, before contact location optimization and (*b*) optimized set of design variables

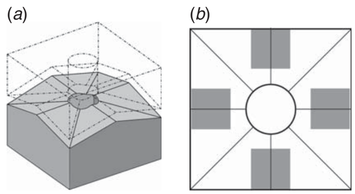

Fig. 11 Case study IV illustration, 3D serration: (*a*) illustrated model and (*b*) PCZs (grayed) in the interface

Downloaded From: https://manufacturingscience.asmedigitalcollection.asme.org on 04/02/2019 Terms of Use: http://www.asme.org/about-asme/terms-of-use

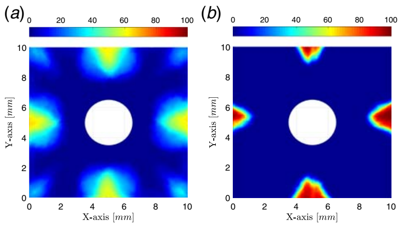

Fig. 12 Variation simulation 3D serration: (*a*) surface variation, using eight variables, before contact location optimization and (*b*) optimized set of design variables

be seen in Figs. 12(*a*) and 12(*b*). The correlating variables are presented in Table 5 and result for each run is presented in Table 6 in Appendix C.

4 Discussion

The first case study shows a negligible loss in accuracy when numerical data is used compared to analytical data. This allows for more complex models to be analyzed. The reliability of the found optimum was validated in the second case study by comparing the results to DMC simulations of the performance function. The FORM algorithm calculates the reliability instantaneously while DMC with 100, 000 simulations takes roughly 7.8 s. This difference is notable, and FORM will prove to be of great importance for larger systems containing more variables and for larger populations in the genetic algorithm. The third and fourth case study expand the complexity of the interface further and show the effectiveness of the presented approach with regards to restricting the contact variations to the PCZ. However, the chosen state limits, $\mathbf{g}_s^{\mathbf{II}\cdots\mathbf{IV}}$, that define the stress ratio σ_r are chosen ad hoc. The size of the PCZ will vary depending on the application, altering the state limit criteria. For future implementations, this issue needs to be taken into consideration.

Defining where and how large the contact area is between two bodies can be difficult. Using the concept of full contact, i.e., that contact exists if a node is equal to or exceed the compressive yield strength of the material, can give misleading contact formulation as stress concentrations can occur in areas without contact, i.e., in areas with high curvatures. However, using a minimum distance criterion between the target (tool body interface) and master (carbide insert) surface can also give a misleading contact since fulfilling this criterion does not necessarily contribute to a load-bearing contact, which means that the master and slave nodes are in the vicinity but not carrying any load, thus giving a larger contact area. The minimum distance criteria have not been considered in the presented paper. However, any future implementations of the framework should take consideration for both full contact and minimum distance criteria in order to avoid incorrect contact areas.

5 Conclusion

Current methodologies within positioning and tolerance analysis do not take account for surface-to-surface contacts and nonlinear material behavior. Addressing this issue, a framework for reliability-based design optimization for locating schemes with surface-to-surface contacts was proposed. The framework uses a FORM-based approach on numerical data to reduce computational time when calculating the reliability of the design. Future applications are required to:

- reduce computational time of the FEA,
- investigate the effect of load-bearing surfaces and implement surface topography to the algorithm,
- implement an algorithm to suggest GD&T based on the found optimum, and
- investigate the effect of time-dependent cutting forces found in drilling and milling operations.

Acknowledgment

This work was carried out at the Wingquist Laboratory within the Area of Advance—Production at Chalmers, supported by the Swedish Governmental Agency for Innovation Systems (VINNOVA). The support is gratefully acknowledged. A deep gratitude goes toward the Department of Metal Cutting Modelling at AB Sandvik Coromant for the help and support.

Appendix A: GA Results Case II

Table 1 Correlation factors for study case II with three variables

	x_1	x_2	x_3
$\mathbf{g}_1$	−0.5098	−0.3820	0.0000
$\mathbf{g}_2$	−0.2390	−0.8165	0.0000

Table 2 Results from 10 GA runs for case II

Run	x_1	x_2	x_3
1	−0.08	−0.89	−0.34
2	−0.16	−0.85	0.79
3	0.06	−0.85	−0.16
4	0.05	−0.84	0.60
5	0.06	−0.83	0.48
6*	−0.05	−0.88	0.45
7	−0.09	−0.89	0.70
8	−0.39	−0.88	−0.05
9	−0.10	−0.86	0.84
10	−0.08	−0.89	0.51
Avg.	−0.08	−0.87	0.38
Std	0.14	0.02	0.42

Appendix B: GA Results Case III

Table 3 Correlation factors for study case III with four variables

	x_1	x_2	x_3	x_4
$\mathbf{g}_1$	0.4345	−0.5318	−0.1911	0.0000
$\mathbf{g}_2$	0.0000	0.0000	0.5515	−0.4144

Table 4 Results from 10 GA runs for case III

Run	x_1	x_2	x_3	x_4
1	1.52	−0.11	−0.07	−1.53
2	1.39	−0.41	0.42	−1.64
3	1.69	−0.31	1.16	0.14
4	1.24	−0.63	0.65	−1.61
5*	1.58	−0.48	1.03	−1.04
6	1.44	−0.26	0.26	−1.45
7	1.68	−0.38	0.80	−1.31
8	1.59	−0.66	1.21	−0.50
9	1.70	−0.81	1.34	−0.34
10	1.57	−0.44	1.12	−0.23
Avg.	1.54	−0.45	0.79	−0.95
Std	0.15	0.21	0.47	0.66

Downloaded From: https://manufacturingscience.asmedigitalcollection.asme.org on 04/02/2019 Terms of Use: http://www.asme.org/about-asme/terms-of-use

Paper III

Nonlinear Material Model in Part Variation Simulations of Sheet Metals

S. Camuz, S. Lorin, K. Wärmefjord, R. Söderberg

Journal of Computing and Information Science in Engineering (Jun 2019), Vol. 19, Issue 2, p.19(2)

https://doi.org/10.1115/1.4042539

Soner Camuz[1]
Department of Industrial and Materials Science,
Chalmers University of Technology,
Gothenburg SE-41296, Sweden
e-mail: soner@chalmers.se

Samuel Lorin
Fraunhofer Chalmers Centre,
Chalmers University of Technology,
Gothenburg SE-41288, Sweden

Kristina Wärmefjord
Department of Industrial and Materials Science,
Chalmers University of Technology,
Gothenburg SE-41296, Sweden

Rikard Söderberg
Department of Industrial and Materials Science,
Chalmers University of Technology,
Gothenburg SE-41296, Sweden

Nonlinear Material Model in Part Variation Simulations of Sheet Metals

Current methodologies for variation simulation of compliant sheet metal assemblies and parts are simplified by assuming linear relationships. From the observed physical experiments, it is evident that plastic strains are a source of error that is not captured in the conventional variational simulation methods. This paper presents an adaptation toward an elastoplastic material model with isotropic hardening in the method of influence coefficients (MIC) methodology for variation simulations. The results are presented in two case studies using a benchmark case involving a two-dimensional (2D) quarter symmetric plate with a centered hole, subjected to both uniaxial and biaxial displacement. The adaptation shows a great reduction in central processing unit time with limited effect on the accuracy of the results compared to direct Monte Carlo simulations. [DOI: 10.1115/1.4042539]

Keywords: variation simulation, FEM, nonlinear material, method of influencing coefficients

1 Introduction

Dimensional part deviations induced by the manufacturing process are impossible to avoid and can lead to parts and assemblies not fulfilling their specified functional requirements. In recent years, the variations caused by the manufacturing process have been given more attention in response to an increase in computational efforts in simulating the processes. Being able to predict the variations caused by the manufacturing process will enable companies to reduce the number of inspections and take account for any uncertainties in early product development stages. Over time, different methodologies have been developed to specify tolerance limits to ensure that specific functional requirements are fulfilled. Each one has certain advantages and disadvantages compared to the other [1]. Söderberg and Lindkvist [2] present an approach on robustness evaluations and coupling analysis based on Suh's Axiom which states that, in a good uncoupled design, each functional requirement is satisfied by one and only one design parameter [3]. The overall main objective within geometry assurance is to increase the reliability of the manufactured part, thereby increasing the overall quality of the product. To achieve this, variations caused by the process must be taken into consideration during tolerance analysis. Most manufacturing processes plastically deform the workpiece into its desired shape and size. This induces residual stresses into the workpiece which will cause geometric variations as the stresses are relaxed. Most applications within variation simulation do not take the nonlinear properties of the workpiece material into consideration due to extensive simulations.

Variation simulation of deformable, i.e., nonrigid, sheet metal assemblies is a common industrial application of variation simulation. Here, the material model is typically assumed to be within the elastic region of its material properties. The most common approach for deformable sheet metal assemblies uses the method of influence coefficients (MICs) [4] to form a linear relationship between the part deviations and the springback deviations of the spot-welded assembly. This allows a great reduction in central processing unit time compared to direct Monte Carlo simulations (MCS), where the full finite element analysis (FEA) model is solved at each randomly generated disturbance. The MIC methodology within variation simulations laid the basis for continued development of the methodology and the field of variation simulations. Dahlström and Lindkvist [5] present an approach for implementing a contact search algorithm in the MIC methodology to avoid penetration of contacting surfaces. The implementation shows great significance in reducing computational time with limited loss of accuracy. Physical experiments have shown that plastic strains occur in the contacts between parts and fixtures, and plastic strains are induced in the material through the manufacturing process. Adopting the MIC methodology with these conditions will reduce its accuracy due to nonlinearities in the material and is a source of error in variation simulations. The importance of using nonlinear material models in variation simulations is discussed in Ref. [6].

The most common types of joining operations for sheet metal assemblies within the automotive industry are either riveting or spot welding, with the latter being the method of choice due to weight requirements. Resistance spot welding involves using two copper alloy electrodes to deliver a high current in a small contacting area while clamping two sheet metal plates together. A major benefit of this process is that the energy required to melt the metal can be delivered in a very short amount of time, 10–100 ms. As a result of this, the remainder of the plate does not gain any excessive heat. It can, therefore, be assumed that the largest contribution to assembly deviation is from the clamping of two metal sheet rather than the heat generated from the spot welding process. Moos and Vezzetti [7] found that for resistance spot welding, the effects of plastic deformation in the contacting region between the electrodes have an effect on the assembly deviations. The position deviation of the spot welds will also have an impact on the assembly deviations. Söderberg et al. [8] analyzed scanned data from the automotive industry. They found that the variation and position of the spot welds have a significant effect on assembly deviations. Wärmefjord et al. [9] investigated the effect of part variation on assembly variation in a welding operation. One of the main contributors to assembly deviations from the welding operations is the release and redistribution of residual stresses on the parts. The residual stresses are most likely induced through plastic deformation of the material during manufacturing. By determining the magnitude and distribution of the plastic strains on a part level, it is possible to have more accurate variation simulations of spot welding and welding operations.

[1]Corresponding author.

Contributed by the Computers and Information Division of ASME for publication in the JOURNAL OF COMPUTING AND INFORMATION SCIENCE IN ENGINEERING. Manuscript received April 8, 2018; final manuscript received December 13, 2018; published online March 18, 2019. Assoc. Editor: Krishnan Suresh.

Copyright © 2019 by ASME

Downloaded From: https://computingengineering.asmedigitalcollection.asme.org on 04/02/2019 Terms of Use: http://www.asme.org/about-asme/terms-of-use

Variation simulation has gone from rigid simulations to linear compliant simulations, and in the future, will advance to nonlinear compliant simulations. The aim of this paper is to present an adaptation of the MIC toward use for nonlinear material models, which will be referred to as the nonlinear MIC(NLMIC). This can greatly reduce the simulation time of nonlinear simulations and allows for larger samples to be simulated in order to get statistical significance. The information obtained, i.e., the plastic strain distribution of all nodes, can be used as input for welding and heat treatment simulations which can improve the accuracy of predicting warping in heated sheet metals. Reduced simulation time can make it possible to carry out fatigue simulations, with respect to assembly and geometric deviations, faster. This opens up for the possibility of more efficiently optimizing parameters in life-cycle analyses.

1.1 Scope of the Paper. It is important to capture plastic deformation in order to predict springback deviations after heat treatments and welding due to built-in stresses. It can also be related to fatigue and life expectancy predictions. Furthermore, it is important for assemblies with interchangeable parts to avoid malfunctions when replacing parts due to wear and tear. In this paper, an adaptation of the nonlinear material model by Han and Reddy [10,11] is applied for variation simulation. The material model used is an elastoplastic with isotropic hardening. The approach is based on using displacement and plastic strain components as the primary variables, compared to a strain rate dependent model, such as Havner and Patel [12], or a stress-dependent model, such as Johnson [13].

The methodology is presented in Sec. 3, and two case studies are evaluated as proof of concept on a two-dimensional (2D) quarter symmetric plate with a centered hole that is subjected to a prescribed displacement(s) [14]. The first case study, found in Sec. 4.1, focuses on the accuracy and validity of the method as it is subjected to a uniaxial strain. The second case study, found in Sec. 4.2, shows the validity of the assumption that the superposition principle can be applied to the linearized models. The material model and the finite element approach by Han and Reddy [10] are presented in the Sec. 2. Finally, the results are discussed and conclusions are drawn in Sec. 5. Future work is outlined in Sec. 6.

2 Boundary-Value Problem for Elastoplasticity

The MIC, described earlier, is based on the assumption of linearity; that is geometric linearity (small strain theory) and material linearity (the relation between strain and stress is linear). In this paper, we are considering the MIC for models using an elastoplastic material model that is not linear. This section provides a brief description of the finite element method for a small strain elastoplastic model. The nonlinear MIC described in Sec. 3 is based on this formulation.

The elastoplastic problem is to find the displacement $\boldsymbol{u}$, plastic strain $\boldsymbol{p}$, and internal parameters $\boldsymbol{\xi}$ (e.g., back-stress or kinematic hardening). These are written collectively as $\boldsymbol{w} = (\boldsymbol{u}, \boldsymbol{P})$, where $\boldsymbol{P} = (\boldsymbol{p}, \boldsymbol{\xi})$ is the generalized plastic strain. The region of admissible generalized stresses, $\boldsymbol{\Sigma} = (\boldsymbol{\sigma}, \boldsymbol{\chi})$, consisting of stress $\boldsymbol{\sigma}$ and internal forces $\boldsymbol{\chi}$ is defined using a yield function $\phi(\boldsymbol{\Sigma})$

$$K = \{\boldsymbol{\Sigma}\colon \phi(\boldsymbol{\Sigma}) \le 0\} \tag{1}$$

The flow law [10] can be written as

$$\boldsymbol{\Sigma} \in \partial D(\dot{\boldsymbol{P}}) \tag{2}$$

where $\partial D(\dot{\boldsymbol{P}})$ is the set of subgradients to the plastic dissipation function $D(\dot{\boldsymbol{P}})$

$$\partial D(\dot{\boldsymbol{P}}) = \{\boldsymbol{\Sigma} \in K\colon \quad D(\boldsymbol{Q}) \ge D(\dot{\boldsymbol{P}}) + \boldsymbol{\Sigma}\colon (Q - \dot{\boldsymbol{P}}) \quad \forall \boldsymbol{Q}\} \tag{3}$$

where $\boldsymbol{Q}$ is the space of generalized plastic strain.

The relations in Eqs. (1)–(3) can be used to formulate the primal problem of elastoplasticity, i.e., find the displacement $\boldsymbol{u}$, $\boldsymbol{p}$, and $\boldsymbol{\xi}$ that satisfy the equilibrium equation

$$\nabla \cdot \boldsymbol{\sigma} + \boldsymbol{f} = 0 \quad \text{in}\,\Omega \tag{4}$$

The strain–displacement relation

$$\boldsymbol{\varepsilon} = \frac{1}{2}\left(\nabla \boldsymbol{u} + (\nabla \boldsymbol{u})^{\mathrm{T}}\right) \tag{5}$$

The constitutive relations

$$\begin{aligned} \boldsymbol{\sigma} &= \boldsymbol{C}(\boldsymbol{\varepsilon}(\boldsymbol{u}) - \boldsymbol{p}) \\ \boldsymbol{\chi} &= -\boldsymbol{H}\boldsymbol{\xi} \end{aligned} \tag{6}$$

where $\boldsymbol{C}$ is the elasticity tensor and $\boldsymbol{H}$ is the hardening modulus and the plastic flow

$$(\dot{\boldsymbol{p}}, \dot{\boldsymbol{\xi}}) \in \boldsymbol{K}_p D(\boldsymbol{q}, \boldsymbol{\eta}) \ge D(\dot{\boldsymbol{p}}, \dot{\boldsymbol{\xi}}) + \boldsymbol{\sigma}\colon (\boldsymbol{q} - \dot{\boldsymbol{p}}) + \boldsymbol{\chi}\colon (\boldsymbol{\eta} - \dot{\boldsymbol{\xi}}) \;\; \forall (\boldsymbol{q}, \boldsymbol{\eta}) \in \boldsymbol{K}_p \tag{7}$$

where $\boldsymbol{K}_p = \operatorname{dom} D(\dot{\boldsymbol{P}})$ is the effective domain of D, i.e.,

$$\operatorname{dom} D = \{\dot{\boldsymbol{P}}\colon D(\dot{\boldsymbol{P}}) < \infty\} \tag{8}$$

For details of the formulation of this problem, see Ref. [11].

2.1 Variation Formula for the Plasticity Problem and the Solution Strategy. In this section, we will formulate a variation inequality based on the formulation above. We begin by defining $a(\boldsymbol{w}, z)$

$$a(\boldsymbol{w}, z) := \int_\Omega \mathrm{C}(\varepsilon(\boldsymbol{u}) - \boldsymbol{p})\colon (\varepsilon(\boldsymbol{v}) - \boldsymbol{q}) + \boldsymbol{\chi}\colon \boldsymbol{H}\boldsymbol{\eta}\, dx \tag{9a}$$

and the linear form $l(z)$

$$l(z) := \int_\Omega \boldsymbol{f}(t) \cdot \boldsymbol{v}\, dx \tag{9b}$$

and the (nondifferentiable) functional

$$j(z) := \int_\Omega D(\boldsymbol{q}, \boldsymbol{\eta})\, dx \tag{9c}$$

where $\boldsymbol{w}$ is defined above and $z = (\boldsymbol{v}, \boldsymbol{q}, \boldsymbol{\eta})$ (here z is a trial function), and the plastic dissipation, $D(\boldsymbol{q}, \boldsymbol{\eta})$. For a material model with von Mises yield criteria and with kinematic and isotropic hardening, the dissipation is

$$D(\boldsymbol{q}, \boldsymbol{\eta}) = \begin{cases} c_0 |\boldsymbol{q}| & \text{if} \quad |q| \le \mu \\ +\infty & \text{if} \quad |q| > \mu \end{cases} \tag{10}$$

where c_0 is related to the flow stress σ_y as $c_0 = \sqrt{\frac{2}{3}}\sigma_y$. If we integrate Eq. (7), multiply Eq. (4) with $\boldsymbol{v} - \dot{\boldsymbol{u}}$, integrate over Ω, and use integration by parts, we obtain the variation inequality of the form; find $\boldsymbol{w}$ such that for all t

$$a(\boldsymbol{w}, z - \dot{\boldsymbol{w}}) + j(z) - j(\dot{\boldsymbol{w}}) \ge l(z - \dot{\boldsymbol{w}}), \quad \forall z \in \boldsymbol{Z} \tag{11}$$

where $j(z) = \infty$ for $z \notin \boldsymbol{Z}_P$. The space $Z = V \times Q_0 \times M$ is a Hilbert space with norm $||z||_Z = (z, z)^{1/2}$ where

$$(\boldsymbol{w}, z)_Z = (\boldsymbol{u}, \boldsymbol{v})_V + (\boldsymbol{p}, \boldsymbol{q})_Z + (\boldsymbol{\xi}, \boldsymbol{\eta})_M \tag{12}$$

Downloaded From: https://computingengineering.asmedigitalcollection.org on 04/02/2019 Terms of Use: http://www.asme.org/about-asme/terms-of-use

where $\boldsymbol{w} = (\boldsymbol{u}, \boldsymbol{p}, \boldsymbol{\xi})$, $\boldsymbol{z} = (\boldsymbol{v}, \boldsymbol{q}, \boldsymbol{\eta})$ and

$$V = [H_0^1(\Omega)]^3 \tag{13}$$

$$Q = \{\boldsymbol{q} = (q_{ij})_{3\times 3}: \quad q_{ji} = q_{ij}, q_{ij} \in L^2(\Omega)\} \tag{14}$$

$$Q_0 = \{\boldsymbol{q} \in Q: \quad \mathrm{tr}\boldsymbol{q} = 0 \quad \text{a.e. in } \Omega\} \tag{15}$$

$\boldsymbol{Z}_p$ is the space of admissible states defined by

$$\boldsymbol{Z}_p = \{z \in Z: \quad (\boldsymbol{q}, \boldsymbol{\eta}) \in K_p \quad \text{a.e. in } \Omega\} \tag{16}$$

where $K_p = \mathrm{dom}(D)$ and

$$D(\dot{\boldsymbol{P}}) = \sup\{\boldsymbol{T} : \dot{\boldsymbol{P}}: \quad \boldsymbol{T} \in K\} = \boldsymbol{\Sigma} : \dot{\boldsymbol{P}} \tag{17}$$

with

$$K = \{\boldsymbol{\Sigma} : \phi(\boldsymbol{\Sigma}) \le 0\} \tag{18}$$

for yield function $\phi(\boldsymbol{\Sigma})$. In the case of kinematic hardening only, we have the simple form

$$D(\boldsymbol{q}) = c_0|\boldsymbol{q}| \tag{19}$$

for the dissipation. For a more general discussion about the dissipation function in connection to elastoplasticity, we refer to Ref. [11]. The variation inequality formulation Eq. (11) is equivalent to finding the argument that minimizes the energy functional

$$\mathcal{L}(\boldsymbol{w}) := \frac{1}{2}a(\boldsymbol{w}, \boldsymbol{w}) + j(\boldsymbol{w}) - l(\boldsymbol{w}), \quad \forall \boldsymbol{w} \in \boldsymbol{Z} \tag{20}$$

In this paper, this minimization problem is solved using Newton's method with a pseudo-Jacobian approach to handle the nondifferentiable functional $j(\boldsymbol{w})$; see Jeyakumar [15]. In other words, in every iteration, we solve

$$\partial^2\mathcal{L}(\boldsymbol{w}_n)\Delta\boldsymbol{w}_n = \partial\mathcal{L}(\boldsymbol{w}_n) \quad \boldsymbol{w}_{n+1} = \boldsymbol{w}_n + \Delta\boldsymbol{w}_n \tag{21}$$

The convergence criterion for the minimization problem is the norm of the residuals, such that $||\mathcal{R}(\boldsymbol{w})|| < 10^t$. The residual and the tangent stiffness of the model are defined, respectively, as

$$\partial\mathcal{L}(\boldsymbol{w}) = l(\boldsymbol{w}) - [a(\boldsymbol{w}, \boldsymbol{w})\boldsymbol{w} + \partial D(\boldsymbol{w})] \tag{22a}$$

$$\partial^2\mathcal{L}(\boldsymbol{w}) = a(\boldsymbol{w}, \boldsymbol{w}) + \partial^2 D(\boldsymbol{w}) \tag{22b}$$

To solve Eq. (22), in every iteration, the computational region is divided into the section that has undergone plastic deformation and the region that has not. It is only in the plastic region that the plastic strain is allowed to be nonzero; see Han and Reddy [11] for details.

3 Adaptation of the Method of Influencing Coefficients

The basic idea of the MIC is to find a linear relationship between states by forming a sensitivity matrix of the change in the stiffness matrix [4]. This formulation treats plastic strain as a primary variable which is natural for variation simulation of plastic strain, for example, in fatigue simulation. The first-order Taylor expansion of the primary variable around a nominal load is defined as

$$\tilde{\boldsymbol{w}}(v + \delta v) = \boldsymbol{w}(v) + \Delta\hat{\boldsymbol{w}}(v)\delta v + \mathcal{O}^2(v) \tag{23}$$

where v is the primary variable related to the nominal solution. The derivative of the primary variable, $\Delta\boldsymbol{w}(v)$, is the Newton step from Eq. (21). The step size is chosen arbitrarily by adding a

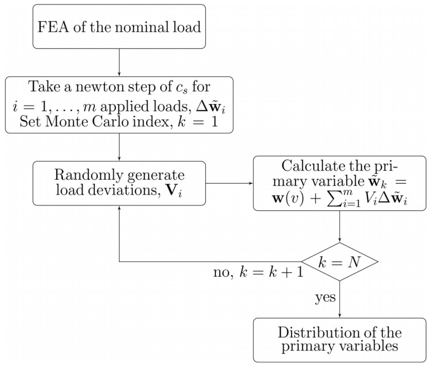

Fig. 1 Flow chart of the proposed method, toward NLMIC, for *N* direct Monte Carlo simulation based on MIC with elastoplastic material

deviation, $c_s \ne 0$, to the applied load $l(\boldsymbol{w})$ such that the residual in Eq. (22*a*) can be formulated as

$$\partial\hat{\mathcal{L}}(\boldsymbol{w}_n) = l(\boldsymbol{w}_n)(1 + c_s) - [a(\boldsymbol{w}_n, \boldsymbol{w}_n)\boldsymbol{w}_n + \partial D(\boldsymbol{w}_n)] \tag{24a}$$

$$\Delta\hat{\boldsymbol{w}}_n = \partial^2\mathcal{L}(\boldsymbol{w}_n)^{-1}\partial\hat{\mathcal{L}}(\boldsymbol{w}_n) \tag{24b}$$

where $\boldsymbol{w}_n = \boldsymbol{w}(v)$ is the nominal solution of the primary variables, the solution of the mean prescribed displacement. This will give a scaled step size that allows one to add a normalized deviation of

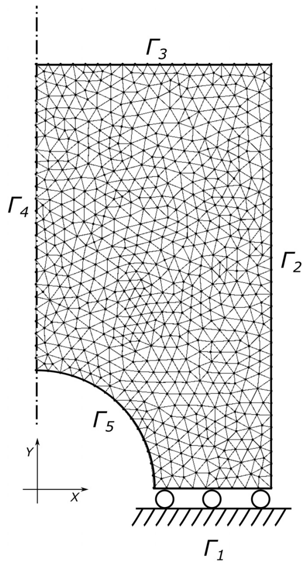

Fig. 2 Boundaries of a 2D quarter symmetric plate

Downloaded From: https://computingengineering.asmedigitalcollection.asme.org on 04/02/2019 Terms of Use: http://www.asme.org/about-asme/terms-of-use

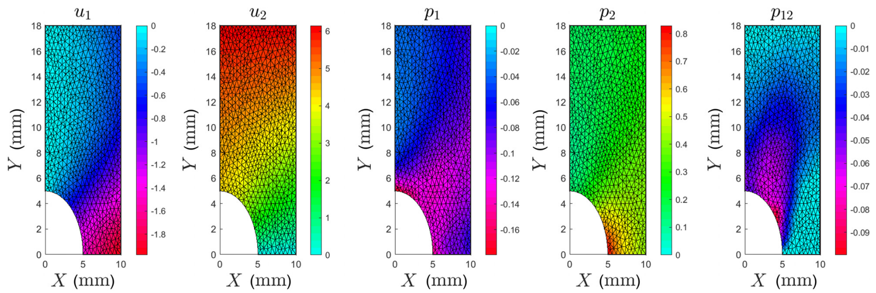

Fig. 3 Nominal prescribed displacement $u_{y|\Gamma_3} = 6.15$ (mm)

Table 1 Boundary conditions

	Case I		Case II	
Boundary	x	y	x	y
Γ_1	Free	0	Free	0
Γ_2	Free	Free	u_x	Free
Γ_3	Free	u_y	Free	u_y
Γ_4	0	Free	0	Free
Γ_5	Free	Free	Free	Free

the loads. The derivative of the nominal load δv can be formulated with respect to the scaled variation

$$\delta v = \frac{v_k - v}{c_s v} \tag{25}$$

To conform with the MIC methodology, Eqs. (23) and (25) are rewritten as

$$\Delta \tilde{\boldsymbol{w}} = \frac{\Delta \hat{\boldsymbol{w}}_n}{c_s v} \tag{26a}$$

$$\tilde{\boldsymbol{w}} = \boldsymbol{w}_n + \mathbf{V}\Delta \tilde{\boldsymbol{w}} \tag{26b}$$

where $\mathbf{V}$ is the load deviation vector containing the deviation from the affected degrees of freedoms. For multiple load cases, the superposition principle is used since the system is assumed to be linear around a nominal point v. This implies that the collective response of all loads acting on a system is equivalent to the sum of loads acting individually

$$\tilde{\boldsymbol{w}} = \boldsymbol{w}_n + \sum_{i=1}^{m} \mathbf{V}_i \Delta \tilde{\boldsymbol{w}}_i \tag{27}$$

where m is the total number of displacements acting on the system and $\Delta \tilde{\boldsymbol{w}}_i$ is the decoupled primary variable containing only the values that are affected by the ith load. The steps in the MIC adaptation for nonlinear materials are presented as a flowchart in Fig. 1 for N Monte Carlo Simulations.

4 Case Studies

Two case studies were selected to demonstrate the applicability and efficiency of the NLMIC. They both involve a 2D quarter symmetric plate with a hole in the center under plane stress conditions. The first case study is subjected to a uniaxial tensile load and proves the validity of the FEA approach by comparing it to similar studies presented in Ref. [14]. The second case study is subjected to tensile loads in two directions to show the validity of the superposition principle. The boundary conditions for the two cases can be seen in Fig. 2 and Table 1.

Positive and negative directions of the boundary conditions are given by the coordinate axis in Fig. 2. See Ref. [14] for any further information about the quarter-symmetric plate.

4.1 Case I: Uniaxial Tensile Loading. A linear kinematic hardening material model is used for demonstration of the presented method. The dissipation function corresponds to Eq. (9c), however, any arbitrary nonlinear material that is reasonably smooth can be applied. The material properties for both cases are given in Ref. [14]. The elastic properties are given as $E = 70$ MPa, $\nu = 0.2$, and the hardening parameters are $\bar{K} = 0.243$ MPa and a strain rate of $\alpha = 1$. The FEA was conducted using an implementation in MATHEMATICA[1] and the results were exported to MATLAB, where the nonlinear adaptation was performed according to the flow chart in Fig. 1. The FE mesh used in both cases consists of triangular elements with linear element shape functions.

The same load deviation vector was applied for both the proposed method and FEA with 1000 generated numbers with a normal distribution $u_y \sim N(6.15, 0.2)$.[2] The primary variables for the nominal prescribed displacement can be seen in Fig. 3 and the L^2 normalization of the residual between FEA and NLMIC is calculated as

$$r_{L^2} = ||\mathbf{w}_{\text{fea}} - \mathbf{w}_{\text{NLMIC}}|| \tag{28}$$

Results are presented in Fig. 4. This indicates that the correlation between the simulated and the approximated solution is coherent. The time comparisons are summarized in Table 2, where it can be observed that the simulation time is improved by a factor of 10^3.

4.2 Case II: Biaxial Tensile Loading. The second case is intended to show the validity of the superposition principle assumption made in Eq. (27). The quarter symmetric plate is subjected to a uniformly distributed prescribed displacement $u_x \sim U(5, 0.2)$ on Γ_2 and $u_y \sim U(6.15, 0.2)$ on Γ_3. A FE simulation is conducted with the mean prescribed displacements, where the components in the energy functional, Eq. (24), are obtained for the NLMIC. The assumption of superposition requires that the affected degrees-of-freedom due to the prescribed displacement are decoupled for each load case. Once the components of the matrices are decoupled, the load deviation vector is applied and the primary variables can be calculated. A 2-level full factorial

[1] MATHEMATICA is used due to its capabilities of solving symbolic integrals.
[2] Normal distribution of a variable x, $x \sim N(\mu, \sigma)$, where μ is the mean of the variable x and σ is the standard deviation.

Downloaded From: https://computingengineering.asmedigitalcollection.asme.org on 04/02/2019 Terms of Use: http://www.asme.org/about-asme/terms-of-use

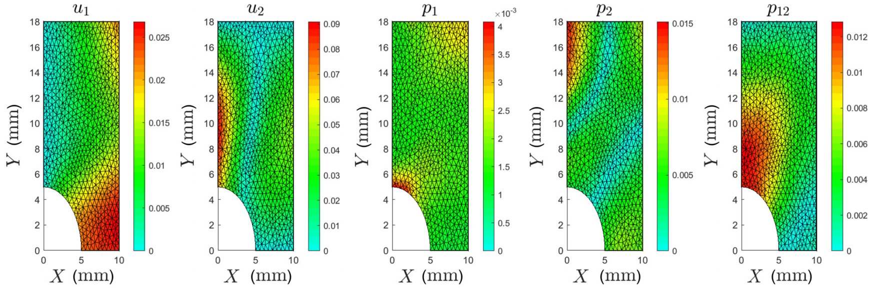

Fig. 4 L^2 **normalization of the residual between FEA and NLMIC, uni-axial**

Table 2 Time comparison between FEA and the proposed method

	# FE-sim	t (s)	Monte Carlo simulations	t (s)	$\sum t$ (s)
FEA	1000	96×10^3	—	—	96×10^3
NLMIC	1	104.01	1000	0.04	104.05

test space was created to validate the NLMIC for multiple boundary conditions. The primary variables, with nominal prescribed displacement applied to the boundaries, are presented in Fig. 5 and the L^2-normalization of the residuals is presented in Fig. 6.

5 Conclusion and Discussion

It can be observed in Table 2 that there is a simulation time difference of a factor 10^3 between the direct Monte Carlo FE

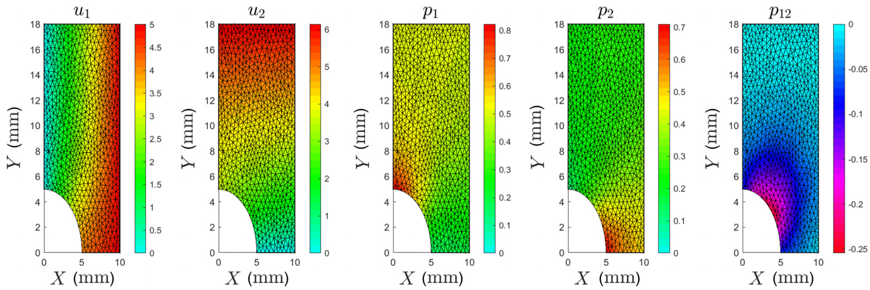

Fig. 5 Nominal prescribed displacement $u_{x|\Gamma_2} = 5\,(\mathrm{mm})$ **and** $u_{y|\Gamma_3} = 6.15\,(\mathrm{mm})$

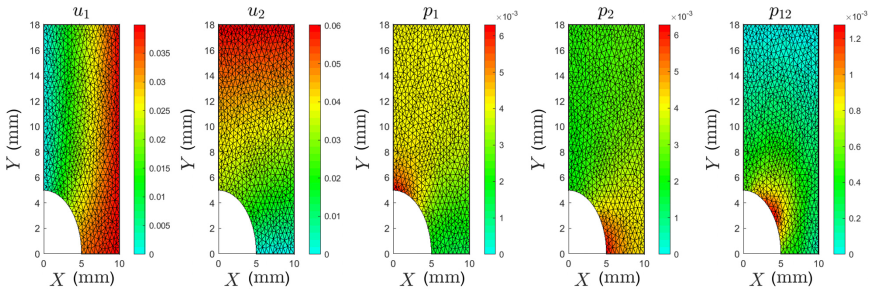

Fig. 6 L^2 **normalization of the residual between FEA and NLMIC of the 2-level full factorial test space**

Downloaded From: https://computingengineering.asmedigitalcollection.asme.org on 04/02/2019 Terms of Use: http://www.asme.org/about-asme/terms-of-use

simulations and the NLMIC. This shows large potential for using NLMIC in situations where it is applicable. With the proposed model, it is possible to greatly reduce computer resources and increase the accuracy of variation simulations for parts and assemblies subjected to plastic deformations. The first case study is a proof of concept where the methodology is validated with known research of a deterministic case and extended to a nondeterministic case. Both the NLMIC and the MIC use MCS to generate the sources of variation. Because the distributions of variables are not bound to any specific distributions, skewed or non-normal distributions can be used. For the isotropic hardening, it can be expected that the plastic strain distribution of each node is equivalent to displacement distribution. For nonlinear kinematic hardening models, it can be expected that the distribution of the plastic strains will be skewed.

In the second case study, it was shown that the principle of superposition can be used with limited loss in accuracy; see Fig. 6. Once the affected degrees-of-freedom are decoupled, it is possible to summarize the effects of each individual boundary condition. This is valid due to the linearization around the nominal prescribed displacement. Due to nonlinearities in the material model, the accuracy of the NLMIC decreases as a point further away from the simulated point is generated. Furthermore, for nonlinear hardening models or larger tolerance limits of the prescribed displacement, it may be necessary to simulate several points to obtain multiple sensitivity vectors, $\Delta\tilde{\mathbf{w}}^d$ where $d = 1,\ldots, D$ and D is the number of discretizations of the prescribed displacement. Depending on the applied variation, a sensitivity vector closest to the point d can be chosen in order to reduce the errors caused by the linearization and the dissipative nature of plasticity.

A milestone within the variation simulation research field is the incorporation of nonlinear material models. With the current methodologies, such as the MIC methodology, it is not possible to incorporate nonlinear material behavior without losing accuracy and necessary information. This paper presented an adaptation of the MIC, NLMIC, for variation simulation of sheet metal parts with nonlinear material models. The presented approach incorporates an elastoplastic material model with isotropic hardening through a first-order Taylor expansion of the primary variable around a nominal load. The derivative of the primary variable is identified as the Newton step and can be retrieved from the FE formulation. An elastoplastic material model with isotropic hardening was used for demonstration purposes. For highly nonlinear material models, it is expected that the error will increase as the distance from the nominal load increases. The presented case studies show that it is possible to incorporate plastic strains for single and multiple loads in variation simulations with limited effect on accuracy.

6 Future Work

In future work, the linearization error will be handled by a discrete point NLMIC. It is also assumed that the linearization error will diverge faster for more general material models, such as nonlinear kinematic hardening models. Future work will also incorporate welding and heat treatment simulations with the NLMIC model. It is also necessary to investigate the applicability and limits of the proposed method, for example, appropriate use of the NLMIC can be assured for a given material model. The formulation can be expanded to fatigue simulations and life-cycle expectancy analyses. This will require the NLMIC to incorporate cyclic load behavior.

Acknowledgment

This work was carried out at the Wingquist Laboratory within the Production Area of Advance at Chalmers, supported by VINNOVA (Sweden's government agency for innovation). The support is gratefully acknowledged.

References

[1] Chase, W., and Parkinson, A. R., 1991, "A Survey of Research in the Application of Tolerance Analysis to the Design of Mechanical Assemblies," Res. Eng. Des., **3**(1), pp. 23–37.
[2] Söderberg, R., and Lindkvist, L., 1999, "Computer Aided Assembly Robustness Evaluation," J. Eng. Des., **10**(2), pp. 165–181.
[3] Suh, N. P., 1990, *The Principles of Design*, Oxford University Press, New York.
[4] Liu, S. C., and Hu, S. J., 1997, "Variation Simulation for Deformable Sheet Metal Assemblies Using Finite Element Methods," ASME J. Manuf. Sci. Eng., **119**(3), pp. 368–374.
[5] Dahlström, S., and Lindkvist, L., 2007, "Variation Simulation of Sheet Metal Assemblies Using the Method of Influence Coefficients With Contact Modeling," ASME J. Manuf. Sci. Eng., **129**(3), pp. 615–622.
[6] Söderberg, R., Lindkvist, L., Wärmefjord, K., and Carlson, J. S., 2016, "Virtual Geometry Assurance Process and Toolbox," Procedia CIRP, **43**, pp. 3–12.
[7] Moos, S., and Vezzetti, E., 2013, "An Integrated Strategy for Variational Analysis of Compliant Plastic Assemblies on Shell Elements," Int. J. Adv. Manuf. Technol., **69**(1–4), pp. 875–890.
[8] Söderberg, R., Wärmefjord, K., Lindkvist, L., and Berlin, R., 2012, "The Influence of Spot Weld Position Variation on Geometrical Quality," CIRP Ann. Manuf. Technol., **61**(1), pp. 13–16.
[9] Wärmefjord, K., Söderberg, R., Ericsson, M., Appelgren, A., Lundbäck, A., Lööf, J., Lindkvist, L., and Svensson, H-. O., 2016, "Welding of Non-Nominal Geometries—Physical Tests," Procedia CIRP, **43**, pp. 136–141.
[10] Han, W., Daya Reddy, B., and Schroeder, G. C., 1997, "Qualitative and Numerical Analysis of Quasi-Static Problems in Elastoplasticity," Soc. Ind. Appl. Math., **34**(1), pp. 143–177.
[11] Han, W., and Reddy, B. D., 2013, "Plasticity," *Interdisciplinary Applied Mathematics*, Vol. 9, Springer, New York.
[12] Havner, K. S., and Patel, H. P., 1976, "On Convergence of the Finite-Element Method for a Class of Elastic-Plastic Solids," Q. Appl. Math., **34**(1), pp. 59–68.
[13] Johnson, C., 1975, "On Finite Element Methods for Plasticity Problems," Numer. Math., **26**(1), pp. 79–84.
[14] Simo, J. C., and Hughes, T. J. R., 1998, "Computational Inelasticity," *Interdisciplinary Applied Mathematics*, Vol. 7, Springer, New York.
[15] Jeyakumar, V., 2008, "Nonsmooth Vector Functions and Continuous Optimization," *Optimization and Its Applications*, Vol. 10, Springer, Boston, MA.

Downloaded From: https://computingengineering.asmedigitalcollection.asme.org on 04/02/2019 Terms of Use: http://www.asme.org/about-asme/terms-of-use

Paper IV

Algorithm for Detecting Load-Carrying Regions within the Tip Seat of an Indexable Cutting Tool

S. Camuz, A. Liljerehn, K. Wärmefjord, R. Söderberg

Journal of Computing and Information Science in Engineering (Apr 2024), Vol. 24, Issue 4

https://doi.org/10.1115/1.4064255

Check for updates

ASME Journal of Computing and Information Science in Engineering
Online journal at:
https://asmedigitalcollection.asme.org/computingengineering

Soner Camuz[1]
Metal Cutting Research,
AB Sandvik Coromant,
Sandviken 811 34, Sweden
e-mail: soner.camuz@sandvik.com

Anders Liljerehn
Metal Cutting Research,
AB Sandvik Coromant,
Sandviken 811 34, Sweden
e-mail: anders.c.liljerehn@sandvik.com

Kristina Wärmefjord
Department of Industrial and Materials Science,
Chalmers University of Technology,
Gothenburg 412 58, Sweden
e-mail: kristina.warmefjord@chalmers.se

Rikard Söderberg
Department of Industrial and Materials Science,
Chalmers University of Technology,
Gothenburg 412 58, Sweden
e-mail: rikard.soderberg@chalmers.se

Algorithm for Detecting Load-Carrying Regions Within the Tip Seat of an Indexable Cutting Tool

Maintaining an even pressure distribution in an indexable cutting tool interface is crucial to the life expectancy of a carbide insert. Avoiding uneven pressure distribution is highly relevant for intermittent cutting operations because two load cases arise for full immersion, inside and outside the cutting zone, which can cause alternating contact positioning. Current positioning methodologies, such as 3-2-1 principles, do not consider external mechanical forces, which must be considered for insert-tool body positioning designs. Therefore, this paper proposes an algorithm to calculate a contact index to aid in the design of locating schemes for the early design phases of insert-tool body interface design. The results indicate that it is possible to visualize where a contact condition needs to exist to give support based on the mechanical loads acting on the insert.
[DOI: 10.1115/1.4064255]

Keywords: computer-aided design, computer-aided engineering, data-driven engineering, model-based systems engineering

1 Introduction

Cutting tool manufacturers are constantly improving their cutting tools' reliability and durability to satisfy the demand for predictable and long-lasting tools. Insert grade and geometry, machining parameters, and the tool-workpiece configuration are the primary determinants of the cutting tool's reliability and durability.

There is a gap in current research within the machining industry that looks at interface between the tool holder and the insert for indexable cutting tools; the focus has been on cutting process optimization, insert chemical composition, fixture-workpiece positioning, and insert macro geometries for different workpiece materials. Tuysuz and Altintas [1] and Altintas et al. [2] presented a method to predict optimal tool paths for ball-end mills in five-axis machining to reduce deflection errors in blade machining. Merdol and Altintas [3] presented a computationally efficient generalized milling mechanics method to predict the chip, cutting forces, spindle torque, and power distribution along an arbitrary cutting-edge geometry. Merdol and Altintas [4] presented the mechanics and dynamics of a serrated cylindrical and tapered helical end mill, which allows for the optimization of the serration profile.

In recent years, efforts to increase the robustness of the cutting point of an insert have been in focus. These efforts have involved both chamfered and serrated interfaces in the tool body. The results have often had the unfortunate, unintended effect of overdetermining the positioning in the interface, causing multiple points of contact that alternate depending on the loads acting on the indexable insert.

Alternating positions or uneven pressure distribution of an indexable cutting tool insert can reduce the life expectancy rate of the tool [5] and result in failure modes such as fatigue in the clamping mechanism and increased wear-rate on the insert. Effects that can alter the positioning of an insert are mainly cutting force direction and magnitude. However, the clamping mechanism also impacts the positioning for intermittent machining processes. In these processes, when the insert is outside the cutting zone, the cutting forces will be zero, and the clamping conditions are the only mechanism that affect the insert's positioning. When the insert is inside the cutting zone, the cutting forces are greater than zero and will impact the positioning of the insert. Thus, any discrepancies in the positioning caused by the two load cases can lead to deviations in the insert positioning. Indexable inserts must function for various machining parameters using the same tool holder. As such, it can prove challenging to design a tool holder that can establish even contact pressure for all possible combinations of machining parameters and operations.

Different modeling approaches to variation propagation through an assembly have advantages and disadvantages [6]. The most common approaches in various industries can ensure the dimensional accuracy of the insert positioning with point-to-point-based contacts, such as N-2-1 for compliant assemblies [7–10] or a skin model-based approach with surface-to-surface contact [11–13]. A common method for variation simulation in deformable sheet metal assembly, frequently used within the automotive industry, is the method of influencing coefficients (MIC) [8]. The MIC approach forms a linear relationship between the part deviations and the spring back deviation of a welded/riveted assembly. Dahlstrom and Lindkvist [14] presented an approach for

[1]Corresponding author.
Manuscript received June 30, 2023; final manuscript received November 24, 2023; published online January 29, 2024. Assoc. Editor: NABIL ANWER.

Copyright © 2024 by ASME

Downloaded from http://asmedigitalcollection.asme.org/computingengineering/article-pdf/24/4/041006/7235490/jcise_24_4_041006.pdf by Chalmers University of Technology user on 21 February 2024

implementing a contact search algorithm to avoid surface penetration of contacting surfaces. Camuz et al. presented an extension of the MIC to that incorporates elasto-plastic material models with isotropic hardening [15].

The skin model approach is preferable for simulating variation propagation, with surface-to-surface contacts, in an assembly. A quantitative study on tolerance analysis [16] compares a skin model approach to three established methods: tolerance stack- up, vector loops, and small displacement. The authors also highlight the importance of integrating deformation and thermal effects in the skin model approach to improve simulation accuracy. Integrating thermal effects for a skin model approach is also presented in Garaizar et al. [17], who added systematic and random variations to each degrees-of-freedom for a node in the mesh. Using finite element analysis (FEA), it is possible to calculate the thermal expansion of the skin model. Junnan et al. [18] took a similar approach, incorporating deformation due to static loads. Nevertheless, skin models with integrated effects require numerous FE simulations to obtain statistical data, resulting in time-consuming and computational-demanding simulations.

The research on variation analysis within the machining industry has mainly focused on the fixturing of the workpiece and fixture design optimization [19–21] to ensure dimensional accuracy of the finished workpiece. Research on insert positioning variations is limited. Lopatukhin et al. [5] concluded that maintaining an even pressure distribution between the insert and tool holder is critical; failure to achieve this can reduce life expectancy at the cutting edge. In previous work, Camuz et al. [13] presented a reliability-based design optimization framework to distribute pressure evenly among preferred contact zones (PCZs). However, the given PCZ was chosen arbitrarily based on the user experience. For a body with simple geometries and static loads, it can be intuitive to see where to designate the PCZ to minimize movement and tensile stresses in the body based on the direction of the force. However, this process can be complicated for non-ideal surfaces with time-dependent loads as the force direction continuously changes.

With current tolerance analysis and allocation methodologies, ensuring the expected robustness is challenging due to the interface's sheer complexity and external loads acting on the carbide insert. For new tool designs, issues regarding uneven pressure distribution are often captured during the machining test or after product release. This results in costly design reiterations and loss in expected quality. Therefore, in the early product development phases, a method is necessary to identify load-carrying surfaces in the interface of the carbide insert and the tool holder. By doing so, the engineer can design a tool holder tip seat to accommodate the loads acting on the carbide insert.

This paper presents an algorithm for identifying load-carrying surfaces for homogenous elastic cutting tool interfaces with respect to time-dependent loads. The methodology uses FEA to analyze the kinematics of a rigid body resting on homogeneous elastic springs subjected to mechanical loads to identify the PCZ based on the applied load. The methodology also considers the clamping mechanism on the carbide insert and its effect on the positioning.

The methodology is presented in Sec. 2, and three case studies are evaluated to show the method's effectiveness. The first case study, found in Sec. 3.1, validates the result of the contact index and its application for a simple geometry with a static load. Second case study, Sec. 3.2 is an extension of the first case study and visualizes the effectiveness of a body with applied torque. Third case study, Sec. 3.3 is an industrial application on a CoroMill R390-11T308M-MM carbide insert with time-dependent cutting forces and an offset clamping screw.

2 Method

The methodology aims to identify suitable load-carrying surfaces in early design phases within cutting tool manufacturing by calculating a contact index dependent on the elastic springs' displacement and the object surface's orientation. To achieve this, the outer surface perimeter of the object of interest (white body in Fig. 1) is suspended in linear elastic springs (gray section in Fig. 1). The springs are modeled in the FEA as solid elements with a significantly lower elastic stiffness than the object of interest. The utmost nodes of the elastic springs are fixed in space to ensure that no rigid body motions exist. The methodology builds on the following three assumptions:

(1) the tool body interface material is homogeneous,
(2) the direction of the forces is significant for positioning an indexable insert,
(3) the force magnitude is relative to the elastic displacement.

The first step of the methodology involves collecting data through FEA and exporting the nodal position, and displacement fields for post-processing using matlab. Based on the applied mechanical loads, the nodal position and normalized displacement are the only requirements for calculating the contact index. This information makes it possible to determine the object's under these conditions, thereby giving engineers the necessary information to design the cutting tool interface during the early design phases.

2.1 Finite Element Model.

The data collection through FEA is performed using the commercially available software ansys workbench. The carbide insert, or the object of interest (white body in Fig. 1), rests on homogenous elastic springs (gray section in Fig. 1) modeled as 3D solid tetrahedral elements (SOLID185) with an elastic stiffness of 100 MPa and a Poisson's ratio of $\nu = 0.3$. Furthermore, the outer end of the elastic springs is fixed in space to constrain rigid body movements (Fig. 2). The material model of the object of interest requires a sufficiently high elastic stiffness so that it will not deform under the applied load. The interface between the object of interest and the homogenous elastic springs is connected using bonded pair-based contact elements (CONTA174/TARGE170), which inherit material properties from the underlying element SOLID185. Mesh independence was ensured through the h-refinement method, as the shape function of the elements is linear, Appendix B. Assuming a linear relationship through material linearity or Taylor expansion, the super-positioning principle is valid, thus allowing simulations of each load case separately.

The outputs from the FEA are the stiffness matrix, nodal positions, and displacement, which determine the normalized displacement and the normal vector and allow for further linearization to increase the number of simulations with limited effect on accuracy [15].

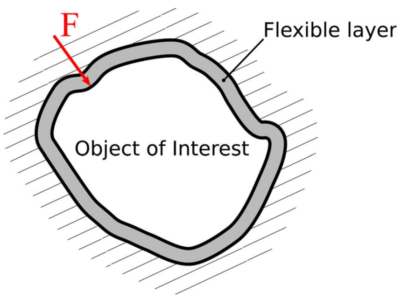

Fig. 1 Object of interest suspended in linear elastic springs

Downloaded from http://asmedigitalcollection.asme.org/computingengineering/article-pdf/24/4/041006/7235490/jcise_24_4_041006.pdf by Chalmers University of Technology user on 21 February 2024

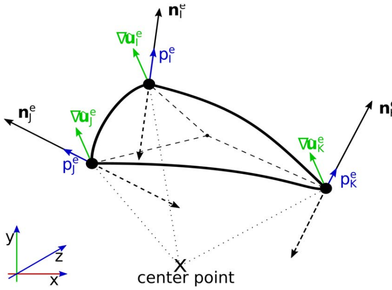

Fig. 2 Surface element for the contact index algorithm

2.2 Contact Index. The contact index $\boldsymbol{c}(F)$ aims to detect suitable surfaces on an arbitrary body under mechanical loads to design appropriate supporting contacts in its assembled state in the early design phases. The first step in defining the contact index is calculating the surface normal vectors $\left(\boldsymbol{n} \in \mathbb{R}^{(m\times3)}\right)$ of the body of interest and calculating the two-argument arctangent (arctan 2) of a vector $\left(\overrightarrow{V}_1 \in \mathbb{R}^{(m\times3)}\right)$ from the center point[2] to a node $i \le m$, where m is the total number of nodes in the mesh.

$$\overrightarrow{V}_1 = \left(x_{cp} - x_i, y_{cp} - y_i, z_{cp} - z_i\right), \quad i \le m \tag{1}$$

$$\theta = \arctan 2\left(\frac{|\overrightarrow{V}_1 \times \boldsymbol{n}|}{\overrightarrow{V}_1 \boldsymbol{n}^T}\right) \tag{2}$$

The two-argument arctangent removes the quadrant compensation step, and the normal vector's can easily be corrected to point away from the centroid (Eq. (2)).

$$\boldsymbol{n} = -\boldsymbol{n}, \quad \text{if } \theta > \frac{\pi}{2} \quad \text{or } \theta < -\frac{\pi}{2} \tag{3}$$

The second step is determining the object's movement direction using the displacement vector. While an object is moving, the only possible contact is on the surfaces where the surface normal vector moves in the same direction as the displacement vector. By calculating the normalized displacement vector's projection (scalar dot product) onto the surface normal vector, we can identify if the object is moving in the same or opposite direction of its surface normal vector.

$$\boldsymbol{p}(F) = (\boldsymbol{n} \cdot \hat{\boldsymbol{u}}(F)) \in (-1, 1) \subset \mathbb{R}^{(m\times3)} \tag{4}$$

where $\boldsymbol{p}(F)$ is the scalar projection of the normal vector $\boldsymbol{n} \in \mathbb{R}^{(m\times3)}$ on the normalized displacement field $\hat{\boldsymbol{u}}(F) \in \mathbb{R}^{(m\times3)}$. For $\boldsymbol{p}(F) < 0$, the object moves in the opposite direction of the surface normal vector, and for $\boldsymbol{p}(F) = 0$, the object moves along the surface normal vector. For $\boldsymbol{p}(F) > 0$, the object moves in the same direction as the surface normal vector, which generates a plausible contact since contact can occur.

The third step is calculating the reaction forces for each node using Hooke's Law's constitutive relationship, where the reaction force in a spring is linearly dependent on its displacement, $R = -ku$. The spring forces are normalized to the maximum displacement in the FEA solution.

$$\boldsymbol{R}_r(F) = \frac{-k|\boldsymbol{u}(F)|}{-k|\boldsymbol{u}(F)|_{\max}} = \frac{|\boldsymbol{u}(F)|}{|\boldsymbol{u}(F)|_{\max}} \in \mathbb{R}^{(m\times1)} \tag{5}$$

where $k \in \mathbb{R}^*_+$ is the spring stiffness in the flexible layer. The contact index, $\boldsymbol{c}(F)$, can now be formulated by combining Eqs. (4) and (5).

$$\boldsymbol{c}(F) = \boldsymbol{p}(F)\boldsymbol{R}_r(F) = \cdots \left((\boldsymbol{n} \cdot \hat{\boldsymbol{u}}(F))\frac{|\boldsymbol{u}(F)|}{|\boldsymbol{u}(F)|_{\max}}\right) \in (-1, 1) \subset \mathbb{R}^{(m\times1)} \tag{6}$$

The contact index inherits its sign convention from the projection of the normalized displacement gradient onto the surface normal vector (Eq. (4)). A negative contact index indicates a point moving opposite to the surface. Thus, a negative contact index would not provide any support and can be ignored and all $\boldsymbol{c}(F) < 0$ are treated as equal to zero.

2.3 Contact Index Algorithm. The common approach for loads with time dependencies and/or distributions is calculating the average response over time or with a statistical distribution. However, for machining, outliers could result in critical failure of the workpiece and tool, which can be costly for the end user. It is therefore necessary to take a worst-case scenario approach in calculating the contact index, updating the contact index at a node $i \in m$ for each step, and storing the highest index.

2.3.1 Algorithm for Mechanical Loads With a Statistical Distribution. Performing MCSs by applying a static load with a given distribution $F \sim P(X \le x)$, the displacement response $\boldsymbol{u}(F \sim P(X \le x))$ is trivially found through linearization of the primary variable at the nominal load. Therefore, the contact index with a statistical distribution is found by calculating each possible outcome through Monte Carlo simulations (MCS). In machining, this type of load is generally a representation of the offset clamping screw force, $F_s(T, x_{os}, y_{os})$[3]. $T \sim N(\mu_t, \sigma_t)$ is the normally distributed torque with a mean value μ_t and standard deviation σ_t, and, $(x_{os}, y_{os}) \sim N(\mu_t, \sigma_t)$ is the in-plane offset position of the insert hole center relative to the threaded hole center.

2.3.2 Algorithm for Mechanical Loads With a Transient Dependency. Cutting tools function for a variety of machining parameters. A traditional shoulder milling tool expects to function for a depth of cut a_p from > 0 to its entire cutting-edge length b, and a feed rate, f_z of 0.08 mm to 0.3 mm. Further exacerbating the complexity, transient or cyclic mechanical loads such as intermittent cutting in milling operations have varying chip thicknesses depending on the immersion angle. Thus, calculating the cutting forces at each discrete time-step for different machining parameters is crucial for accurately representing the cutting force resultant in the calculations of the contact index. The calculations of the cutting forces follow a general algorithm for helical flute milling forces [22], with added effects for rake angle and edge rounding compensation retrieved through experimental data from AB Sandvik Coromant. The calculations for the cutting forces are written in the finite element model software language ansys apdl to allow for accurate calculations in each time-step.

Following steps 6–11 in Appendix D, the contact index at each time-step is compared to the current highest contact index and updated if needed, resulting in a super-positioning update process as described in Appendix E.

[2]center point subscript cp.

[3]Subscript os denotes the offset x, y-coordinates to the center of the offset hole.

Downloaded from http://asmedigitalcollection.asme.org/computingengineering/article-pdf/24/4/041006/7235490/jcise_24_4_041006.pdf by Chalmers University of Technology user on 21 February 2024

3 Case Studies

Three case studies present the contact index algorithm capability to identify appropriate supporting contact surfaces. The proposed algorithm can detect areas requiring more support due to movements in the direction of the surface normal vector. The first case study shows the algorithm for a uniaxial static load to visualize and validate the magnitude of the contact index for different shapes and angles. The second case study validates the algorithm for rotational degrees-of-freedom by applying a static torque to the body of interest. The third case study adds further complexity by subjecting a CoroMill R390-11T308M-MM insert for shoulder milling to two load cases, one with a normal distribution and the second with a time-dependent load. The required CPU time for each case study is summarized in Table 2[4] in Appendix A.

3.1 Case Study I: Uni-Directional Movement With Static Load. The object of interest in the first case study (Fig. 3(*a*)) includes geometries that are common on an arbitrary machined part. Applying a static uni-directional load of $F = 1(\mathrm{N})$ will give a uniform displacement (green arrows in Fig. 3(*b*)) at all nodes, and the contact index will mainly depend on the face orientation with respect to the direction of the displacement, or more specifically, the projection of the surface normal vector on the displacement vector. This results in surface normal vectors parallel to the displacement vector having $c_i = 1$. Hence, in uni-directional cases, planar surfaces with normal vectors aligned with the displacement vectors are most suitable to design as a contacting surface.

3.2 Case Study II: Rotational Movement With Static Load. The second case study implements the proposed method on a uniform static rotation (torque) in the mass center of a cog-shaped object (white; see Fig. 4(*a*)). The magnitude of the torque is arbitrarily chosen as $T = 1$ (N/mm) so that the cog-shaped object is not deformed due to the torque. The displacement is no longer uniform, and the maximum displacement $R_r(T) = 1$ is obtained at the peaks of the convex surfaces, see Fig. 4(*b*). The maximum scalar projection of the normal vector on the normalized displacement field $p(T) = 1$ is obtained at the center of the flat surface. Using the contact index algorithm, the PCZ is found between the convex surface and the flat surface at the tangent point.

3.3 Case Study III: Cutting Tool Insert With Time-Dependent Load. The third case study significantly expands the complexity of the geometry and load-case by implementing the proposed method on a CoroMill 390-11T308M-MM[5] shoulder milling tool. The body of interest, which is a carbide insert used for shoulder milling (see Fig. 5) and that is subjected to an analytically calculated

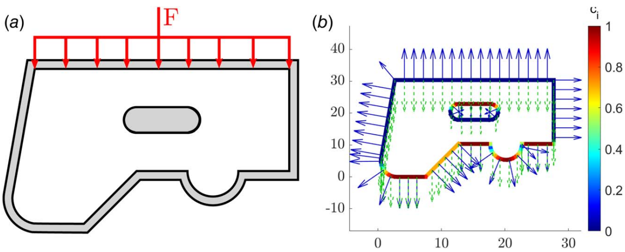

Fig. 3 Case I: Illustration of the boundary conditions in the FE model: (*a*) case I illustration, red arrows indicate the force direction and (*b*) contact index of case I with outer boundary normal vectors (blue arrows) and displacement direction (green-dashed arrows)

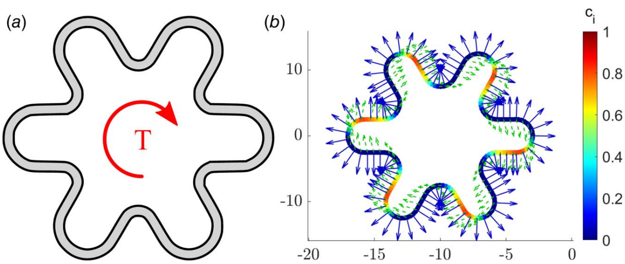

Fig. 4 Case II: Illustration of the boundary conditions in the FE model: (*a*) case II illustration, red arrow indicates the torque direction and (*b*) contact index of case II with outer boundary normal vectors (blue arrows) and displacement direction (green arrows)

[4]Intel® Core™ i7 – 10850H CPU @ 2.70 GHz, 32 GB 2133 MHz RAM, Windows 10 Enterprise.

[5]Corner radius, 0.8 (mm), approach angle 90 (deg), primary rake angle 5 (deg), secondary rake angle 25 (deg), and primary land width 0.12 (mm).

Downloaded from http://asmedigitalcollection.asme.org/computingengineering/article-pdf/24/4/041006/7235490/jcise_24_4_041006.pdf by Chalmers University of Technology user on 21 February 2024

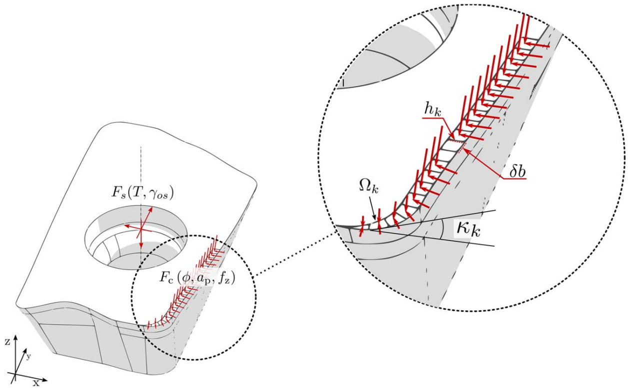

Fig. 5 Case III illustration, CoroMill 390-11T308M-MM, red arrows indicate force vectors

screw clamping force and a time-dependent cutting force retrieved from mechanistic modeling of the cutting conditions.

As mentioned, the elastic springs are linear, which validates the super-positioning principle, and the two load cases are solved separately following Algorithm 1–3 in Appendices C–E. The load case for the offset clamping screw only requires a single FEA to calculate the contact index using the method proposed by Camuz et al. [15]. The applied nominal screw torque is $T = 1.2$ N/mm with a 10% tolerance range, $T \sim \mathcal{U}(0.9T, 1.1T)$. The offset positioning tolerance is assumed to contribute to the direction of the resulting clamping force and not the magnitude. All the other machine screw tolerances, such as pitch and angle, are set to their nominal values as they remain unknown and are assumed to have a limited impact on the resulting force. From handbook data [23] for unlubricated machine screws, a friction coefficient of μ_t, $\mu_h = 0.15$ is set for the thread-tool holder combination and screw head-insert combination.

$$F_s = \frac{T}{\left(\frac{p}{2\pi}\right) + \left(\frac{\mu_t r_t}{\cos\frac{\beta}{2}}\right) + \left(\frac{\mu_h r_m}{\sin\frac{\alpha}{2}}\right)} \tag{7}$$

where p is the thread pitch, μ_t is the friction coefficient in the thread, r_t is the mean thread radius, β is the thread angle, μ_h is the friction coefficient between the socket head and clamping body, r_m is the mean radius of the socket head, and α is the screw head angle. The reaction forces acting on the insert can be derived as

$$F_{s,x} = F_s \cos\frac{\alpha}{2} \cos\gamma_{os} \tag{8}$$

$$F_{s,y} = F_s \cos\frac{\alpha}{2} \sin\gamma_{os} \tag{9}$$

$$F_{s,z} = F_s \sin\frac{\alpha}{2} \tag{10}$$

where $\gamma_{os} \sim \mathcal{U}(\gamma_{os,\min}, \gamma_{os,\max})$ is the offset angle determining the direction in which the insert is pushed. Figure 6(*a*) displays the load distribution of the clamping forces for 100,000 MCSs. The contact index is calculated using MCSs and saves the highest index for each node using the linearization of the primary variable due to the clamping forces.

In the time-dependent load case with cutting forces, linearizing the primary variable will induce high inaccuracies in the model due to the change in the uncut chip area. To prevent this, creating a three-level full factorial test space with the depth of cut $a_p\{0.5, 4.25, 8\}$ and feed rate $f_z\{0.15, 0.225, 0.3\}$ as the controllable parameters, the effect of the machining parameter space is covered. The cutting forces are calculated using a modified Kienzle's Equation, with edge radius (e_r) and rake angle (α_r) compensation, and simulated as shown in Algorithm 2 in Appendix D, where Fig. 6(*b*) shows the variation of the minimum and maximum cutting forces acting on the uncut chip area of the insert for full immersion. The modified Kienzle's Equation is separated into two cases, below and above the nose radius in the axial direction. The force equation below the nose radius is stated as

$$\delta F_t = K_c \delta b h_k^{1-m_c}(1 - p_c\alpha_r)\left(1 + \frac{h}{e_r}\right)^{m_{er|c}} \tag{11}$$

$$\delta F_r = K_n \delta b \sin(\kappa_k) h_k^{1-m_n}(1 - p_n\alpha_r)\left(1 + \frac{h}{e_r}\right)^{m_{er|n}} \tag{12}$$

$$\delta F_a = K_n \delta b \cos(\kappa_k) h_k^{1-m_n}(1 - p_n\alpha_r)\left(1 + \frac{h}{e_r}\right)^{m_{er|n}} \tag{13}$$

where K_c, K_n, m_c, and m_n are the specific cutting force coefficients, p_c and p_n are scaling parameters to accommodate the effect of the rake angle and $m_{er|c}$ and $m_{er|n}$ are exponential coefficients for the edge radius compensation, and κ_k is the segment (k) approach angle. The segment length and the uncut chip thickness segment is given by

$$\delta b = \delta a_p / \sin\kappa_k \tag{14}$$

$$h_k = f_z \sin\phi_t \sin\kappa_k \tag{15}$$

where ϕ_t is the immersion angle at time t. Following Algorithm 2, the cutting forces are applied in each discrete surface Ω_k by dividing the cutting forces by the sum of nodes in Ω_k. This process is repeated for each increment of the immersion angle $\phi_i \in (0, \pi)$. The numerical values for the combination of $SS2541$ workpiece material and the CoroMill 390-11T308M-MM insert are given through empirical studies conducted by AB Sandvik Coromant.

Downloaded from http://asmedigitalcollection.asme.org/computingengineering/article-pdf/24/4/041006/7235490/jcise_24_4_041006.pdf by Chalmers University of Technology user on 21 February 2024

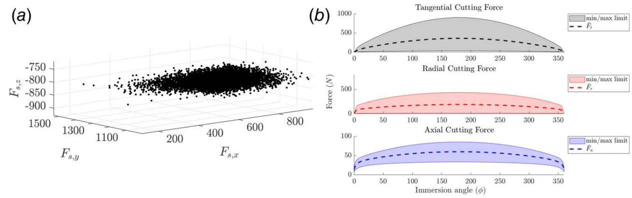

Fig. 6 Load cases for case study III: (*a*) load case I, MCS for clamping screw forces, F_s and (*b*) load case II, cutting forces for full immersion with varied depth of cut and feed rate

The results of the contact index algorithm in Fig. 7 demonstrate that, as expected, the contact index varies depending on the machine parameters. At a low depth of cut, $a_p < r_e$, the radial (*y*-axis) and axial (*x*-axis) cutting forces are prominent and mainly direct the cutting forces in the insert axial direction. Increasing the depth of cut results in the axial forces becoming less dominant, thus redirecting the cutting forces toward the insert radial direction. Observing Fig. 7 it is evident that two load cases exist. Any convexity in the bottom surface due to inaccurate manufacturing or plastic deformations may lead to a reduced life expectancy of the cutting tool as shown in Ref. [5].

4 Discussion

The first case study indicates that if a uniformly static load is applied to an arbitrary machined part the surfaces with normal vectors parallel to the displacement vector is most suitable for use as contact support, which also validates the algorithm's functionality in finding suitable contact surfaces. In the second case study, a similar result is found. The highest c_i is found at the start of the convex radii, where the trade-off between displacement and perpendicularity is optimal. The third case study implements the contact index algorithm for a CoroMill R390-11T308M-MM shoulder milling insert during a full immersion cutting operation. Observing the bottom surface of the insert in Fig. 7, it is evident that there is a discrepancy between the load cases for higher depths of cut and feed rates. At lower depths of cut and feed rates, the cutting forces are lower than the offset clamping force, resulting in the clamping screw load case being dominant over the cutting forces load case.

The contact index algorithm makes it possible to determine where on the insert surface support is necessary. Failure to do so can result in excessive insert movement in the tip seat, which can cause fatigue failure in the clamping screw. In future implementations of the contact index algorithm in locating scheme optimization tools, the contact index can act as a penalty function in the optimization routine to pick areas of higher contact index. By doing this, we will incorporate information on mechanical loads acting on a body before we define our locating scheme. Thus, giving an insert that is robust, in a geometrical sense, and has contact where it is crucial with respect to external mechanical loads. The drawback of the proposed algorithm is that if the engineer does not consider a particular load distribution or uses the tool with machine parameters that significantly alter the contact index distribution, it can lead to a decrease in the tool's life expectancy. However, product

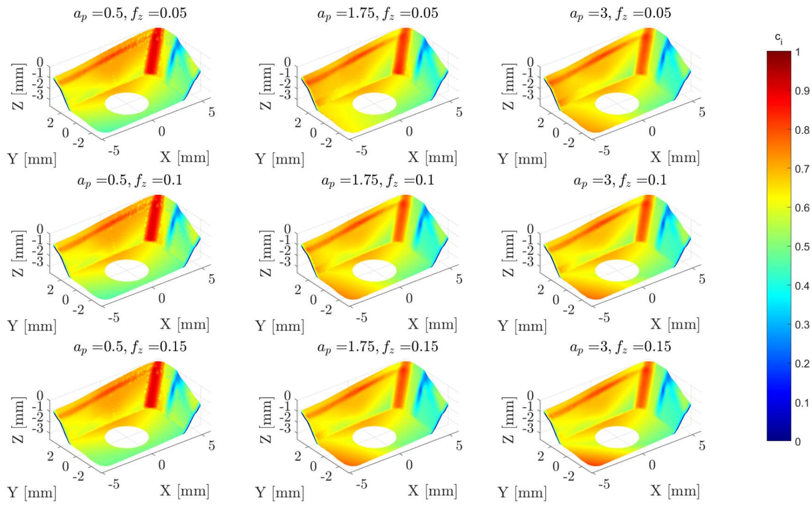

Fig. 7 Case III results for different depths of cuts and feed rates

Downloaded from http://asmedigitalcollection.asme.org/computingengineering/article-pdf/24/4/041006/7235490/jcise_24_4_041006.pdf by Chalmers University of Technology user on 21 February 2024

development projects typically have enough redundancy to cope with unintentional machine parameters to detect errors in the design of the indexable cutting tool.

5 Conclusion

Maintaining an even pressure distribution over the surface of the interface is critical to ensure the reliability and durability of an indexable insert. To address this issue, a method was proposed to calculate a contact index that aids in the design of locating schemes in the early phases of insert-tool body interface design. The method uses FEA to analyze the displacement of an indexable insert resting on homogeneous linear elastic springs and subjected to cutting and clamping forces. Future applications of this algorithm must

(1) implement a locating scheme optimization,
(2) verify the locating scheme optima with physical experiments,
(3) implement a nonlinear spring material model.

Acknowledgment

This work was carried out at the Wingquist Laboratory within the Production Area of Advance at Chalmers, supported by VINNOVA (Sweden's government agency for innovation). The support is gratefully acknowledged. A deep gratitude goes toward the Department of Metal Cutting Research at AB Sandvik Coromant for the help and support.

Conflict of Interest

There are no conflicts of interest.

Data Availability Statement

The datasets generated and supporting the findings of this article are obtainable from the corresponding author upon reasonable request.

Appendix A: Computational Time Comparison

Table 1 Computational time comparison

Case study (#)	FE-sim (#)	t/sim (s)	MCS (#)	t/sim (s)	$\sum t$ (s)
I	1	1.72	–	–	–
II	1	5.72	–	–	–
III load case 1	1	63.1	100,000	0.0016	163.91
III load case 2	9	900	–	–	8100

Appendix B: Mesh Convergence

Table 2 Mesh convergence for case studies

	Maximum deformation (mm)									
Mesh size (mm)	1	0.9	0.8	0.7	0.6	0.5	0.4	0.3	0.2	0.1
Case 1	0.01011	0.01011	0.01011	0.01011	0.01011	0.01011	0.01011	0.01011	0.01011	0.01011
Case 2	0.00020	0.00020	0.00019	0.00019	0.00019	0.00019	0.00019	0.00019	0.00019	0.00019
Case 3	0.08859	0.08862	0.08823	0.08877	0.08877	0.08936	0.08923	0.08902	0.09006	0.09076

Appendix C: Pseudocode for the Contact Index for a General Statistical Distribution

Algorithm 1 Pseudocode for the contact index for a general statistical distribution

$\mathbf{c} \leftarrow$ empty array size $(m \times 1)$
for j from 1 to the number of MCS **do**
  $F_j^{mcs} \leftarrow$ sample random value from given distribution
  $\delta F \leftarrow F^{nom} - F_j^{mcs}$
  $\tilde{\mathbf{u}}(F^{nom} + \delta F) \leftarrow \mathbf{u}(F^{nom}) + \Delta\hat{\mathbf{u}}(F^{nom})\delta F + O^2$
  $$\mathbf{c}^{tmp}\left(F_j^{mcs}\right) \leftarrow \left(\left(\mathbf{n}\cdot\tilde{\mathbf{u}}\left(F_j^{mcs}\right)\right)\left(\frac{|\tilde{\mathbf{u}}\left(F_j^{mcs}\right)|}{|\tilde{\mathbf{u}}\left(F_j^{mcs}\right)|_{\max}}\right)\right)$$
  for i from 1 to the number of nodes, m **do**
    if $c_i^{tmp}\left(F_j^{mcs}\right) > c_i$ **then**
      $c_i \leftarrow c_i^{tmp}\left(F_j^{mcs}\right)$
    end if
  end for
end for

Appendix D: Pseudocode for Time-Dependent Cutting Forces

Algorithm 2 Pseudocode for time-dependent cutting forces

for a_p from min to max depth of cut [mm] **do**
  for f_z from min to max feed rate [mm/rev] **do**
    Set cutting forces (F_t, F_r, F_a) to zero
    for t, immersion angle 0–180 deg (time-step) **do**
      for k from min to max number of discrete uncut chip areas Ω_k **do**
        $\delta F_t \leftarrow$ tangential cutting force in the kth area
        $\delta F_r \leftarrow$ radial cutting force in the kth area
        $\delta F_a \leftarrow$ axial cutting force in the kth area
        $\sum \Omega_k \leftarrow$ Sum of nodes in the kth area
        Add cutting forces to the FE load vector for the kth discrete area $\left\{\begin{array}{l} F_t \leftarrow \delta F_t / \sum \Omega_k \\ F_r \leftarrow \delta F_r / \sum \Omega_k \\ F_a \leftarrow \delta F_a / \sum \Omega_k \end{array}\right.$
      end for
      Run FE simulation and store displacement response $u\left(F_{t,r,a}(t)\right)$
    end for
  end for
end for

Downloaded from http://asmedigitalcollection.asme.org/computingengineering/article-pdf/24/4/041006/7235490/jcise_24_4_041006.pdf by Chalmers University of Technology user on 21 February 2024

Paper V

Robustness Optimization of the Tip Seat of an Indexable Cutting Tool

S. Camuz, L. Lindkvist, A. Liljerehn, R. Söderberg, K. Wärmefjord

Journal of Computing and Information Science in Engineering (Apr 2025), Vol. 25, Issue 4

https://doi.org/10.1115/1.4067919

Check for updates

ASME Journal of Computing and Information Science in Engineering
Online journal at:
https://asmedigitalcollection.asme.org/computingengineering

Soner Camuz[1]
Metal Cutting Research,
AB Sandvik Coromant,
811 34 Sandviken, Sweden
e-mail: soner.camuz@sandvik.com

Anders Liljerehn
Metal Cutting Research,
AB Sandvik Coromant,
811 34 Sandviken, Sweden
e-mail: anders.c.liljerehn@sandvik.com

Lars Lindkvist
Department of Industrial and Materials Science,
Chalmers University of Technology,
412 58 Gothenburg, Sweden
e-mail: lali@chalmers.se

Kristina Wärmefjord
Department of Industrial and Materials Science,
Chalmers University of Technology,
412 58 Gothenburg, Sweden
e-mail: kristina.warmefjord@chalmers.se

Rikard Söderberg
Department of Industrial and Materials Science,
Chalmers University of Technology,
412 58 Gothenburg, Sweden
e-mail: rikard.soderberg@chalmers.se

Robustness Optimization of the Tip Seat of an Indexable Cutting Tool

In the machining industry, fixturing of indexable inserts in the tool holders plays a critical role in ensuring high-quality outcomes by minimizing insert movement during operations. Ensuring consistent pressure distribution in an indexable cutting tool interface is essential for extending the lifespan of a carbide insert. However, existing methods either lack the necessary complexity to accommodate varying loads or are overly intricate for implementation in the early stages of product development. To address this gap, a novel approach was developed that integrates the contact index algorithm into a robust locating scheme optimization. The results show that it is possible to design an indexable cutting tool where clearly defined contacting points (half-spheres) can support and maintain minimal movement in an indexable insert during its expected lifetime. [DOI: 10.1115/1.4067919]

Keywords: computer aided engineering, multidisciplinary optimization, topology and shape optimization

1 Introduction

Cutting tool manufacturers strive to enhance their products' reliability and longevity to meet the increasing demand for tools that offer predictable and lasting performance. Key factors influencing the reliability and durability of cutting tools include insert grade and geometry, machining parameters, and the tool's configuration relative to the workpiece. Recent efforts to increase reliability have led cutting tool manufacturers to explore both chamfered and serrated interfaces within the tool body. However, the outcomes have sometimes unintentionally led to excessive contact in the interface positioning, resulting in multiple contact points that vary depending on the loads exerted on the indexable insert, thus decreasing the life expectancy of the cutting tool.

Indexable cutting tools are common in metal-forming applications such as milling, drilling, and turning, where the materials are sheared off from the workpiece in the form of chips. In the removal process, forces arise between the tool and the workpiece. These loads and their transfer paths between the insert and the tool body must be considered at the design stages of the cutting tool. Here, two separate load cases can be defined. The first case considers the tool inside the cut, where both cutting forces and clamping forces between the insert and tool body are active. The second case considers the tool out of cut, where only clamping forces are active. Rotating applications (such as milling and drilling) give rise to a third case where centripetal forces act on the insert. The magnitude of the force depends on the rotational speed and distance between the insert and the center of rotation. Any discrepancies in the positioning of the indexable insert caused by these loads can lead to deviations in the insert positioning. Therefore, it is crucial to control the rigidity and predictability of the insert positioning, ensuring an increase in the life expectancy rate of the cutting tool by maintaining an even pressure distribution [1] throughout a machining operation.

Recent advancements in metal cutting research primarily center around optimizing cutting processes, tool design, and workpiece-fixture interactions to enhance machining efficiency and precision [2]. Most relevant research within cutting process optimization focuses on predicting optimal tool paths for ball-end mills to reduce deflection in blade machining using five-axis milling machines [3,4], in turn minimizing the reaction forces on the fixturing.

Various methods for modeling variation propagation in assembly processes have been developed, with point-to-point positioning schemes like 3-2-1 and N-2-1 being widely used in machining to ensure fixture stability and dimensional accuracy. Modeling variation

[1]Corresponding author.
Manuscript received August 20, 2024; final manuscript received January 14, 2025; published online March 6, 2025. Assoc. Editor: Wenmeng Tian.

Copyright © 2025 by ASME

Downloaded from http://asmedigitalcollection.asme.org/computingengineering/article-pdf/25/4/041005/7433163/jcise-24-1446.pdf by Chalmers University of Technology user on 11 April 2025

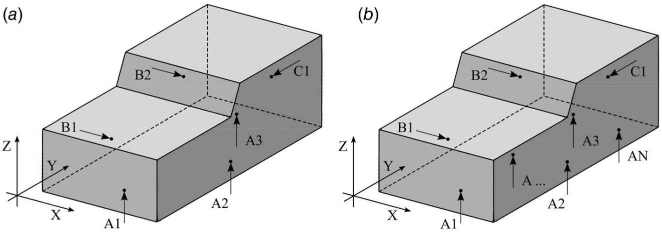

Fig. 1 Positioning systems: (*a*) illustration of the 3-2-1 positioning and (*b*) illustration of the N-2-1 positioning

propagation through an assembly can involve numerous approaches depending on its application and industry, each with its advantages and disadvantages [5,6]. Most common approaches use a point-to-point positioning scheme, such as 3-2-1 (Fig. 1(*a*)) for rigid assemblies and N-2-1 (Fig. 1(*b*)) for compliant assemblies [7–9]. The machining industry commonly uses the 3-2-1 and N-2-1 positioning approaches for fixture-workpiece positioning, where high fixture stiffness is required to minimize displacement during machining. The significance of this method was proven by Shawki and Abdel-Aal [10–12] by investigating the dimensional accuracy of fixturing under working conditions for different contact formulations. Hurtado and Melkote [13] expanded the approach further by adding a tolerance budget for the machined part to the stiffness optimization of machining fixtures. Research on fixturing during machining has shifted toward the use of a finite element-based approach with neural networks and evolutionary algorithms to find optimal fixture layout designs [14–17] and can often result in time-consuming simulations.

Research on fixturing sheet metal assemblies within the automotive industry has instead increased simulation speed by implementing a method of influencing coefficients (MIC) on deformable sheet metal assemblies [18], which has some effect on accuracy. The MIC methodology linearizes the part deviation and the springback deviation of a welded/riveted assembly, which will only require one finite element simulation, with the drawback being that it is only valid within the elastic region of the material model. The MIC methodology was expanded by Camuz et al. [19] through incorporation of elastoplastic material models with isotropic hardening in the MIC methodology, allowing for more accurate variation simulations that are subjected to plastic strains.

Research on sheet metal assembly and fixture optimization has explored various algorithms and routines to enhance assembly precision, robustness, and efficiency, addressing challenges to these processes. Dahlström and Lindkvist [20] presented a contact search algorithm to prevent surface penetration between sheet metals. The optimization of sheet metal assembly and fixtures varies compared to machining fixtures. Lööf et al. [21] presented an optimization routine aimed at maximizing robustness in critical product dimensions through a heuristic approach. Tabar et al. [22] presented an efficient optimization routine for spot welding sequences aimed at reducing solution time by calculating the relative displacement of the spot welds in the fixture. Rezaei Aderiani et al. [23] used a genetic algorithm (GA) to consider both spring back and flexibility for multistation-compliant assemblies.

Current fixture optimization routines require a finite element approach for each set of contact positions, even for rigid 3-2-1 positioning. This requirement is time consuming, and sheet metal assembly fixtures using the MIC approach do not consider external loads. It is necessary that methods are in place during early cutting tool development processes to position and analyze the tip seat and avoid expensive reiterations further down the development stream. An optimization routine is needed for cutting tool holders that can combine the complexity of machine fixture optimization with the time effectiveness of sheet metal fixturing optimization.

In previous studies using reliability-based design optimization [24], efforts were made to evenly distribute pressure over an existing tip seat interface by choosing which contact areas were needed. For nonideal surfaces and time-dependent loads, it can be challenging for the designer to determine the positioning of the insert. Hence, it is necessary to develop methods and tools that assist in finding and determining the optimal positioning of an indexable insert. Camuz et al. [25] developed a method to detect load-carrying surfaces by considering the varying loads acting on a body and calculating a contact index (CI) with respect to surface topology and load direction and magnitude. However, the placement of a positioning system is not considered.

This article presents an optimization routine that finds the optimal positioning that incorporates insert movement with cutting forces for different machine parameters and clamping screw variations to increase tip seat interface robustness through the CI from the study by Camuz et al. [25] as overdetermined or ill-defined support surfaces reduce the life expectancy of indexable cutting tools due to insert movements and uneven pressure distributions. Current methodologies and research for fixturing or positioning do not generally consider external loads or are too complex to incorporate in early design phases. The methodology presented in this article uses a genetic algorithm with a CI as a reward function to minimize the cutting point's deviation through its root-mean-square (RMS) value. The aim is to create a prototype based on the results of the optimization routine, and any referral to a prototype is the result of the presented optimization routine. The validation process is divided into four parts:

(1) Repeatability of the robustness optimization.
(2) Finite element simulations ensure that the contact points are not too far apart by checking that the tensile stresses do not exceed a failure rate of 0.01%, corresponding to 600 MPa [26].
(3) Fatigue machine testing to measure the insert movement and find the clamping screw fatigue limit.
(4) The final test is the machining test, where tip seat deformation is measured, the flank wear of the insert, or if any further failure modes are present.

The methodology is presented in Sec. 2 with a detailed description of the steps in the methodology in Secs. 2.1–2.3, where in Sec. 2.1, the CI algorithm is explained; in Sec. 2.2, the approach for the stability analysis is presented; and in Sec. 2.3, the desirability function and its constraints, used as a fitness function, for the genetic algorithm is presented. The validation process is described in Sec. 2.4 where each subsection explains the chosen validation methods. The results from the validation process are presented in Sec 3. The validation results of the robustness optimization is presented in Sec. 3.1. The finite element analysis (FEA) of the stresses in the insert is presented in Sec. 3.2, the measured flank wear of the

Downloaded from http://asmedigitalcollection.asme.org/computingengineering/article-pdf/25/4/041005/7433163/jcise-24-1446.pdf by Chalmers University of Technology user on 11 April 2025

machine tests is presented in Sec. 3.3, and insert movement and clamp screw fatigue results are presented in Sec. 3.4. A discussion of the results and the validation process is presented in Sec. 4 with suggestions for future work in Sec. 5.

2 Method

The robust locating scheme optimization methodology seeks to establish an optimal rigid positioning system for indexable cutting tools by integrating the CI algorithm [25] (as described in Sec. 2.1) as a reward function and incorporating stability analysis [8] within the 3-2-1 locating principle to minimize the RMS value at the cutting point. The primary surfaces required for the 3-2-1 locating principle are retrieved through density-based cluster analysis of the surface normal vectors and ranking based on cluster size, thus resulting in surface A being the tangential direction support, surface B being the radial direction support, and surface C being the axial direction support (Fig. 2). The stability analysis is simulated using commercially available software RD&T and controlled in MATLAB, which performs the optimization (Sec. 2.2).

The optimization of the positioning system is divided into two parts: the first aims to determine the positioning system that gives the lowest RMS value Eq. (4), and the second aims to determine the positioning system that maximizes the desirability function Eq. (8) that incorporates the CI algorithm and cutting point RMS value, and triangulates the points on the A-surface such that the center axis of the clamping screw is within the prescribed triangle of reference points A_1, A_2, and A_3 (Sec. 2.3). The optimization routine uses a standard GA with a gray encoder to retrieve the position coordinates of the locating points. A random tournament selection approach selects which individuals reproduce for the next generation, and each bit on the chromosome has a mutation rate of 5%. The best individual with the highest fitness score is stored and used in the next generation to increase the likelihood of high-performing individuals being produced in the next generation. This process is also referred to as an elitist selection. A more detailed explanation of the genetic algorithm is found in the studies by Camuz et al. [24] and Wahde [27].

For validation purposes, a prototype of the found optimum is created and compared to a reference tool holder with no modifications and one modified tool holder with an overconstrained A-surface, which causes movement of the insert in the tool body interface during machining operations. The insert's strength is validated through FEA simulations (Sec. 2.4.1), ensuring that the stresses generated during operation do not exceed the tensile yield limit of the material. Machining tests (Sec. 2.4.2) were conducted using a Mori Seiki SV-500 milling machine to verify the performance of the prototype tool holder compared to the reference

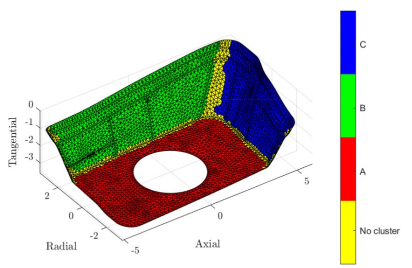

Fig. 2 Primary surfaces retrieved through density-based cluster analysis

Table 1 Overview on validation methods for each tool holder design

	Tool holder		
Validation method	Reference	Reference (deformed)	Prototype
Optimization repeatability			x
FEA simulation			x
Fatigue test	x	x	x
Machine test	x		x

tool. Flank wear was measured after 21 min of machining time, directly comparing wear resistance between the prototype and the reference. Additionally, the machining tests were checked for further failure modes that were not considered in the previous tests. Fatigue tests (Sec. 2.4.3) were performed using a Zwick Roell HB250 servo hydraulic fatigue testing machine to evaluate clamping screw fatigue and insert movement. These tests applied cyclic loads that mimicked the direction and magnitude encountered in conventional planning operations. A table of the validation methods and which tool holder was tested is shown in Table 1.

An overall description of the steps in the methodology is shown in Fig. 3.

2.1 Contact Index Algorithm.

The CI algorithm is an approach that is used to retrieve a CI value to detect suitable surfaces for support by analyzing the displacement by resting an object on homogeneous linear elastic springs and subjecting it to mechanical loads. The scalar projection of the normal vector $\mathbf{n} \in \mathbb{R}^{m\times 3}$ on the normalized displacement field $\hat{\mathbf{u}}(F) \in \mathbb{R}^{m\times 3}$ is given by:

$$\mathbf{p}(F) = \mathbf{n} \cdot \hat{\mathbf{u}}(F) \in (-1, 1) \subset \mathbb{R}^{m\times 3} \tag{1}$$

The reaction forces of the homogeneous linear elastic springs are calculated using Hooke's law of constitutive relationships, in which the reaction force of a spring is linearly dependent on its displacement, thus giving:

$$\mathbf{R}_r(F) = \frac{-k|\mathbf{u}(F)|}{-k|\mathbf{u}(F)|_{\max}} = \frac{|\mathbf{u}(F)|}{|\mathbf{u}(F)|_{\max}} \in \mathbb{R}^{m\times 1} \tag{2}$$

where $k \in \mathbb{R}_+^*$ and the contact index can be formulated as follows:

$$\begin{aligned} \boldsymbol{c}(F) &= \boldsymbol{p}(F)\boldsymbol{R}_r(F) = \cdots \\ &\cdots \left((\boldsymbol{n} \cdot \hat{\boldsymbol{u}}(F)) \frac{|\boldsymbol{u}(F)|}{|\boldsymbol{u}(F)|_{\max}} \right) \in (-1, 1) \subset \mathbb{R}^{(m\times 1)} \end{aligned} \tag{3}$$

The contact index inherits its sign convention from the projection of the normalized displacement gradient onto the surface normal vector. A negative contact index indicates a point moving opposite to the surface. Thus, a negative contact index would not provide any support and can be ignored, and $\boldsymbol{c}(F) < 0$ is treated as equal to zero. A more detailed explanation of the contact index is found in the study by Camuz et al. [25].

2.2 Stability Analysis.

To match the 3-2-1 locating scheme methodology for rigid positioning systems, A, B, and C surfaces of the cutting tool insert are defined using density-based spatial clustering of the surface normal vectors to identify surfaces oriented in the same general direction. The three most significant clusters, which are also the main surfaces, are then chosen.

The sensitivity of the measuring point ($Y(x, y, z)_{\mathrm{rms}}$) is quantifiable by varying each locating point individually in its normal direction and calculating each axial direction's RMS value [8].

Downloaded from http://asmedigitalcollection.asme.org/computingengineering/article-pdf/25/4/041005/7433163/jcise-24-1446.pdf by Chalmers University of Technology user on 11 April 2025

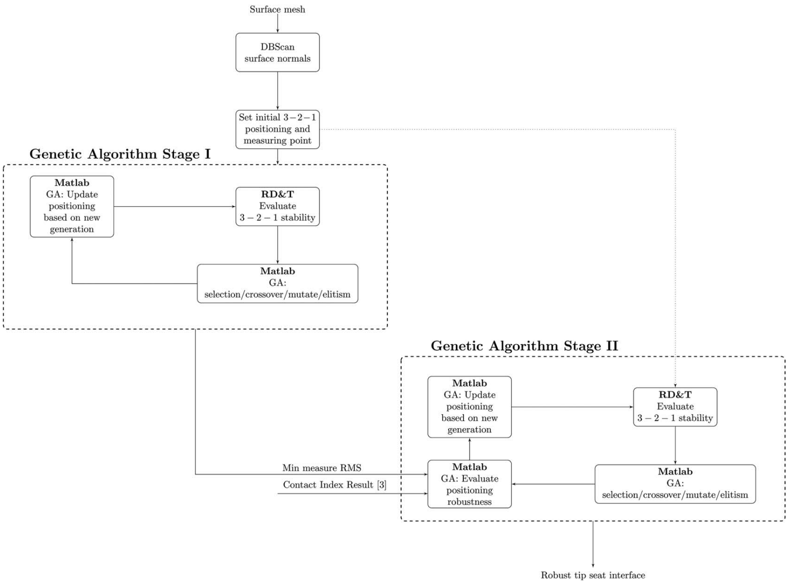

Fig. 3 Overall methodology for the robust locating scheme optimization algorithm

$$Y(x,\,y,\,z)_{\text{rms}} = \sqrt{\sum_{\gamma}^{x,y,z}\frac{1}{n}\sum_{1}^{n}\left(\frac{\gamma-\gamma_{\text{nom}}}{\Delta_{\text{input}}}\right)^{2}} \tag{4}$$

where n is the number of degrees-of-freedom and $n = 6$ in rigid locating schemes (Fig. 4).

2.3 Positioning System Optimization Using a Genetic Algorithm. The desirability function methodology consists of one to several individual desirability functions where a function $d(x) \longrightarrow 1$ when it is nearing its target value, and $d(x) \longrightarrow 0$ when it is moving away from its target; this allows each function to be normalized and thus comparable. If one desirability function is deemed to be more significant than the other, a weighting constant $s \in (0.1,\, 10)$ could be added to the desirability function $d(x)^s$. In this article, the weighting constants are equal and set to $s = 1$. In Eq. (4), the minimum RMS value for the cutting point $Y(x,\,y,\,z)_{\text{rms}}^{\min}$ is retrieved through the GA optimization of the stability in the locating points are visualized in Fig. 5, where the fitness function rewarded $y(x,\,y,\,z)_{\text{rms}}^{\min} \longrightarrow 0$. The optimization of the locators uses the same GA as shown in Fig. 5 but with different desirability functions. The desirability function d_{rms}, Eq. (5), minimizes the RMS value of the cutting point $Y(x,\,y,\,z)$; d_{c_i}. Equation (6) retrieves the combined contact index value for each locator from simulation results based on Ref. [25], and the d_{tri} (Eq. (7)) rewards the locators on the A-surface as being symmetric and having the center of the clamping hole within the prescribed triangle. The desirability functions and their constraints are formulated according to Eqs. (5)–(7).

$$d_1 = d_{\text{rms}} = \begin{cases} 0 & \text{if } Y(x,y,z)_{\text{rms}} > Y(x,y,z)_{\text{rms}}^{\max} \\ \frac{Y(x,y,z)_{\text{rms}}^{\min}}{Y(x,y,z)_{\text{rms}}} & \text{if } Y(x,y,z)_{\text{rms}}^{\min} \geq Y(x,y,z)_{\text{rms}} \geq Y(x,y,z)_{\text{rms}}^{\max} \\ 1 & \text{if } Y(x,y,z)_{\text{rms}} < Y(x,y,z)_{\text{rms}}^{\min} \end{cases} \tag{5}$$

$$d_2 = d_{c_i} = \prod_{i=1}^{n} \boldsymbol{c}(\text{REF}_i) \tag{6}$$

$$d_3 = d_{\text{tri}} = \begin{cases} \left[3\left(\frac{\text{Area}_1(P,\,A_2,\,A_3)}{\text{Area}(A_1,\,A_2,\,A_3)}\right)\right] \times \left[3\left(\frac{\text{Area}_2(P,\,A_1,\,A_3)}{\text{Area}(A_1,\,A_2,\,A_3)}\right)\right] \times \left[3\left(\frac{\text{Area}_3(P,\,A_1,\,A_2)}{\text{Area}(A_1,\,A_2,\,A_3)}\right)\right] & \text{if Area} = \text{Area}_1 + \text{Area}_2 + \text{Area}_3 \\ 0 & \text{if Area} \neq \text{Area}_1 + \text{Area}_2 + \text{Area}_3 \end{cases} \tag{7}$$

where $\boldsymbol{c}(\text{REF}_i) \in (0,\,1) \subset \mathbb{R}$ is the vector containing the contact index value, as described in Sec. 2.1, for each node of the mesh, and REF_i is the Cartesian coordinates for the ith point in the reference positioning system. The product of sequence, $\prod$, approaches a value of one only if all n points of the contact index value at the ith point in the REF is equal to one. This condition reflects a scenario where each

Downloaded from http://asmedigitalcollection.asme.org/computingengineering/article-pdf/25/4/041005/7433163/jcise-24-1446.pdf by Chalmers University of Technology user on 11 April 2025

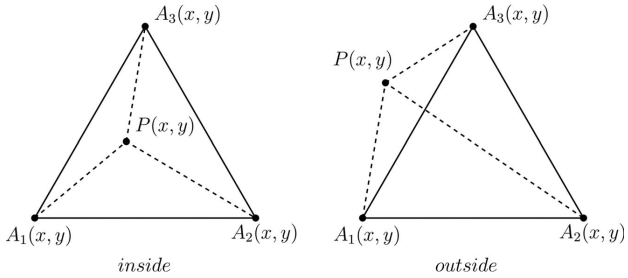

Fig. 4 Inside or outside of triangle illustration

contact index value achieves its maximum, ensuring optimal contact and stability across all defined points in the system.

Let the point $P(x, y)$ be the center of the clamping screw hole, and $A_1(x, y)$, $A_2(x, y)$, and $A_3(x, y)$ be the vertices of the triangle $\mathrm{tri}(A_1, A_2, A_3)$. Then, the sum of areas formed by $\mathrm{Area}_1(P, A_2, A_3)$, $\mathrm{Area}_2(P, A_1, A_3)$, and $\mathrm{Area}_3(P, A_1, A_2)$ is equal to the area of $\mathrm{Area}(A_1, A_2, A_3)$ if the point $P(x, y)$ is within the prescribed triangle. If the center of the clamping screw hole is within the prescribed triangle of the locators A_1, A_2, and A_3, then $d_{\mathrm{tri}} = 1$, if it is outside the prescribed triangle, then $d_{\mathrm{tri}} = 0$.

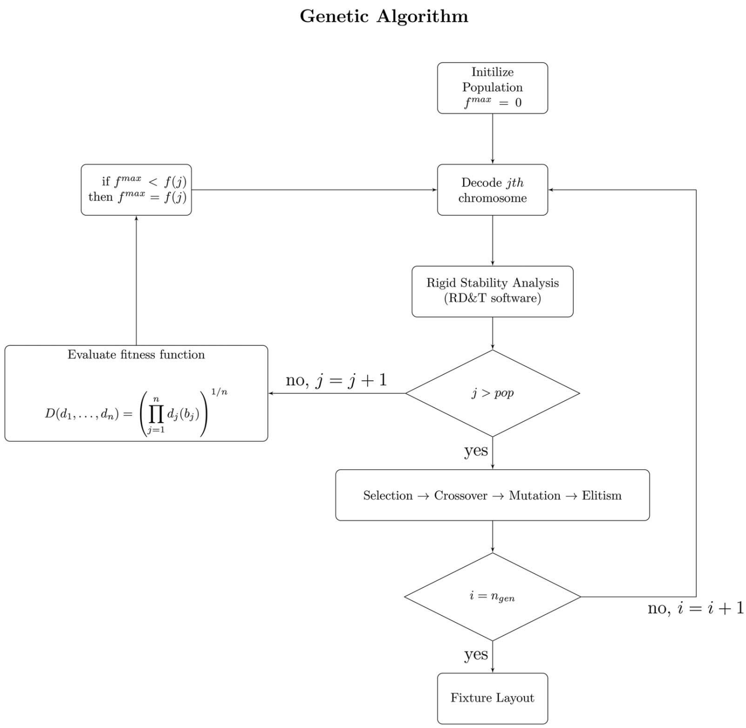

Fig. 5 Robust optimization work flow

Downloaded from http://asmedigitalcollection.asme.org/computingengineering/article-pdf/25/4/041005/7433163/jcise-24-1446.pdf by Chalmers University of Technology user on 11 April 2025

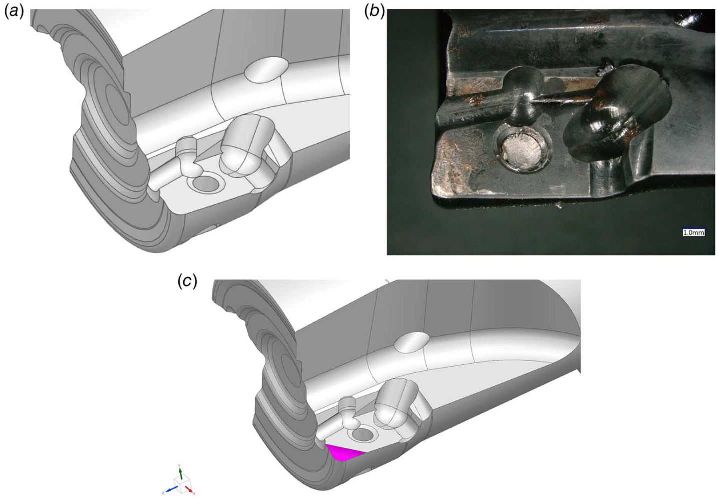

Fig. 6 Tip seat interfaces used in the validation process: (*a*) model of the reference tip seat interface, (*b*) image of a highly deformed tip seat interface in a CM390 tool holder, and (*c*) model of a highly deformed (chamfer marked in magenta) tip seat interface

The fitness function for the GA can now be written as follows:

$$f(\boldsymbol{x}) = \left(\prod_{i}^{3} = d_i(\boldsymbol{x}) \right)^{1/3} \tag{8}$$

where $\boldsymbol{x} \in \mathbb{R}^{1\times18}$ is a row vector containing the x, y, z-positions for the locators in a rigid system.

2.4 Validation Method.

To validate the results from the proposed robust optimization algorithm for indexable cutting tool interfaces, an extensive validation process is required. The results from the proposed optimization routine to reduce excessive movements in the tip seat were validated using FEA simulations to confirm that no excessive stress is put on the indexable insert due to the locating scheme. Machine tests were used to identify failure modes and load cycles, and a Zwick Roell HB250 servo hydraulic fatigue testing machine was used to compare screw clamp fatigue and insert movement.

The validation process involves three cutting tool bodies:

(1) Reference: with no modifications, Fig. 6(*a*)
(2) Reference (deformed): reference holder with a chamfered edge below the cutting point Fig. 6(*c*), representing a heavily deformed cutting tool body Fig. 6(*b*)
(3) Prototype: The prototype was retrieved using the proposed robust locating scheme optimization methodology (Fig. 12)

2.4.1 *Finite Element Analysis of the Tip Seat.*

FEA is carried out using the commercially available software ANSYS WORKBENCH 2021 R2. The tool holder material is 34CrNiMo6, which has a hardness of 43.1 HRc, and the insert is seen as a homogenous cemented carbide with a grade of H10F. Both the indexable insert and the tool holder are modeled using 3D solid tetrahedral elements (SOLID187) with quadratic displacement behavior, and the interface between them is modeled using frictional pair-based contact elements (CONTA174/TARGE170) with a frictional coefficient of $\mu = 0.5$, which also inherits all its material properties from its parent element. The boundary conditions for the simulation can be seen in Table 2 and Fig. 7.

A torque of $T = 1.2\,\text{N/mm}$ is applied to an M2.5 clamping screw, and the axial force in the bolt pretension boundary ζ_3 is calculated according to the following equation:

$$F_s = \frac{T}{\left(\frac{p}{2\pi}\right) + \left(\frac{\mu_t r_t}{\cos\frac{\beta}{2}}\right) + \left(\frac{\mu_h r_m}{\sin\frac{\alpha}{2}}\right)} \tag{9}$$

where p is the thread pitch, μ_t and μ_h are the friction coefficients in the thread and between the screw head and insert, r_t is the mean thread

Table 2 FEA boundary condition illustration

Name	Type	Tx	Ty	Tz	Rx	Ry	Rz
ζ_1	Frictionless support	0	Free	Free	Free	0	0
ζ_2	Fixed support	0	0	0	0	0	0
ζ_3	Bolt pretension	0	0	1800 N	0	0	0
ζ_4	Force	450 N	1000 N	−75 N	0	0	0

Downloaded from http://asmedigitalcollection.asme.org/computingengineering/article-pdf/25/4/041005/7433163/jcise-24-1446.pdf by Chalmers University of Technology user on 11 April 2025

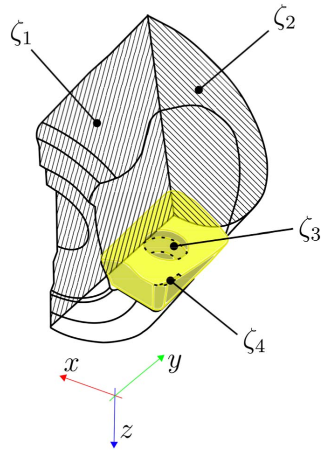

Fig. 7 Illustration of the boundary conditions in the FEA

radius, β is the thread angle, r_m is the mean radius of the clamping screw head, and α is the screw head angle. Numerical values for the standard metric thread are retrieved from handbook data [28].

The cutting forces on boundary ζ_4 are calculated using the modified Kienzle's equation (Eq. (10)), with edge radius (e_r) and rake angle (α_r) compensation and a depth of cut of $a_p = b = 4$ and feed rate $f_z = 0.15$.

$$\begin{aligned} F_t &= K_c b h_k^{1-m_c}(1 - p_c\alpha_r)\left(1 + \left(1 + \frac{h}{e_r}\right)^{m_{er,c}}\right) \\ F_r &= K_n b \sin(\kappa_k) h_k^{1-m_n}(1 - p_n\alpha_r)\left(1 + \left(1 + \frac{h}{e_r}\right)^{m_{er,n}}\right) \\ F_a &= K_c b \cos(\kappa_k) h_k^{1-m_n}(1 - p_n\alpha_r)\left(1 + \left(1 + \frac{h}{e_r}\right)^{m_{er,n}}\right) \end{aligned} \tag{10}$$

where K_c, K_n, m_c, and m_n are the specific cutting force coefficients for the insert and material combination and p_c, p_n, $m_{er,c}$, and $m_{er,n}$ are scaling parameters for the rake angle and edge radii compensation, κ is the approach angle, and h is the uncut chip thickness, which is equal to the feed rate, f_z, at 90 deg immersion angle and approach angle $\kappa = 90$ deg.

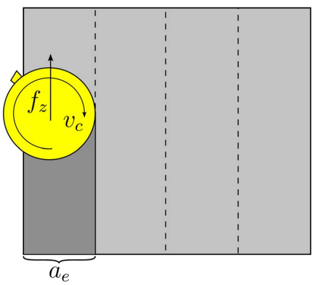

Fig. 8 Illustration of the machining setup and parameters

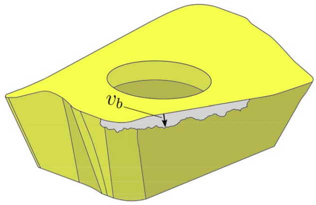

Fig. 9 Measuring flank wear

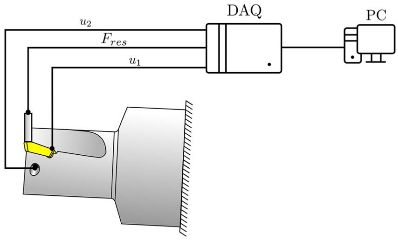

Fig. 10 Illustration of the fatigue test setup

2.4.2 Machine Test. The machine tests are performed in a Mori Seiki SV-500 CNC machine. The radial engagement is set to 80% of the cutting diameter of the tool, with a depth of cut, $a_p = 4$ mm, and tooth feed $f_z = 0.15$ mm, Fig. 8. The workpiece material is 34CrNiMo6 steel alloy with a dimension of 250 mm × 200 mm × 250 mm, resulting in ten passes per depth of cut and a total of 590 passes per workpiece, giving roughly 983, 333 load cycles per workpiece with a spindle speed of 2546 rpm. The machine tests are performed using only one tooth.

Flank wear (v_b, see Fig. 9) is measured for two prototypes and one reference at every tenth pass. Afterward, for the remaining tests, it is measured every 30th pass, and if the flank wear is larger than 0.2 mm, a new cutting edge is used, and the clamping screw is also changed to avoid critical failures, as the clamping screw fatigue will be measured in the fatigue machine.

2.4.3 Fatigue Test. Tests in the fatigue testing machine are conducted at room temperature. The temperature at the tool holder interface during milling operations is roughly 300 °C. In order to simulate deformations at higher temperatures, the edge of the tool holder interface is chamfered.

The tool holder is oriented in the fatigue testing machine so that the cutting force direction is parallel to the axial actuator. This requires that the cutting point of the $CoroMillR390 - 11T308M - MM$ insert be ground perpendicular to the axial actuator. Placing two Mahr 5313180 1318 dial test indicator inductive probes, u_1 and u_2, on the insert and the screw bottom surface allows researchers to collect data regarding the insert movement. Placing two probes, Fig. 10, allows the movement of the insert to be isolated from the tool holder. A Kistler 9712B quartz modal force sensor measures the piston force applied to the cutting tool. The piston runs at 5 Hz, with a resulting force of 1470 N, 2100 N, and 2940 N, corresponding to a semi-finishing and roughing operation. The data acquisition unit is sampling at a rate of 200 Hz. The run-off limit is set to 200, 000 cycles to reduce machine test time.

Downloaded from http://asmedigitalcollection.asme.org/computingengineering/article-pdf/25/4/041005/7433163/jcise-24-1446.pdf by Chalmers University of Technology user on 11 April 2025

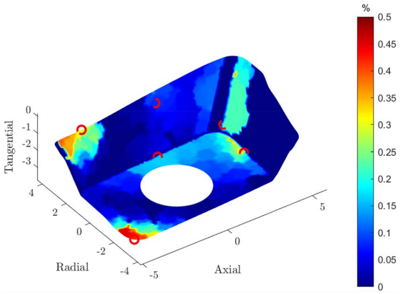

Fig. 11 Heat map of the found reference points

3 Results

The validation process of the found optimum is presented in four sections: (1) optimization algorithm repeatability, (2) FEA of contact point placements and insert stresses, (3) wear-rate in machining, and (4) insert movement and screw clamp fatigue tests.

3.1 Robustness Optimization. The robust optimization methodology consequentially finds an optimum that satisfies the conditions in the desirability function. The repetitiveness of the optimization was tested by running the algorithm for a population size of 20 with a maximum of 100 generations. The population was reset after the population achieved the maximum number of generations, and the individual with the highest fitness score was stored. One GA optimization with the given parameters takes 310.8 s and the software RD&T is called 2000 times. The GA optimization routines were repeated 500 times and required roughly 43 h of solution time for the whole validation process of the genetic algorithm. The results are shown in Fig. 11, which displays a heat map of the frequency of each area to be chosen. The circles mark the positioning with the overall highest fitness. The overall fitness results have a normal distribution of $f \sim N(0.7375, 0.0074) \in (0, 1) \subset \mathbb{R}$.

Using the results from the robustness optimization, a prototype tool holder was designed and modeled. This design features an indexable insert supported by half-spheres, as illustrated in Fig. 12. The half-sphere support structure aims to enhance stability by minimizing insert movement and ensuring consistent contact points, even under varying operational loads.

3.2 Finite Element Analysis. Insert movement u_1 is measured in the opposite corner of the cutting point (see Fig. 13), to replicate the fatigue test probe location, see Sec. 2.4.3. The results are given in the radial ($\delta_r = 28\,\mu$m), axial ($\delta_a = 26\,\mu$m), and tangential ($\delta_t = 23\,\mu$m) directions of the cutting tool and signify the maximum deformation of the cutting point, while $\Delta_t = 5.5\,\mu$m is the difference in translation in the tangential direction between the loading and unloading of the cutting force.

The maximum principal stress in the insert was found at the clamping hole radius of surface A with a magnitude of 625 MPa. The elapsed time for the simulation was 3.3 h.

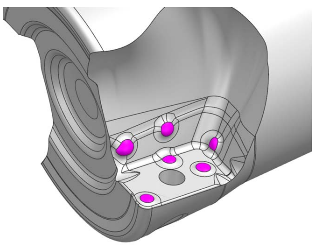

Fig. 12 Model of the prototype tip seat interface using 3-2-1 methodology (contact surfaces marked in magenta)

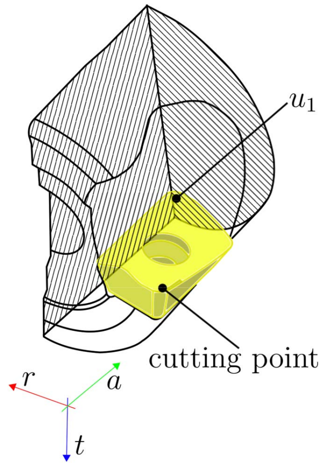

Fig. 13 Insert movement measurement

3.3 Machine Test. The flank wear of the indexable carbide inserts $R390-11T308M-MM2030$ was measured after 30 passes, corresponding to 21 min of machining time. The results of the machining tests are presented in Fig. 14, where the median flank wear of the insert is measured at 0.192 mm, while the reference was measured at 0.183 mm. The trailing ends in the boxplot represent the minimum and maximum values of flank wear

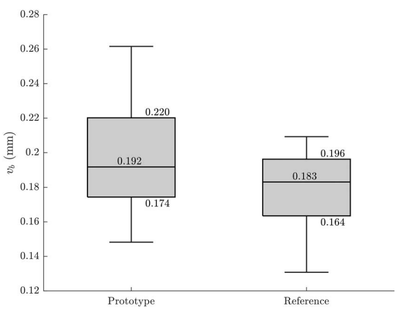

Fig. 14 Flank wear v_b after 21 min

Downloaded from http://asmedigitalcollection.asme.org/computingengineering/article-pdf/25/4/041005/7433163/jcise-24-1446.pdf by Chalmers University of Technology user on 11 April 2025

Table 3 Insert movement results

Name	Load (N)	Run 1 (cycle)	Run 2 (cycle)	Run 3 (cycle)	Run 4 (cycle)	Δ_m (μm)
Reference	2940	200,000	200,000	–	–	5.60
Reference (deformed)	1470	200,000	200,000	200,000	–	77.20
Reference (deformed)	2100	200,000	200,000	200,000	–	30.35
Reference (deformed)	2940	46,661	125,576	72,724	34,850	47.93
Prototype	2940	200,000	200,000	200,000	–	8.67

observed in the machining tests. A total of 15 samples were measured: nine samples for the prototype and six for the reference. However, two edges of the reference samples critically failed during machining: one before the 21 min mark and one after.

3.4 Fatigue Test. The results from the fatigue tests are shown in Table 3. The inserts were fatigued for the deformed tool with a load of 2940 N on the cutting point, which corresponds to heavy machining operations. The mean translation of the reversed cutting point between tests is presented in the Δ_m column and is calculated as the maximum difference in a steady-state interval between the two displacement probes, u_1 and u_2, as shown in Fig. 10.

4 Discussion

In order to minimize insert movements in the tool body interface, a robust locating scheme optimization algorithm for indexable cutting tools was created and validated. The validation process of the robustness optimization was divided into four parts: (1) optimization algorithm repeatability to ensure that a global optimum is found (Fig. 11), (2) FEA simulations to confirm stress levels below the yield in the insert, (3) fatigue machine testing to measure insert movement relative to the tool holder and screw clamp fatigue (Table 3), and (4) machine tests to determine overall performance and flank wear due to heat generation (Fig. 14).

The optimization algorithm was repeated 500 times, and approximately 50% of the found optima's support was located directly under the cutting load on the A-surface (Fig. 11). The remaining contact points were spread out over a larger area, with some concentration toward the radial supports (B-surface) and in the corner between the radial and axial support (C-surface). The overall spread of the found contact point solutions are in line with the stochastic behavior of a genetic algorithm, and several runs are necessary to ensure that the found optima is most likely a global optimum for the given conditions. However, the normal distribution of the fitness $f \sim N(0.7375, 0.0074) \in (0, 1) \subset \mathbb{R}$ showed a small variance between the solutions, indicating that they should perform similarly in relation to the stated desirability function (Eq. (8)). Thus, varying the positions of the half-spheres would most likely have a small impact on the results. The final solution of the robust positioning of the indexable insert in the tool holder is seen in Fig. 12 where the contacting points, or half-spheres, are marked in magenta.

The fracture toughness of the WC-CO carbide inserts has a normal distribution of σ_{TRS} $N(2811, 714)$ MPa [26,29] for the whole hardness spectra and gives the 0.1% percentile as 632 MPa. Through the simulations, the maximum principal tensile stress on the bottom surface of the insert was found to be 625 MPa, which is close to the estimated limit. However, it should be noted that the given limit is for all hardness levels of the uncoated grades.

In the fatigue tests (Table 3), it was essential to evaluate both undeformed and deformed tool holders since the applied loads alone were insufficient to plastically deform the interface. However, during machining, tool holders can reach temperatures as high as 300 °C, which lowers the material's yield strength, making plastic deformation more likely. The fatigue tests were conducted under various load conditions, with a run-off limit set at 200,000 load cycles. In the reference tool holder, under maximum loads of 2940N, no signs of clamping screw fatigue were detected, and the tangential movement of the insert was recorded at 5.60 μm, with no indications of severe plastic deformation. In the deformed reference tool holder, at loads of 1470 N and 2100 N, no clamping screw fatigue was observed, but the insert showed movements of 77.20 μm and 30.35 μm, respectively. The 77.20 μm movement at 1470 N seems unusually high, as it is more than twice that at 2100 N and should be treated as an outlier. Under maximum load (2940 N), clamping screw fatigue occurred after 35, 000–125, 000 load cycles, with a mean tangential insert movement of 47.93 μm. For the prototype tool holder, results were comparable to the undeformed reference, showing no clamping screw fatigue and an insert movement of 8.67 μm. Although there was an initial large deformation (as also seen in FEA simulations), this reduced the pretension of the clamping screw, but it did not affect the result of the tests.

During the machining tests, the flank wear was measured at every 10th pass at the beginning and every 30th pass when the wear-rate had stabilized, corresponding to a 21 min machining time. The wear-rate between the prototype and the reference showed no significant difference and is dependent on the sample size, see Fig. 14. However, two reference tests ended in critical failure due to a fracturing of the cutting edge. The cause of the critical failures is difficult to determine, since no indication of a heavily deformed tip seat was detected prior to failure. This behavior was not found in the prototype tip seat tests. With the current machining process parameters, approximately 30 passes correspond to 50,000 load cycles. This suggests that for a worn reference tool holder, clamping screw failure is likely imminent. To mitigate this risk and prevent critical failures, the clamping screw was replaced with each indexation and insert replacement. This practice ensured that the tool could continue operating safely without the risk of fatigue-induced screw failure

The half-spheres where the insert was positioned showed expected heavy plastic deformation but maintained contact with the insert even when changing inserts. Thus, an adequately constrained insert with necessary supports functions similarly to reference tool holders, throughout its life time. A similar outcome was found in the fatigue machine tests, where the prototype had large deformations in the tip seat. Still, the insert showed stable behavior, with a mean translational movement of 8.67 μm, similar to the reference holder, and the clamping screw withstood 200, 000 load cycles. The FEA simulations underpredicted the translational movement of the insert. This could be because heat generation is not considered in the simulations.

The robust locating scheme optimization algorithm finds optimal contact in the tool body with consideration of operation type and clamping solution using the contact index algorithm [25]. Previous tool holder solutions have an overdetermined tip seat or experience large plastic deformations that create new contact points, resulting in uneven pressure distribution and excessive insert movement that leads to fatigue in the clamping screw.

The reduced size of the contact surfaces in the prototype may result in lower heat transfer between the insert and tool body. Elevated temperatures catalyze tool wear, and this effect could be considered in the optimization algorithm. In these tests, the difference in wear-rate was insignificant, but improvements in heat transfer could lead to the new fixturing concepts of indexable inserts having improved heat transfer capabilities. A noticeable advantage

Downloaded from http://asmedigitalcollection.asme.org/computingengineering/article-pdf/25/4/041005/7433163/jcise-24-1446.pdf by Chalmers University of Technology user on 11 April 2025

of the prototype design is that no grinding of the bottom surface is required, thereby reducing manufacturing costs.

5 Conclusion

Fixturing methodologies are a fundamental part of the machining industry. Minimizing insert movement during a machining operation is crucial to ensuring quality aspects such as durability, reliability, and repeatability. Current fixturing methodologies either do not have enough complexity to handle varying loads or are too complex to implement in early product development phases. For this reason, a method was proposed to incorporate the contact index algorithm into a robust locating scheme optimization algorithm. The optimization consists of two steps: (1) obtaining the lowest root-mean-square value at the cutting point and (2) using a genetic algorithm by considering the contact index, A-surface point distribution, and the normalized root-mean-square value of the cutting point to get an optimized robust insert positioning. By avoiding overdetermination in the tip seat interface, the cutting tool can achieve a significantly longer operational life compared to conventional tool holders, with a minimal impact on performance. This optimization improves tool longevity while maintaining the required operational efficiency. Future applications of this robust locating scheme optimization algorithm for indexable cutting tools must:

(1) validate the methodology's effectiveness for other cutting operations, such as drilling and turning,
(2) consider heat transfer between the indexable insert and tool body,
(3) include cutting point translation due to plastic deformation in the initial tool design, and
(4) incorporate finite element analysis in the genetic algorithm optimization routine.

Acknowledgment

This work was carried out at the Wingquist Laboratory within the Production Area of Advance at Chalmers, supported by VINNOVA (Sweden's government agency for innovation). This support was gratefully acknowledged. Gratitude is extended toward the Department of Metal Cutting Research at AB Sandvik Coromant for all of the help and support.

Conflict of Interest

There are no conflicts of interest.

Data Availability Statement

The datasets generated and supporting the findings of this article are obtainable from the corresponding author upon reasonable request.

References

[1] Lopatukhin, I., Ber, A., and Rotberg, J., 2011, "Analysis and Optimization of the Contact Pressure Distribution Between an Insert and Its Pocket Due to the Clamping and the Cutting Action," J. Manuf. Sci. Prod., **2**(1), pp. 17–26.
[2] Melkote, S., Liang, S., Özel, T., Jawahir, I. S., Stephenson, D. A., and Wang, B., 2022, "100th Anniversary Issue of the Manufacturing Engineering Division Paper: A Review of Advances in Modeling of Conventional Machining Processes: From Merchant to the Present," ASME J. Manuf. Sci. Eng., **144**(11), p. 110801.
[3] Altintas, Y., Tuysuz, O., Habibi, M., and Li, Z. L., 2018, "Virtual Compensation of Deflection Errors in Ball End Milling of Flexible Blades," CIRP Ann., **67**(1), pp. 365–368.
[4] Tuysuz, O., and Altintas, Y., 2018, "Time-Domain Modeling of Varying Dynamic Characteristics in Thin-Wall Machining Using Perturbation and Reduced-Order Substructuring Methods," ASME J. Manuf. Sci. Eng., Trans., **140**(1), p. 011015.
[5] Schleich, B., and Wartzack, S., 2016, "A Quantitative Comparison of Tolerance Analysis Approaches for Rigid Mechanical Assemblies," 14th CIRP CAT 2016 – CIRP Conference on Computer Aided Tolerancing, Göteborg. Sweden.
[6] Shen, Z., Ameta, G., Shah, J. J., and Davidson, J. K., 2005, "A Comparative Study of Tolerance Analysis Methods," ASME J. Comput. Inf. Sci. Eng., **5**(3), pp. 247–256.
[7] Cai, W., Hu, S. J., and Yuan, J. X., 1996, "Deformable Sheet Metal Fixturing: Principles, Algorithms, and Simulations," ASME J. Manuf. Sci. Eng., Trans., **118**(3), pp. 318–324.
[8] Söderberg, R., and Lindkvist, L., 1999, "Computer Aided Assembly Robustness Evaluation," J. Eng. Des., **10**(2), pp. 165–181.
[9] Söderberg, R., Lindkvist, L., and Dahlström, S., 2006, "Computer-Aided Robustness Analysis for Compliant Assemblies," J. Eng. Des., **17**(5), pp. 411–428.
[10] Shawki, G. S., and Abdel-Aal, M. M., 1965, "Effect of Fixture Rigidity and Wear on Dimensional Accuracy," Int. J. Mach. Tool Des. Res., **5**(3), pp. 183–202.
[11] Shawki, G. S., and Abdel-Aal, M. M., 1966, "Rigidity Considerations in Fixture Design-Contact Rigidity at Locating Elements," Int. J. Mach. Tool Des. Res., **6**(1), pp. 31–43.
[12] Shawki, G. S., and Abdel-Aal, M. M., 1966, "Rigidity Considerations in Fixture Design-Rigidity of Clamping Elements," Int. J. Mach. Tool Des. Res., **6**(4), pp. 207–220.
[13] Hurtado, J. F., and Melkote, S. N., 2001, "Improved Algorithm for Tolerance-Based Stiffness Optimization of Machining Fixtures," ASME J. Manuf. Sci. Eng., **123**(4), pp. 720–730.
[14] Prabhaharan, G., Asokan, P., Ramesh, P., and Rajendran, S., 2004, "Genetic-Algorithm-Based Optimal Tolerance Allocation Using a Least-Cost Model," Int. J. Adv. Manuf. Technol., **24**, pp. 647–660.
[15] Prabhaharan, G., Padmanaban, K. P., and Krishnakumar, R., 2007, "Machining Fixture Layout Optimization Using FEM and Evolutionary Techniques," Int. J. Adv. Manuf. Technol., **32**(11–12), pp. 1090–1103.
[16] Sundararaman, K. A., Guharaja, S., Padmanaban, K. P., and Sabareeswaran, M., 2014, "Design and Optimization of Machining Fixture Layout for End-Milling Operation," Int. J. Adv. Manuf. Technol., **73**(5–8), pp. 669–679.
[17] Wu, D., Zhao, B., Wang, H., Zhang, K., and Yu, J., 2020, "Investigate on Computer-Aided Fixture Design and Evaluation Algorithm for Near-Net-Shaped Jet Engine Blade," J. Manuf. Processes, **54**, pp. 393–412.
[18] Charles Liu, S., and Jack Hu, S., 1997, "Variation Simulation for Deformable Sheet Metal Assemblies Using Finite Element Methods," ASME J. Manuf. Sci. Eng., **119**(3), pp. 368–374.
[19] Camuz, S., Lorin, S., Wärmefjord, K., and Söderberg, R., 2019, "Nonlinear Material Model in Part Variation Simulations of Sheet Metals," ASME J. Comput. Inf. Sci. Eng., **19**(2), p. 021012.
[20] Dahlstrom, S., and Lindkvist, L., 2007, "Variation Simulation of Sheet Metal Assemblies Using the Method of Influence Coefficients With Contact Modeling," ASME J. Manuf. Sci. Eng., **129**(3), pp. 615–622.
[21] Lööf, J., Lindkvist, L., and Söderberg, R., 2010, "Optimizing Locator Position to Maximize Robustness in Critical Product Dimensions," Proc. ASME Des. Eng. Tech. Conf., **2**(Parts A and B), pp. 515–522.
[22] Tabar, R. S., Lorin, S., Cromvik, C., Lindkvist, L., Warmefjord, K., and Soderberg, R., 2021, "Efficient Spot Welding Sequence Simulation in Compliant Variation Simulation," ASME J. Manuf. Sci. Eng., **143**(7), p. 071009 .
[23] Rezaei Aderiani, A., Wärmefjord, K., Söderberg, R., Lindkvist, L., and Lindau, B., 2020, "Optimal Design of Fixture Layouts for Compliant Sheet Metal Assemblies," Int. J. Adv. Manuf. Technol., **110**(7–8), pp. 2181–2201.
[24] Camuz, S., Bengtsson, M., Söderberg, R., and Wärmefjord, K., 2019, "Reliability-Based Design Optimization of Surface-to-Surface Contact for Cutting Tool Interface Designs," ASME J. Manuf. Sci. Eng., **141**(4), p. 041006.
[25] Camuz, S., Liljerehn, A., Wärmefjord, K., and Söderberg, R., 2024, "Algorithm for Detecting Load-Carrying Regions Within the Tip Seat of an Indexable Cutting Tool," J. Comput. Inf. Sci. Eng., **24**(4), p. 041006 (8 pages).
[26] Chychko, A., García, J., Collado Ciprés, V., Holmström, E., and Blomqvist, A., 2022, "HV-K IC Property Charts of Cemented Carbides: A Comprehensive Data Collection," Int. J. Refract. Met. Hard Mater., **103**, p. 105763.
[27] Wahde, M., 2008, *Biologically Inspired Optimization Methods—An Introduction*, WIT Press, Southampton.
[28] Bjoorklund, S., Gustafsson, G., Hageryd, L., and Rundqvist, B., 2015, *Karlebo Handbok*, 16th ed., Liber, Lund, Sweden.
[29] García, J., Collado Ciprés, V., Blomqvist, A., and Kaplan, B., 2019, "Cemented Carbide Microstructures: A Review," Int. J. Refract. Met. Hard Mater, **80**, pp. 40–68.

Downloaded from http://asmedigitalcollection.asme.org/computingengineering/article-pdf/25/4/041005/7433163/jcise-24-1446.pdf by Chalmers University of Technology user on 11 April 2025